

Fundamental Aspects of DNA-Mediated Charge Transport

Thesis by

Tashica Tréshun Williams

*Submitted in Partial Fulfillment of the Requirements for the
Degree of Doctor of Philosophy*

California Institute of Technology
Pasadena, CA 91125
March 2004
(Defended March 26, 2004)

© 2004
Tashica Williams
All Rights Reserved.

ACKNOWLEDGEMENTS

Every day you may make progress. Every step may be fruitful. Yet there will stretch out before you an ever-lengthening, ever-ascending, ever-improving path. You know you will never get to the end of the journey. But this, so far from discouraging, only adds to the joy and glory of the climb.

Sir Winston Churchill

Although I have reached the end of my educational tenure at Caltech, I am indebted to a great many people who have aided my efforts here at the Institute. First and foremost, I would like to thank Dr. Jacqueline K. Barton, who introduced me to a world of research that was both intellectually stimulating and engaging. To adroitly convince the most hardened critic to consider one's point of view is certainly a skill that I have learned from her and will try to effectively utilize in law practice! Additionally, I appreciate the support and encouragement that she has provided me over the years. Her passion for chemistry is an inspiration to all-especially me. I also thank Mo Renta, who is the oil (high quality!) that allows the Barton scientific machine to operate smoothly and efficiently. I certainly will miss her discussions and sharp wit. Dian Buchness and Lena Lenore should also be acknowledged for they assisted me in both administrative and personal matters.

During my time at Caltech, I have befriended a great many people; however, I will only highlight some here. Marissa Mock, Sarah Heilshorn, and

Niki Zacharias are friends who kept me grounded when I was driving *myself* insane. They were great friends with whom to hang out, explore Los Angeles and as emotional and scientific soundboards. Candace Rypisi, Brandi Jones, Parandeh Kia, and Erica O'Neal always kept me encouraged, gave me the name of a *great* beautician (yes, Virginia, vanity is a sin, but one *must* stay fabulous; thanks Ed!), occasionally reminded me to eat and provided me with tons of free food! I also broadly thank the numerous faculty members and staff whom I was privileged to serve with on various committees. To the students who enabled me to form the Caltech Black Graduate Student Association, I appreciate all of you for your interesting discussions and desire to initiate change! Past and present members of the Caltech Chamber Singers and the Caltech Women's Glee Club should also be noted for both of these clubs allowed me to find a musical release every week and allowed me to interact with interesting students and staff.

Micheal Babamazid, John McKey, and Paul Winze are friends who moved out here from Texas to break into the Hollywood scene and were great roommates who kept me laughing until my sides hurt, hence permitting me to forget about science every now and then. I also want to express my appreciation to my numerous sorors of Delta Sigma Theta for their support, particularly Lindsey Malcom, Stephanie Brown, and Jackie Robinson. Chantal Morgan D'Apuzzo and Sherice Nivens provided me with unequivocal support of my career choice of

patent law and valuable advice. My gratitude also extends to Dr. Jesse Jones (Baylor University), Barbara Rauls (Baylor University) and Dr. Hyun Ok (Merck Laboratories, Rahway, NJ) for their continued support. I also give a special thanks to Dr. Thomas Franklin (Baylor University) who had faith in my scientific abilities as a freshman and allowed me to work in his laboratories, hence starting me on my scientific journey. Sir, you will be missed.

My excellent thesis committee should also be acknowledged. Professor Harry B. Gray, the chairman of my committee, is one of the most entertaining faculty members that I have ever encountered! He always provided a soothing mental balm for my extraordinarily frayed nerves during defense of my candidacy report, Ph.D. proposals, and thesis. Professor David Tirrell is truly one of the most insightful and thoughtful scientists that I have been privileged to know. Professor Rudolph A. Marcus provided the theoretical framework for this thesis and is truly a chemical pioneer. I thank them all for their great advice and also for passing me!

Jackie has the incredible ability to attract extremely intelligent and motivated people to the Barton group. A number of these individuals have guided me through numerous emotional and scientific jungles. Megan Núñez and Scott Rajske helped me get started and armed me with the necessary biochemical skills. Other individuals made my graduate life enjoyable and

provided me with scientific clarity on numerous occasions: Olav Schiemann, Pratip Bhattacharya (thanks for saving my candidacy report!), Roshi Pakadaman, Matthias Pascaly, Henrik Junicke, Jen Kisko, Jae Yoo, Eva Rüebea, Alex Schnyder, Maria DeRosa and Dave Vicic. Both Jon Hart and Greg Drummond, my fuzzy head duo, were great sports, always allowing me to rub their heads for good luck! I especially want to thank Kitty Erkkila Calahan and Duncan Odom for their warm friendship and excellent counsel. Kimberly and Rebekah Copeland (my Friday lunch buddies) and Elizabeth Boon Carrico always had a kind word and provided me with warm Christian fellowship; they also kept me from going absolutely crazy during my candidacy preparation and continue to keep me sane! Additional thanks are extended to Sarah Delaney, Anne Petitjean, Melanie O'Neill, and Donato Ceres. All championed me and pushed me toward graduation in various ways; my heart will *never* stop singing their praises.

Another anchor throughout my graduate career was my family. The unconditional love of my mother, father, brother, and sister was the wind for my flagging emotional sails when I did not feel like continuing at Caltech and was feeling discouraged. I also would like to thank, whole-heartedly, my extended family of Abe Amirgholizadeh and Laverne Menser. I love you all and would not have made it this far without you. I know, Dad, "God is good. All the time, God is good."

Finally, my love and thanks goes to a person who has emotionally endured more than any human being should: Sasan Amirgholizadeh. What can I say that would adequately describe all that he has done for me? He is the love of my life and has weathered so many storms with me. God certainly knew what he was doing when he sat me behind you in pre-calculus at Ellison High. You are the kindest and most selfless person I have ever known. Although you have yet to make an honest woman of me, I will love you forever.

ABSTRACT

The π -stacked array of DNA base pairs has fascinated scientists since its structural delineation. Here are described fundamental studies to probe how this π -stacked array mediates DNA charge transport (CT). Intercalators, such as dipyridophenazine (dppz) complexes of ruthenium and phenanthrenequinone diimine (phi) complexes of rhodium, serve as powerful and systematic probes of DNA CT in these studies.

In a series of rhodium-tethered DNA assemblies, with varying A/T sequences intervening between guanine doublet sites (5'-GG-3'), long-range oxidative DNA damage is examined. The guanine doublet sites are known as sites of low oxidation potential in DNA, and the rhodium complex serves as a spatially separated, potent photooxidant. Although these studies are inconsistent with a mechanism involving guanine hopping and tunneling through A/T sequences, these data illustrate that the sequence of bases is an important determinant in attenuating oxidative damage yields of CT. Based on these data, we propose hopping among domains defined by sequence-dependent structure. Additional studies are also described using rhodium-tethered DNA assemblies to examine how different ionic distributions around the DNA duplex modulate DNA CT. In the rhodium-DNA conjugates, differences in long-range

oxidative damage yield were observed depending on the position of pendent charges on the oligomer.

A direct comparison of DNA CT utilizing a variety of oxidants has also been performed. CT is assayed both through determination of the yield of oxidative guanine damage and, in derivative DNA assemblies, by analysis of the yield of a faster oxidative trapping reaction, ring-opening of N^2 -cyclopropylguanine (^{CP}G) within the DNA duplex. We find clear differences in oxidative damage ratios at the distal versus proximal 5'-CGGC-3' depending upon the photooxidant employed. There is also a correlation seen between absolute yield of oxidative damage and distal/proximal damage ratio; photooxidants that produce higher distal/proximal damage ratios have lower yields. These differences observed among photooxidants as well as the complex distance dependence are attributed to differences in rates of back electron transfer (BET).

A study of the overall effect of bridge energetics on DNA CT has also been performed by constructing rhodium-DNA assemblies containing varying numbers of inosine, a guanine base analog with a higher oxidation potential, between two 5'-GG-3' sites. For the rhodium conjugates, only a slight diminution in distal oxidative yield with increasing distance is observed,

suggesting direct charge injection by rhodium into higher energy sites of the intervening bridge.

These results, taken together, provide insight into salient parameters that govern DNA CT, in particular how energetics, charge distribution, and sequence-dependent DNA structure and dynamics modulate charge migration through DNA.

TABLE OF CONTENTS

Acknowledgements	iii
Abstract	viii
Table of Contents	xi
Lists of Figures and Tables	xiv
CHAPTER 1. Charge Transport in DNA	
Introduction	2
DNA metallointercalators	
Phenanthrenequinone diimine complexes of rhodium	6
Dipyridophenazine complexes of ruthenium	11
Photophysical studies of electron transport in DNA	
Electron transport between ethidium and a rhodium intercalator	13
Ultrafast charge transport in DNA: ethidium and 7-deazaguanine	16
Base-base charge transport	18
DNA-mediated electron transport on surfaces	
Characterization of DNA-modified surfaces	19
Electrochemical probe of redox reactions of intercalators	21
Sensing mismatches in DNA	23
Long-range oxidative damage to DNA	26
Models for long-range DNA charge transport	31
Mismatch influence on long-range oxidative damage to DNA	34
Using charge transport to probe DNA-protein interactions and DNA repair	
DNA binding proteins as modulators of oxidative damage from a distance	36
Detection of transient radicals in protein/DNA charge transport	37
Electrical detection of DNA-protein interactions	39
Repair of thymine dimers	41
Oxidative damage to DNA in nucleosomes	43
DNA charge transport within the nucleus	46
Dissertation overview	47
References	48

CHAPTER 2. Variations in DNA Charge Transport with Nucleotide Composition and Sequence	
Introduction	57
Experimental	58
Results and Discussion	
Assembly design	60
Long-range guanine oxidation: sequence composition and bridge length	62
DNA-mediated charge transport: domain hopping	72
References	76
CHAPTER 3. The Effect of Varied Ion Distribution on Long-Range Charge Transport in DNA	
Introduction	83
Experimental	84
Results and Discussion	
Assembly design	86
Ionic distribution and charge transport	90
Potential differences and long-range charge transport	98
References	100
CHAPTER 4. Effects of the Photooxidant on DNA-Mediated Charge Transport	
Introduction	105
Experimental	110
Results	
Photooxidants and DNA assembly	115
Oxidative damage patterns of the various oxidants	120
Native gel analysis of photooxidant-tethered assemblies	122
Long-range CT studies with thionine	126
Hole-trapping by ^{CPG} with other photooxidants	132
Discussion	
Tethered metallointercalators do not aggregate under assay conditions for DNA CT	139
Differences in both yield and distal/proximal damage ratios are found to depend upon the tethered photooxidant	140
Back electron transfer as a distinguishing characteristic of the photooxidant	142

Implications and Conclusions	147
References	148
CHAPTER 5. Probing the Effects of Bridge Energetics on Long-Range Charge Transport in DNA	
Introduction	154
Experimental	158
Results and Discussion	
Design of assemblies	161
Bridge energetics using the $[\text{Rh}(\text{phi})_2\text{bpy}']^{3+}$ photooxidant	161
The temperature dependence of long-range oxidation in the presence of bridging inosines and utilizing the $[\text{Rh}(\text{phi})_2\text{bpy}']^{3+}$ photooxidant	168
Conclusion	171
References	172
CHAPTER 6. Summary and Perspectives	175

LIST OF FIGURES AND TABLES

CHAPTER 1. Charge Transport in DNA

1.1. The structure of double helical DNA	3
1.2. Crystal structure of $\Delta\text{-}\alpha\text{-}[\text{Rh}(\text{R,R-dimethyltrien})\text{phi}]^{3+}$	8
1.3. Different photochemical reactions of phi complexes of rhodium	9
1.4. Schematic illustration of some DNA assemblies used to probe photoinduced charge transfer	14
1.5. Schematic illustration of alkane-thiol functionalized DNA duplexes, immobilized on a gold electrode	20
1.6. Illustration of the effect of a CA mismatch on electron transport through DNA films	24
1.7. Photooxidants used to probe long-range oxidative damage to DNA	28
1.8. The flash-quench cycle for ruthenium	30
1.9. Schematic illustration of long-range charge transport in a nucleosome core particle	45

CHAPTER 2. Variations in DNA Charge Transport with Nucleotide Composition and Sequence

2.1. Oxidative damage to an assembly containing an A ₄ -tract by $[\text{Rh}(\text{phi})_2\text{bpy}']^{3+}$	63
2.2. Temperature dependence of oxidative damage yield and sequence	65
2.3. Oxidative damage to an assembly containing an A ₆ -tract by $[\text{Rh}(\text{phi})_2\text{bpy}']^{3+}$	67
2.4. Oxidative damage to an assembly containing an A ₈ -tract by $[\text{Rh}(\text{phi})_2\text{bpy}']^{3+}$	69
2.5. Plot of distal/proximal guanine oxidation ratio versus the distance from the site of $[\text{Rh}(\text{phi})_2\text{bpy}']^{3+}$ intercalation	71
Table 2.1. Long-range oxidative damage in DNA assemblies functionalized with the tethered photooxidant $[\text{Rh}(\text{phi})_2\text{bpy}']^{3+}$	61

CHAPTER 3. The Effect of Varied Ion Distribution on Long-Range Charge Transport in DNA

3.1. Oxidative damage to A ₆ -tract assemblies containing either a 5' or 3' ³² P end-label and a pendant Δ-[Rh(phi) ₂ bpy'] ³⁺	88
3.2. Oxidative damage to an A ₆ -tract assembly containing a nonradioactive ³² P 5' end-label, a 3' ³² P radioactive end-label and a pendant Δ-[Rh(phi) ₂ bpy'] ³⁺	91
3.3. Oxidative damage to an A ₆ -tract assembly containing a base overhang, a 5' or 3' end-label, and a pendant Δ-[Rh(phi) ₂ bpy'] ³⁺	93
3.4. Oxidative damage to a mixed sequence assembly containing a 5' or 3' ³² P end-label and a pendant Δ-[Rh(phi) ₂ bpy'] ³⁺	96
Table 3.1. Long-rang oxidative damage obtained in the presence of various charge distributions utilizing tethered Δ-[Rh(phi) ₂ bpy'] ³⁺	87

CHAPTER 4. Effects of the Photooxidant on DNA-Mediated Charge Transport

4.1. Photooxidants, modified nucleosides, and DNA assembly	116
4.2. Oxidative damage with various pendant photooxidants	118
4.3. Native gel of duplexes tethered with Δ-[Rh(phi) ₂ bpy'] ³⁺ , and either an intercalated or an end-capped anthraquinone	125
4.4. The ring-opening reaction of ^{CP} G and products	128
4.5. HPLC profiles of d ^{CP} G oxidation and irradiation time course monitoring d ^{CP} G consumption by thionine	129
4.6. HPLC profiles of nucleoside mixtures from the enzymatic digestion of d ^{CP} G and d ^{iPr} containing DNA/thionine conjugates	133
4.7. Sequences and plot of ^{CP} G-containing DNA/thionine conjugates as a function of distance separating ^{CP} G and thionine	135
4.8. HPLC profiles of nucleoside mixtures from the enzymatic digestion of irradiated ^{CP} G-containing DNA assemblies functionalized with either Δ-[Rh(phi) ₂ bpy'] ³⁺ or end-capped anthraquinone	137
4.9. Schematic illustrating pathways for CT in oxidant-tethered assemblies	144
Table 4.1. A summary of oxidative guanine damage by biochemical analysis and ^{CP} G consumption	123

CHAPTER 5. Probing the Effects of Bridge Energetics on Long-Range Charge Transport in DNA

- | | |
|---|-----|
| 5.1. A schematic illustration of rhodium-tethered assemblies containing intervening inosine bases and structures of guanine and inosine | 162 |
| 5.2. Oxidative damage of inosine-containing assemblies with functionalized $[\text{Rh}(\text{phi})_2\text{bpy}']^{3+}$ | 163 |
| 5.3. Plot of 5'-distal/proximal guanine oxidation ratio versus distance from the intercalation site of $\Delta\text{-}[\text{Rh}(\text{phi})_2\text{bpy}']^{3+}$ for intervening guanine or inosine steps | 165 |
| 5.4. Plot of the temperature dependence of 5'-distal/proximal guanine oxidation ratio for two inosine containing assemblies | 170 |

CHAPTER 1

Charge Transport in DNA

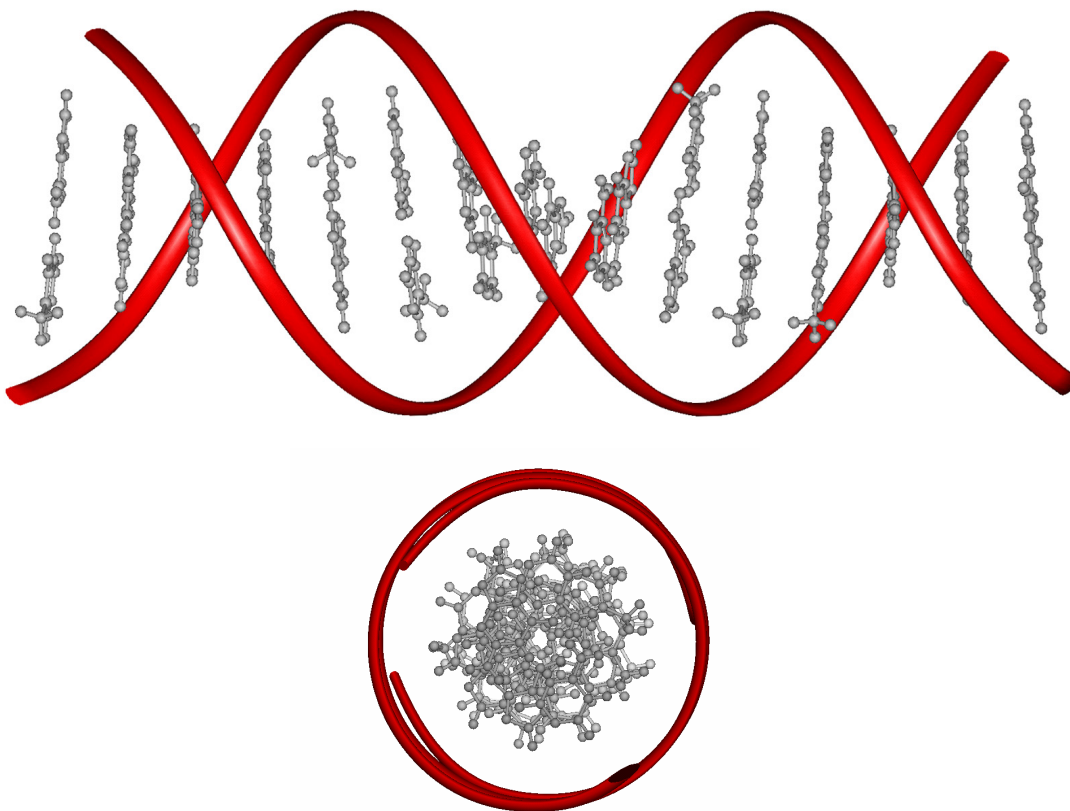
Adapted from Williams, T. T. and Barton, J. K. "Charge Transport in DNA," in *DNA and RNA Binders: From Small Molecules to Drugs*, Vol. 1, Eds. M. Demeunynck, C. Bailly, and W.D. Wilson, pp. 146-172, Wiley-VCH, Weinheim (2003).

INTRODUCTION

Double helical DNA contains within its interior an extended π -stacked array of aromatic, heterocyclic base pairs (Figure 1.1). As such, the DNA double helix represents, almost uniquely, a well-defined molecular π -stack. Solid state π -stacked materials, particularly when doped, can be effective conductors and semiconductors [1,2]. In the years since the delineation of the DNA structure by Watson and Crick [3], then, by analogy, it has been asked whether double helical DNA might similarly display properties associated with molecular conductivity [4,5]. Indeed, whether double helical DNA, owing to its π -stacked structure, might be an effective conduit for charge transport (CT) has intrigued physicists, chemists, and biologists for more than 40 years.

Early studies of DNA charge transport generated significant interest and extensive debate. Physicists carried out varied measurements of electron transport in DNA, resulting in DNA being described by some as an insulator and others as a quantum wire [6-8]. Based upon pulse radiolysis studies, radiation biologists suggested charge could migrate over as short a distance as 3 base pairs [9] or as long a distance as 200 base pairs [10]. More recent studies applied more sophisticated techniques in measurements of DNA conductivity. Differential conductivity depending upon DNA orientation was seen in studies of aligned DNA films [11]; a large current that increased linearly with applied voltage was

Figure 1.1. The structure of double helical DNA. The sugar phosphate backbone is delineated in red and the bases in gray (top). Note the extensive overlap of the base pairs, the path of DNA-mediated charge transport (bottom).



found when the DNA molecules were oriented perpendicular to the electrode, and in contrast, no current was detected with a parallel alignment. Direct conduction measurements were carried out on small collections of DNA duplexes arranged into 600 nm long DNA ropes, and these studies revealed semiconductor behavior, with resistivity values that were comparable to those of other conducting or semiconducting materials [12]. Furthermore, single molecule conduction measurements on dry poly(G)-poly(C) showed no conduction at low voltages, but at higher voltages, DNA seemed to support large currents [13]. While some consensus may now have been reached that DNA possesses properties of a wide band gap semiconductor [14], varied conductivity measurements on dry DNA samples at low temperatures continue to appear consistent with DNA being everything from an insulator to a superconductor [15]. Likely the variability in DNA structure and integrity in these physical measurements adds to the variance in the conclusions obtained.

Chemists first focused on CT in DNA in the context of earlier studies of protein electron transfer [16], and analogously to protein systems, well-defined oligonucleotide duplexes containing pendant donors and acceptors were constructed to measure electron transfer rates and yields as a function of distance on DNA duplexes in solution. The ability of the DNA π -stack to serve as a medium for long-range electron transport was quantified utilizing β , which, from

Marcus theory, is a measurement of the exponential decay with distance of electronic coupling of the medium [17]. For σ -bonded systems, including proteins, the value of β was found to be $\sim 1.0 \text{ \AA}^{-1}$; for comparison, a β value of $\sim 0.1 \text{ \AA}^{-1}$ is found for conjugated polymers [18]. In measurements of electron transfer on DNA assemblies, β was found to range from ≤ 0.2 [19,20] to $\sim 0.6-0.7$ [21], to as high as 1.4 [22] \AA^{-1} . Recent experiments have demonstrated the complexity of experimental evaluation of β for DNA, and have suggested that the apparent disparity in CT distance dependence may arise because different experimental assemblies might operate within different regimes of a mechanistic continuum between one-step superexchange and multi-step hopping [23]. Hence β , in the context of non-adiabatic tunneling models, may not be the most appropriate parameter to characterize DNA-mediated CT.

Other investigations have focused on using DNA assemblies with intercalators and modified bases that serve as donors and acceptors. These CT studies using intercalators permit direct probing of the π -stack and have revealed particularly shallow distance dependence in various systems. CT in DNA is sensitive to π -stacking of the donor, the acceptor, and the intervening base-pair array. As a result, CT may be most usefully applied as a probe of nucleic acid structure and structural dynamics.

DNA METALLOINTERCALATORS

In characterizing the π -stack as a medium for DNA-mediated CT, it is important to have the probes directly coupled into the π -stack. Hence, metallointercalators have been useful in studying long-range electron transfer in DNA, particularly dipyrrophenazine (dppz) complexes of ruthenium(II) (e.g., $[\text{Ru}(\text{phen})(\text{dppz})(\text{bpy}')]^{2+}$ and phenanthrenequinone diimine (phi) complexes of rhodium(III) (e.g., $[\text{Rh}(\text{phi})_2\text{bpy}']^{3+}$) [24]. These ligands afford the octahedral ruthenium and rhodium metal complexes tight DNA binding via intercalation ($K \geq 10^6 \text{ M}^{-1}$), and the DNA interactions of these intercalators have been extensively characterized [25].

Phenanthrenequinone Diimine Complexes of Rhodium

Studies of phi complexes of rhodium have shown that these complexes bind avidly to DNA ($K \geq 10^6 \text{ M}^{-1}$) by intercalation of the phi ligand [26,27]. The sequence specificity of these complexes can be varied by altering the ancillary, non-intercalating ligands. High resolution NMR studies initially provided insight into the binding mode of these phi complexes [28]. The studies revealed that the complexes bound DNA from the major groove, and that intercalation provided a means by which the functional groups on the ancillary ligands and those contained in the major groove could interact. In fact, NMR studies of the

complex, $\Delta\text{-}\alpha\text{-}[\text{Rh}(\text{R,R-dimethyltrien})\text{phi}]^{3+}$, which was designed to recognize the sequence 5'-TGCA-3', revealed site-specific binding of the complex to a decamer that centrally contained a 5'-TGCA-3' sequence and delineated specific, rationally designed hydrogen bonding and methyl-methyl contacts [29]. A 1.2 Å crystal structure was also obtained for the $\Delta\text{-}\alpha\text{-}[\text{Rh}(\text{R,R-dimethyltrien})\text{phi}]^{3+}$ complex, intercalated into a DNA octamer (Figure 1.2) [30]. The structure revealed that intercalation of the complex occurs via the major groove, and, based upon five independent views of the intercalator, minimal perturbation of the π -stack is observed; the phi ligand inserts into and essentially serves as an additional base pair within the π -stack. Hence, intercalation of the complex does not appear to perturb the base stack either globally or locally.

The rich photochemistry of phi complexes of rhodium enables demarcation of binding sites of the metal complexes in addition to providing potent, intercalating photooxidants [27]. Hence, irradiation of the complexes bound to DNA at different wavelengths induces different photochemical reactions [Figure 1.3 and reference 31]. Irradiation of the phi complexes with ultraviolet light ($\lambda = 313 \text{ nm}$) leads to direct strand scission of the DNA sugar-phosphate backbone with products consistent with abstraction of the C3' hydrogen from the sugar that is near the activated phi ligand at the intercalation site.

Figure 1.2. (A) Five Δ - α -[Rh(R,R-dimethyltrien)phi]³⁺-DNA octamer complexes stacked end to end in the asymmetric cell of the crystal. (B) A major groove view of intercalation of Δ - α -[Rh(R,R-dimethyltrien)phi]³⁺ bound to 5'-G-dIU-TGCAAC-3'. As shown in the figure, minor perturbation of the π -stack is observed. The intercalator is inserted as an additional base-pair step. Adapted from [30].

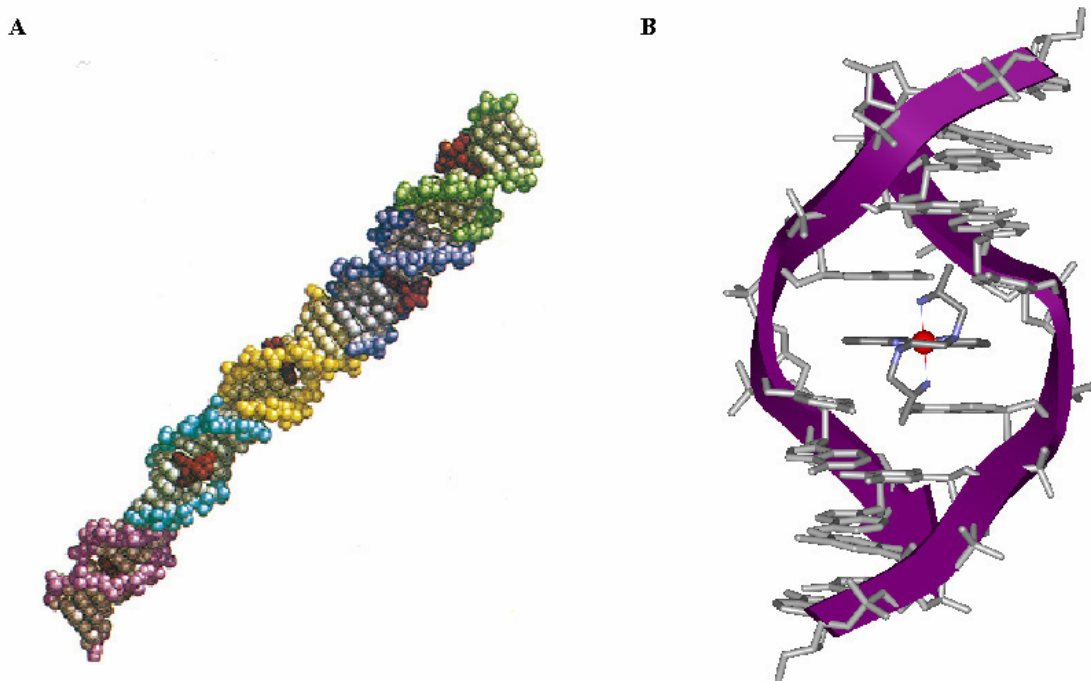
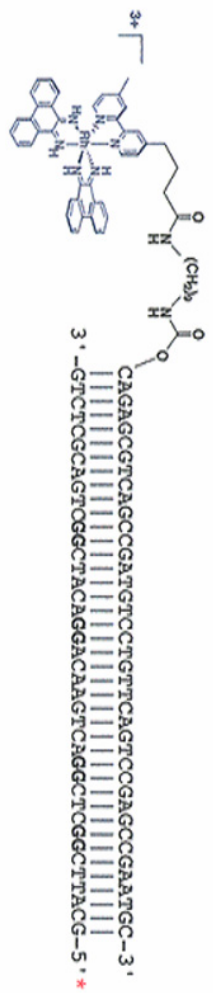


Figure 1.3 Different photochemical reactions of phi complexes of rhodium. Irradiation at 313 nm leads to direct scission of the DNA phosphate backbone, hence demarcating the site of intercalation. Longer wavelength irradiations (i.e., 365 nm) leads to long-range oxidation, which is revealed following treatment with hot aqueous piperidine.

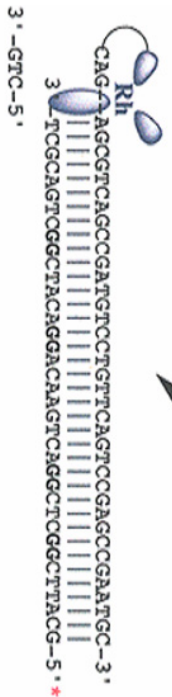


313 nm

Direct Backbone Scission

365 nm

Base Oxidation



10% Piperidine at 90°C



This chemistry then marks the site of binding. If, instead, the DNA bound phi complexes are irradiated with visible light ($\lambda \geq 365$ nm), oxidative damage to the DNA bases results. These phi complexes of rhodium, when photoexcited, appear to be sufficiently potent to promote oxidation of all of the nucleotides.

Dipyridophenazine Complexes of Ruthenium

The dipyridophenazine complexes of ruthenium(II) have been shown to possess remarkable photophysical properties when bound to DNA [32,33]. Irradiation of these complexes with visible light leads to a metal-to-ligand charge transfer excited state, which is localized on the dppz ligand. This localization of the charge on the dppz ligand has been particularly valuable in probing DNA-mediated CT, because excitation of intercalated dipyridophenazine complexes directs the charge transfer directly into the π -stack, not onto an ancillary ligand [34].

Perhaps more important is the interesting differential luminescence quenching seen with the complex free in aqueous solution compared to when bound to DNA. Luminescence of the dppz complex of ruthenium is easily detected in organic solvents; however, none is observed in aqueous solution. This quenching by water has been attributed to proton transfer from the solvent to the nitrogen atoms of the phenazine [35]. Upon intercalation of the dppz into

DNA, however, the luminescence is maintained, for the DNA π -stack protects the phenazine nitrogen atoms from the solvent. Hence dppz complexes of ruthenium serve as sensitive “light switches” for DNA.

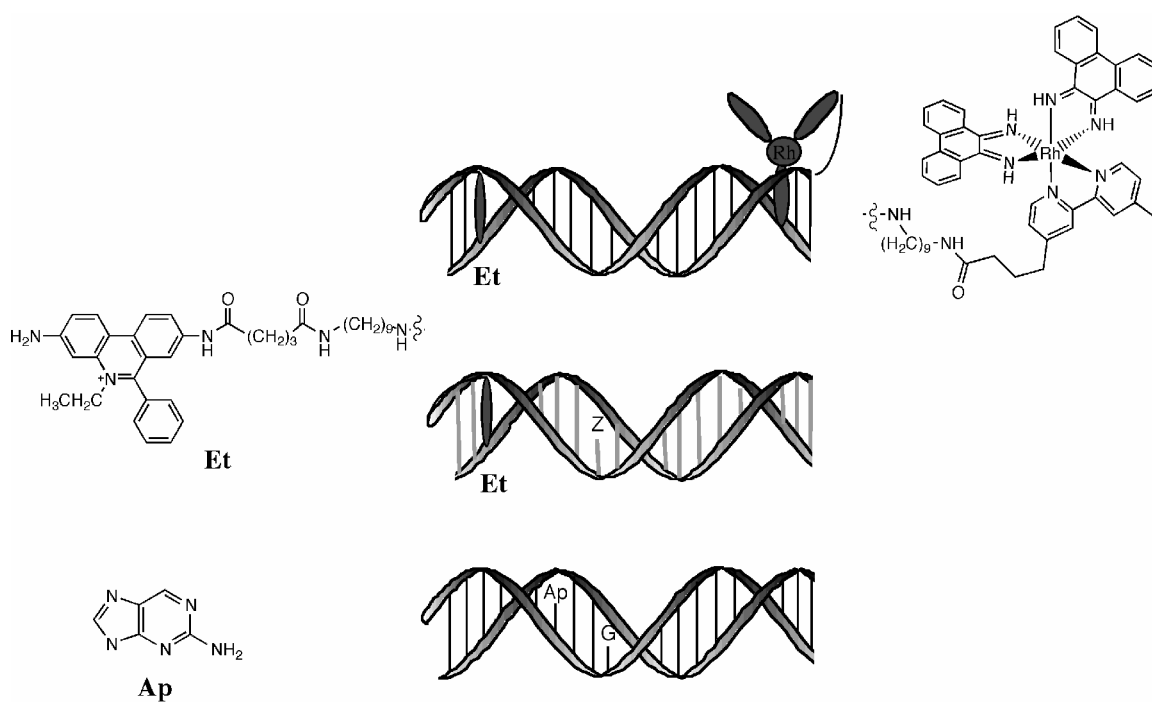
This “light switch” characteristic of the dipyrrophenazine complexes has proven to be a valuable spectroscopic tool in delineating how the intercalated dppz ligand is bound to DNA [36]. NMR studies of partially deuterated [Δ -Ru(phen)₂dppz]²⁺ bound to a hexamer revealed that the dppz ligand prefers to intercalate via the major groove and that two binding orientations (i.e., symmetrical and asymmetrical) were identified [37]. In the symmetrical mode, the phenazine nitrogens are protected from the solvent, whereas in the asymmetrical mode, the phenazine nitrogens are more solvent exposed. Other studies have suggested that some dppz complexes may bind to DNA also from the minor groove side [38]. A DNA intercalator that possesses both major and minor groove orientations has not been previously established. Therefore, it would be valuable to establish whether both binding orientations occur through intercalation and also what truly determines access of the dppz complex to the base-pair stack.

PHOTOPHYSICAL STUDIES OF ELECTRON TRANSPORT IN DNA

Electron Transport between Ethidium and a Rhodium Intercalator

Early photophysical investigations of long-range electron transfer quenching in an assembly containing tethered metallointercalators provided an intriguing introduction to studies of CT through DNA [19]. These early studies underscored clear differences between CT in DNA versus protein systems [39]. To further probe the distance dependence of CT in DNA and to begin to delineate the importance of π -stacking to the CT process, the classic organic intercalator, ethidium, was employed as the photoexcited electron donor and $[\text{Rh}(\text{phi})_2\text{bpy}']^{3+}$ as the acceptor (Figure 1.4) [20]. Both the donor and acceptor molecules were tethered to duplexes of variable length (24-38 Å) to permit systematic investigation of the electron transfer over defined donor-acceptor distances. Photoinduced quenching of the ethidium excited state was monitored for a series of duplexes and the extent of fluorescence quenching provided a measure of electron transfer efficiency. Interestingly, a shallow distance dependence in the quenching yield was observed for this system. Moreover, although the quenching variations appeared to reflect attenuation in the yield of electron transfer, time-resolved measurements showed that dramatic variations in the electron transfer rate were not apparent.

Figure 1.4. Schematic illustration of some DNA assemblies used to probe photoinduced charge transfer. Shown (top to bottom) are duplexes containing donors and acceptors as two pendant intercalators [20], an intercalator and modified base [23,40], and two bases [41,43].



Thus it was proposed that electron transfer through the base-pair stack was faster than the ability to detect it ($>10^9$ s⁻¹) and that electron transfer through DNA was sensitive to π -stacking. Therefore, the distance dependence in quenching yield observed reflected the increased probability of a stacking defect with increasing donor-acceptor distance, not a significant change in rate.

To probe the sensitivity of the electron transfer process to π -stacking, a CA mismatch, which is known to cause local perturbations in base-stacking but not global structural distortions, and a GA mismatch, which continues to be well-stacked in the DNA due to increased aromatic surface area, were introduced into the DNA assemblies. Substantial electron transfer quenching was still evident in the duplex containing the GA mismatch, which had a quenching yield similar to that of the Watson-Crick paired duplex. However, a significant reduction in quenching yield was observed in the presence of the CA mismatch. This result provided a clear demonstration of the sensitivity of the electron transport process to perturbations in the intervening base-pair stack. Moreover, this experiment unambiguously established that the path of CT is through π -stacked bases.

Ultrafast Charge Transport in DNA: Ethidium and 7-Deazaguanine

Having observed photoinduced long-range electron transport between metallointercalators, other studies were performed in which a DNA base could serve as the reactant. The guanine base analog, 7-deazaguanine, possesses an oxidation potential that is ~ 300 mV below that of guanine. Hence, in assemblies containing tethered ethidium as the photoexcited donor, selective oxidative quenching by this analogue but not guanine is possible within a mixed DNA sequence [40].

Fluorescence measurements of the ethidium-deazaguanine system (Figure 1.4) first revealed that electron transport could occur over a range of donor-acceptor separations (6-24 Å) and that the transport occurred on the subnanosecond timescale, with a quenching yield that also exhibited a shallow distance dependence. Furthermore, as in the earlier study [20], upon the incorporation of mismatches into the ethidium/7-deazaguanine duplexes, the quenching yield was significantly diminished. Hence, results were consistent with fast electron transport between the intercalated ethidium and deazaguanine mediated by the DNA π -stack.

The critical importance of DNA dynamics in attenuating the CT process was then underscored in time-resolved studies on the femtosecond timescale of the photooxidation of deazaguanine in a series of tethered ethidium duplexes.

Again the measurements indicated that it was primarily the yield of electron transfer that varied with distance rather than the rate [23]. Transient absorption measurements revealed a 5 picosecond component in the electron transfer decay, which was assigned to direct electron transfer from deazaguanine, and a 70 picosecond component, which corresponded to the timescale for motion of the ethidium within its binding site. With an increase in donor-acceptor separation, it was observed that these components decreased in yield but not significantly in their decay times. Hence, these results were understood in the context of a model in which the initial population of duplexes that were properly stacked and aligned to permit effective coupling were represented by the 5 ps component, yielding fast long-range CT, while CT on the longer 70 ps timescale was gated by the motion of the ethidium within its intercalation site, requiring motion and realignment of the ethidium to permit long-range CT. Interestingly, these studies provided the first direct observation of electron transfer rates through DNA and showed the sensitivity of electron transfer to dynamical motions within the base-pair stack.

Base-Base Charge Transport

While metallointercalators have been useful in probing the DNA-mediated CT process, additional systems were developed to examine base-base electron transfer directly. This was accomplished by exploiting the fluorescence properties of 2-aminopurine and ethenoadenine, analogues of adenine, as well as 7-deazaguanine.

A systematic investigation of DNA-mediated photooxidation of guanine by ethenoadenine and 2-aminopurine was first performed using duplexes with donor-acceptor separations ranging from 3.4 Å to 13.6 Å (Figure 1.4) [41]. The studies revealed fast CT over a range of distances in duplexes containing guanine and 2-aminopurine; the rates for interstrand base-base electron transfer were $\sim 10^8$ s⁻¹ with $\beta = 0.1$ Å⁻¹. These rates indicated efficient coupling among the donor, acceptor, and intervening bases. Notably, however, in duplexes containing ethenoadenine, a bulkier fluorescent analogue of adenine, and guanine, a steeper distance dependence was observed ($\beta = 1.0$ Å⁻¹). Analogously, slow electron transfer kinetics and steep dependence upon increasing distance were also observed in a system using stilbene bridged DNA hairpins ($\beta = 0.6$ Å⁻¹) [21,42].

The base-base electron transfer studies also allowed for differentiation between interstrand and intrastrand electron transfer [41]. In B-form duplexes containing 2-aminopurine, the electron transport kinetics for the intrastrand

reactions were monitored on the femtosecond timescale and were seen to be $> 10^3$ times faster than the interstrand reactions [43]. This difference again is consistent with the path for charge transport being through the stacked bases. In the case of the interstrand reaction, however, because the B-form duplex maintains primarily intrastrand stacking, interstrand electron transfer requires transfer across a hydrogen-bonded base pair.

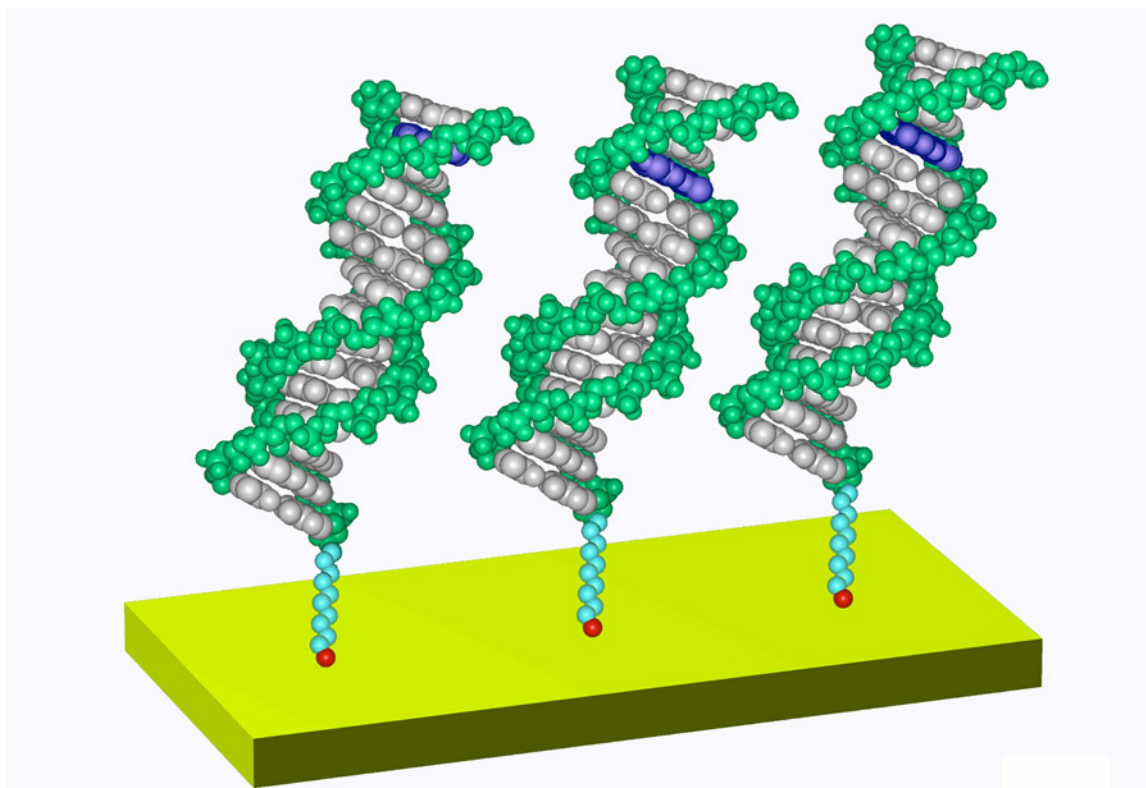
Thus, coupling of the donor, acceptor, and intervening base moieties into the π -stack is paramount for effective CT. In systems that have a well-stacked π -way, lower β values are expected, whereas in systems that do not have significant base stacking, β values approaching those observed in proteins ($\beta \sim 1.0 \text{ \AA}^{-1}$) are expected. From these studies, it can be concluded that fast CT is mediated by an intrastrand, π -stacked pathway.

DNA-MEDIATED ELECTRON TRANSPORT ON SURFACES

Characterization of DNA-Modified Surfaces

The remarkable ability of DNA to form self-assembled monolayers on gold surfaces by way of aliphatic alkane-thiol linkers has also permitted the study of DNA-mediated charge transport utilizing electrochemical techniques that involve ground state reactants [44]. The assembly of DNA films on gold surfaces has been constructed and extensively characterized (Figure 1.5) [45].

Figure 1.5. Schematic illustration of alkane-thiol functionalized DNA duplexes, immobilized on a gold electrode. An intercalator (shown in blue), bound near the top of the DNA monolayer, is reduced by electron transfer from the gold surface through the DNA π -stack.



To immobilize a high density of DNA duplexes on the surface (i.e., close-packing), the DNA is deposited on the surface in the presence of high concentrations of magnesium ion. Direct quantitation of the surface density is achieved by ^{32}P radioactive labeling. Utilizing atomic force microscopy (AFM), a 45° orientation of the duplexes relative to the gold surface was also determined. Moreover, in AFM studies as a function of applied potential, it was found that application of a positive potential caused the DNA, if not closely packed, to lie down upon the surface, hence compressing the monolayer ($\sim 20 \text{ \AA}$), whereas application of a negative potential induced an increase in monolayer thickness ($\sim 50 \text{ \AA}$), consistent with the DNA 15-mer duplexes standing upright, perpendicular to the surface.

Electrochemical Probe of Redox Reactions of Intercalators

Early electrochemical experiments performed involved methylene blue, an aromatic heterocycle that binds to DNA by way of intercalation [46]. The reduction of methylene blue at micromolar concentrations could be easily monitored on an electrode modified to contain densely packed DNA duplexes. The binding affinity of the methylene blue to the DNA film was found to be comparable to that seen with DNA in solution; the binding stoichiometry, however, was significantly lower, consistent with methylene blue having access

only to sites near the top of the film. Because of the large intervening distance expected between the gold and the film-bound methylene blue, these first studies suggested fast rates of DNA-mediated electron transport. As with other methods of analysis, however, well-defined systems were needed to remove the ambiguity of intercalator binding within the DNA-modified surfaces.

A redox active antitumor intercalator, daunomycin, was chosen as a covalently bound intercalator in studies designed to systematically investigate CT as a function of distance on DNA-modified surfaces [47]. Daunomycin also undergoes a reversible reduction within the reduction window of the monolayer. Additionally, upon treatment with formaldehyde, the intercalator can cross-link to the 2-amino group of guanine [48] to form an adduct which has been crystallographically characterized [49]. Hence, thiol-derivatized duplexes were constructed containing a single guanine-cytosine base step to electrochemically probe the effects of distance on long-range electron transport [46]. Structural characterization of the DNA films did not reveal a difference between those films containing cross-linked daunomycin duplexes from those that did not contain the cross-linked moiety.

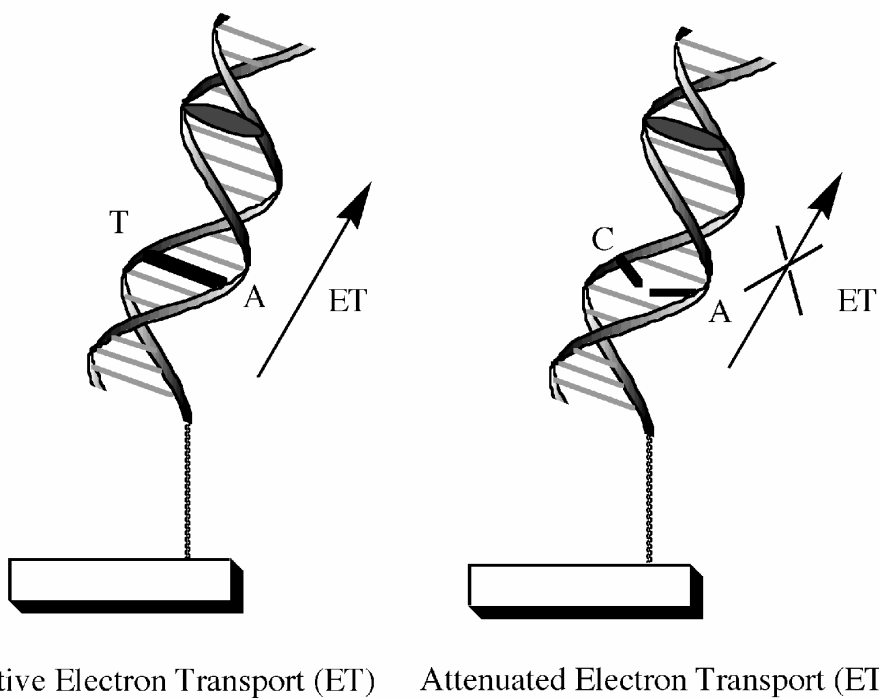
Interestingly, regardless of the position of the daunomycin cross-linked within the 15-mer duplex, reduction of DNA-bound daunomycin was observed and at a comparable rate. Rates of electron transfer through the film could be

estimated in measurements where the scan rate was varied, and these measurements showed slow rates of 10^2 s^{-1} , irrespective of the position of the intercalator; in fact, similar rates were seen with other redox-active probes simply attached to the alkane-thiol linker employed in this investigation. These observations suggested that the rate-limiting step of the process was tunneling through the alkane-thiol linkage; in this context, then, CT through 40 Å distances in DNA was necessarily faster. To explicitly determine the path of CT in these films, a CA mismatch was introduced at a position between the daunomycin and the gold electrode (Figure 1.6). With this intervening mismatch, no detectable reduction of the daunomycin was found. The path for CT is therefore through the base stack, and perturbations in the stack within the films also sensitively attenuate CT.

Sensing Mismatches in DNA

While the CA mismatch experiment represented an important control in early studies, establishing the path for CT, it also provided a demonstration of the electrochemical detection of a single base mismatch in DNA. Current techniques for mismatch discrimination commonly rely upon differential hybridization, thermodynamic measurements of the small and sequence-dependent differences between well-matched and mismatched duplexes.

Figure 1.6. Illustration of the effect of a CA mismatch on electron transport through DNA films. As indicated by the schematic, the introduction of a mismatch, intervening between the gold electrode and intercalator bound near the top of the film, (right) interrupts base-pair stacking locally and effectively attenuates reduction of the intercalator. In the well-stacked duplex (left), in contrast, reduction of the intercalator is efficient.



Hence, it was considered that the sensitivity of long-range CT to stacking might also be exploited in the development of a new class of DNA-based diagnostic tools [50,51].

To amplify the sensitivity of mismatch detection using this strategy, an electrocatalytic cycle was coupled to the electron transport in well-packed DNA-modified films, magnifying signal differences that arise from small stacking perturbations. The cycle begins with the reduction of the methylene blue intercalator, non-covalently bound near the top of the DNA monolayer. The reduced methylene blue, in turn, reduces ferricyanide, that is contained in solution and repelled by the anionic DNA-modified electrode, hence allowing for further reduction of methylene blue. The catalysis is limited only by the amount of ferricyanide contained in the solution. Using chronocoulometry, integrating the current at the methylene blue potential, all of the possible single base mismatches (e.g., GA, CA, etc.) including the difficult purine-purine mismatches, in addition to naturally occurring DNA lesions (e.g., A_{ox}:T), could be detected using electrocatalysis [51]. It has also been shown that mismatches are also sensitively detected in DNA/RNA hybrids [52]. Moreover, this technology can be applied in probing how nucleic acid analogues, such as those utilized for antisense applications, affect duplex stacking [53].

This assay has also been applied in tests of physiologically important sequences where mutations cause disease [51]. For example, hot spots for mutations in the p53 gene were examined; these mutations have been implicated in a variety of human cancers. DNA chips have also been fabricated, prepared using gold surfaces of variable size on silicon wafers. A linear response in charge accumulation with decreasing electrode size (500 μm -30 μm) was found and with high signal: noise; given the dimensions of the gold surfaces, assuming close-packing of the DNA, this corresponds to detection of 10^8 DNA molecules on the chip. The technology, therefore, offers promise as a sensitive, new diagnostic tool to detect mutations and single nucleotide polymorphisms.

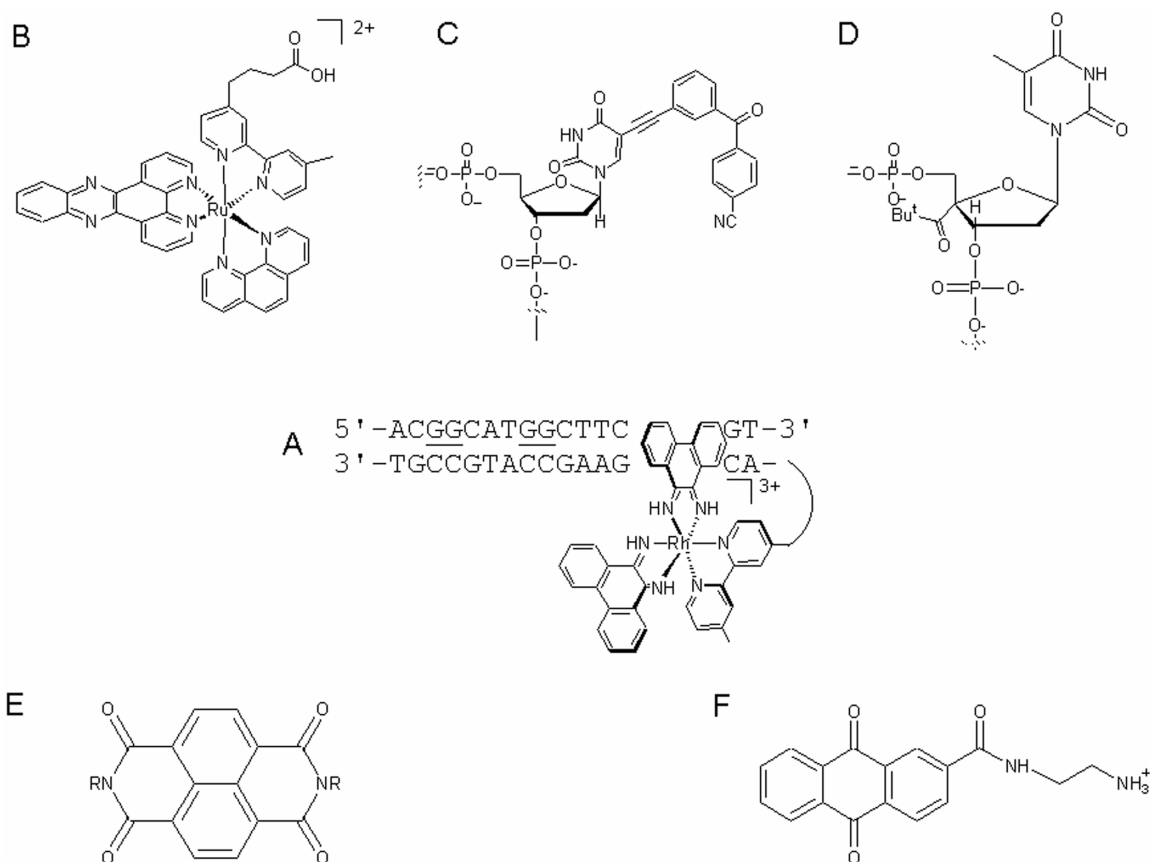
LONG-RANGE OXIDATIVE DAMAGE TO DNA

Within the cell, radical damage to DNA is known to occur. Thus, a physiological role of CT has also been considered. Of the four DNA bases, guanine has been shown to have the lowest oxidation potential ($E^\circ \sim +1.3$ V vs. NHE) [54]. Experimental studies and *ab initio* molecular orbital calculations have revealed that the 5'-G of 5'-GG-3' doublets is preferentially oxidized because the HOMO lies on the 5'-G of a 5'-GG-3' doublet [55,56]. The oxidation of guanine in DNA leads to piperidine-sensitive base lesions, which are revealed as strand breaks [57]. Hence, this damage at the 5'-G of 5'-GG-3' doublets has become a

hallmark for electron transfer chemistry. Oxidative damage to DNA at a distance was first demonstrated in DNA assemblies containing the tethered, intercalating photooxidant $[\text{Rh}(\text{phi})_2\text{bpy}']^{3+}$, spatially separated from two 5'-GG-3' sites (Figure 1.7) [58]. With non-covalent binding of the sequence-neutral intercalator, $[\text{Rh}(\text{phi})_2\text{DMB}]^{3+}$ (DMB = 4,4'-dimethyl bipyridine) and irradiation at 365 nm, oxidation of the 5'-G of 5'-GG-3' was evident; irradiation at higher energy (313 nm) leads instead to direct strand scission, marking the site(s) of metal complex binding. When the rhodium complex was covalently tethered to the duplex, photolysis at 313 nm yielded direct strand breaks near the terminus to which the rhodium complex was tethered. However, with irradiation instead at 365 nm and piperidine treatment, it was found that the two 5'-GG-3' sites were damaged at distances 17 Å and 34 Å away from the bound metallointercalator.

A systematic study of the distance dependence of long-range oxidative damage was performed utilizing a series of duplexes that contained a proximal 5'-GG-3' site that remained at a fixed distance from tethered $[\text{Rh}(\text{phi})_2\text{bpy}']^{3+}$ and a distal 5'-GG-3' site that was marched out in 2 base pair increments relative to the position of the rhodium intercalator [59]. This incremental increase in distal location allowed for exploration of the importance of helical phasing (i.e., stacking of the intercalator and guanine doublet on the same or opposite side of

Figure 1.7. Photooxidants used to probe long-range oxidative damage to DNA. (A) DNA assembly, first used to probe long-range oxidative damage to DNA, containing $[\text{Rh}(\text{phi})_2\text{bpy}']^{3+}$ spatially separated from two 5'-GG-3' doublets, (B) $[\text{Ru}(\text{phen})(\text{dppz})(\text{bpy}')^{2+}$, (C) cyanobenzophenone-modified deoxyuridine, (D) 4-pivavoyl-modified deoxythymine, (E) naphthalene diimide, (F) a substituted anthraquinone.

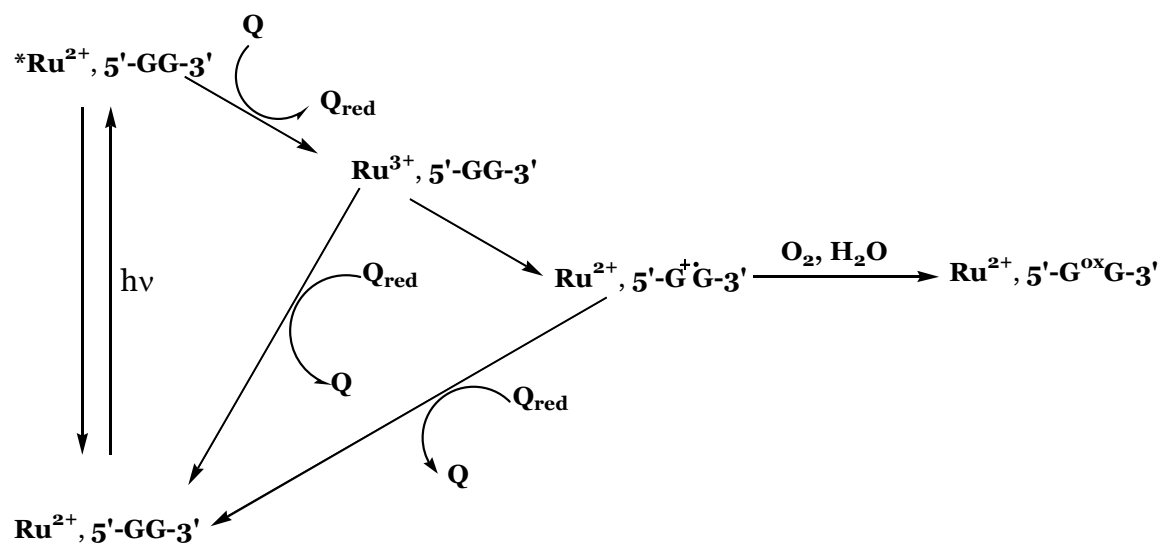


the helix) in charge transport in addition to the distance dependence of the process.

The yield of oxidative damage was not found to be significantly attenuated over a distance of 75 Å. Moreover, the helical phasing of metal complex and the distal guanine site did not appear to be a pertinent parameter. Also, similar to spectroscopic experiments, the long-range CT chemistry was found to be quite sensitive to stacking, both of the oxidant and of the intervening base pairs. Introduction of base bulges (e.g., 5'-ATA-3') in a DNA assembly containing tethered rhodium between 5'-GG-3' sites positioned distal and proximal to the rhodium, for example, caused a dramatic diminution of oxidative damage yield [60].

Additional studies of the distance dependence of the charge transport process investigated 63 base-pair duplexes containing either tethered $[\text{Rh}(\text{phi})_2\text{bpy}']^{3+}$ or $[\text{Ru}(\text{phen})(\text{dppz})(\text{bpy}')]^{2+}$ and six 5'-GG-3' sites, located 31 to 197 Å from the metallointercalator [59]. Ruthenium(III) complexes of dppz, generated *in situ* with quenching of the ruthenium(II) excited state by a non-intercalating quencher (e.g., methyl viologen), had also been shown to promote oxidative damage to DNA from a distance [Figure 1.8 and reference 61]. Remarkably, in the large assemblies, both excited Rh(III) and ground state Ru(III) intercalating oxidants were found to substantially damage DNA over a distance

Figure 1.8. The flash-quench cycle for ruthenium. To generate the ground state Ru(III) oxidant, photoexcitation of the ground state Ru(II) species is performed followed by quenching of the excited state, which is generally executed utilizing either ruthenium hexaamine, methyl viologen, or cobalt pentamine chloride. The Ru(III) species can then oxidize guanine bases.



of 200 Å. Therefore, these studies demonstrated charge migration through DNA to effect damage over a biologically significant distance regime.

Oxidative damage to DNA from a distance does not require a metallointercalator as the oxidant; a variety of oxidants have been used to carry out this long-range chemistry. Figure 1.7 illustrates some of the different photooxidants employed. These include ethidium [62], a cyanobenzophenone-modified deoxyuridine [63], 4-pivaloyl-modified deoxythymine [64], naphthalene diimide [65,66], and anthraquinone [67]. Indeed studies with the anthraquinone moiety bound at a discrete site on long oligonucleotide duplexes confirmed that long-range oxidative damage can be generated from a 200 Å distance [68]. Many of these photooxidants are currently being employed in experiments to explore the mechanism of DNA CT.

Models for Long-Range DNA Charge Transport

Once it became clear that oxidative damage to DNA from a distance through CT was general and not a unique property associated with metallointercalators, new theoretical models were proposed to account for the long-range chemistry that had been delineated. These models focused on descriptions of long-range CT through a combination, to varying extents, of hopping and tunneling mechanisms. In a tunneling mechanism, the orbitals of

the donor and acceptor molecules are significantly below that of the DNA bridge. Therefore, the charge is considered to tunnel through the DNA bridge without forming transient species along the path. The DNA base-pair stack forms a “virtual” bridge of communication between donor and acceptor, and the rate of CT is expected to show an exponential dependence on the distance separating donor and acceptor. At the other extreme, in the hopping mechanism, the donor and acceptor orbitals are energetically close to or above the bridge states. Hence charge is considered to transiently occupy the bridge. If the rate of charge migration through the DNA bridge is faster than irreversible trapping of the transient radical, then the charge would be able to migrate long distances with a quite shallow distance dependence [69,70].

Based upon measurements of oxidative yield, Geise, Jortner, and coworkers proposed that CT through DNA occurs by a mixture of hopping and tunneling mechanisms [71]. Specifically, they proposed that hopping occurs primarily among guanine sites, the lower sites energetically, while tunneling is preferred through TA steps. This proposal was based first upon the observation of little oxidative damage when a 5'-TATA-3' intervened between guanine sites [63,71]. Schuster also described CT through DNA in the context of a hopping model, but one involving phonon-assisted polaron formation [68,72]. In this model, he considered that charge might be delocalized over a polaron within the

DNA bridge, formed in response to the electrostatic perturbations associated with transport of the charge; propagation of the polaron through the DNA would be assisted by phonon interaction. A “domain hopping” model, in which charge hopping proceeds among domains, where delocalization within a given domain depends upon sequence-dependent dynamics and structure has also been proposed [59]. Both the polaron and “domain” hopping models are attractive in the description of the mechanism of charge transport over a distance of 200 Å, for the probability of all of the bases being perfectly aligned over such a distance is improbable.

Likely, however, the description is far more complicated still. In the case of photophysical studies with intercalators bound to DNA, the donor and acceptor orbitals energetically can lie close to the bridge states and are extremely well coupled with the base-pair stack. Conversely, in the case of the electrochemical studies, the redox intercalator potential lies far below that of the DNA bridge. Do these different experiments lie at different ends of a mechanistic continuum or can they be considered together? Heller and coworkers introduced the importance of longitudinal polarizability as a factor in considering these results [73]. If the DNA is polarized along the direction of the helix axis, CT is expected to be facilitated. Photoexcitation or the presence of an

applied potential within the base-pair stack could provide the means to generate a polarized stack.

Additional mechanistic insights will clearly be needed to reconcile all these results. Irrespective of the mechanism, however, it is clear that stacking within the DNA duplex is a critical factor governing and distinguishing long-range CT.

Mismatch Influence on Long-Range Oxidative Damage to DNA

Analogous to photophysical and electrochemical experiments of DNA-mediated charge transport, intervening mismatches, which locally perturb the DNA base-pair stack and sensitively modulated DNA CT, have also been investigated to determine how long-range oxidative damage is attenuated in the presence of mismatches [74]. Using $[\text{Ru}(\text{phen})(\text{dppz})(\text{bpy}')]^{2+}$, a systematic investigation of sixteen possible base-pair and mismatch combinations was explored through biochemical means and ^1H NMR measurements of base-pair opening life times, which also allowed for a concomitant probe of the influence of mismatch dynamics.

Overall, the trend in oxidative damage yields varied in the order $\text{GC} \sim \text{GG} \sim \text{GT} \sim \text{GA} > \text{AA} > \text{CC} \sim \text{TT} \sim \text{CA} \sim \text{CT}$. Generally, the purine-purine mismatches did little to attenuate the amount of oxidative damage observed at the distal

guanine site, while introduction of a pyrimidine-pyrimidine mismatch resulted in much lower oxidative yields. The extent of distal/proximal guanine oxidation in different mismatch-containing duplexes was compared with the helical stability of the duplexes, electrochemical data for intercalator reduction on different mismatch-containing DNA films, and base-pair lifetimes for oligomers containing the different mismatches derived from ^1H NMR measurements of the imino proton exchange rates. While a clear correlation was evident both with helix stability and the electrochemical data, monitoring reduction of an intercalator through DNA films, it was interesting to observe that damage ratios correlated most closely with base-pair lifetimes. Competitive hole trapping at the mismatch site, which had been proposed by others [75], did not appear to be a key factor governing the efficiency of transport through the mismatch. Because of the close correlation with dynamical measurements of DNA, these results served once again to underscore the importance of base dynamics in modulating long-range CT through the DNA base-pair stack [74]. Indeed, it has become increasingly clear that measurements of DNA CT may offer a new and sensitive route to assess sequence-dependent base dynamics within the DNA duplex.

USING CHARGE TRANSPORT TO PROBE DNA-PROTEIN INTERACTIONS AND DNA REPAIR

DNA Binding Proteins as Modulators of Oxidative Damage from a Distance

Proteins that bind DNA do so utilizing a range of structural motifs. Some modes of DNA binding involve significant perturbations in base-pair structure. Because of the sensitivity of charge transport to π -stack perturbations, a variety of studies have been performed utilizing proteins which bind DNA through different, structurally characterized modes [76]. These proteins include the methyltransferase *M.Hha* I, the TATA-binding protein (TBP), the restriction endonuclease *R.Pvu*II, and the Antennapedia homeodomain protein (ANTP).

M.Hha I recognizes the sequence 5'-G*CGC-3' and methylates the target cytosine (*C) after completely flipping the base out of the duplex stack [78]. The π -cavity that is created is filled by insertion of a glutamine side chain (Gln 237) from the enzyme; the glutamine essentially serves as a "bookmark" to hold the place for the cytosine. DNA CT studies have revealed that the yield of oxidative damage at the distal 5'-GG-3' site decreased significantly with *M.Hha* I binding [77]. However, mutant *M.Hha* I, which inserts a π -stacking tryptophan residue (Q237W) into the cavity, found that oxidative damage to the distal guanine doublet site was restored.

Studies of long-range oxidative damage in the presence of other DNA-binding proteins yielded consistent results [76]. For example, crystallographic

studies show that DNA binding of TBP, which plays an important role in transcription initiation, to the sequence 5'-TATAAA-3', induces a 90° kink at either end of the already flexible binding site [79,80]. With this DNA substrate, owing to the flexible 5'-TATAAA-3' site, a low damage ratio was evident even without protein. In the presence of TBP, however, a significant decrease in charge transport to the distal guanine site was also observed as a function of increasing protein concentration. In general, then, it was observed that yields of long-range oxidative damage correlated directly with the nature of the nucleoprotein interaction. Interactions that disturb the DNA π -stack inhibit DNA CT. Alternatively, interactions that promote no helix distortion, such as R.PvuII and ANTP, but, as a result of tight packing may rigidify the π -stack, serve instead to enhance the ability of the DNA base stack to provide a conduit for CT.

Detection of Transient Radicals in Protein/DNA Charge Transport

Both spectroscopic and biochemical techniques have been employed to monitor transient radical intermediates as a result of CT through DNA-protein assemblies [81]. The studies delineated that upon irradiation of an assembly containing the mutant M.Hha I (Q237W) bound 14 base pairs from the site of [Ru(phen)(dppz)(bpy')]²⁺ intercalation and utilizing the flash-quench technique

to generate the Ru(III) oxidant *in situ*, extensive oxidative damage was observed to the guanine located 5' to the tryptophan intercalation site; no similar damage was evident with binding of the wild type protein [81]. Parallel transient absorption experiments also revealed the formation of a radical species. Interestingly, the full transient absorption spectrum of this intermediate contained features that were characteristic both of the guanine and tryptophan radicals. Hence, hole transport proceeded through DNA to the inserted tryptophan from the protein and to the 5'-guanine, where irreversible oxidative damage occurred.

Additional studies have examined the distance dependence of the rate of formation of the tryptophan and guanine radicals, using a series of ruthenium-tethered duplexes that contained *M.Hha* I binding sites located at distances varying from 24 to 51 Å away from the ruthenium intercalator [81]. The yield of oxidative damage observed at the 5'-position to the inserted tryptophan diminished little with increasing distance. Transient absorption measurements also showed no variation in the rate of radical formation with increasing distance; the rate constant for radical formation was $> 10^6 \text{ s}^{-1}$ in each assembly. Hole transport through DNA over this 50 Å distance regime, therefore, was not rate limiting. In fact, these kinetic results complement earlier findings of base-base electron transfer rates on the order of 10^{10} s^{-1} [43]. More recently,

experiments using a methylindole moiety incorporated directly into the DNA as an artificial base [82] yielded comparable results and, in fact, set the lower limit for CT through the stack as $> 10^7 \text{ s}^{-1}$, coincident with formation of the Ru(III) oxidant through diffusional quenching.

Electrical Detection of DNA-Protein Interactions

An electrochemical assay (*vide supra*) on DNA-modified electrodes provided another means to probe protein/DNA interactions by monitoring the effect of protein binding on the DNA base stack [83]. This assay yielded wholly complementary results to biochemical measurements of oxidative damage, despite the fact that here reduction of a bound intercalator was being measured, while in the biochemical experiments photoinduced DNA oxidation chemistry was being probed. Practically, however, in the electrochemistry experiment, the measurement could be made in real time and without gel electrophoresis.

Functionalized with a thiol-terminated linker and with daunomycin cross-linked to a guanine residue near the duplex terminus, DNA assemblies were constructed that contained the binding sites for either *M.Hha* I, uracil-DNA glycosylase (UDG), TBP, or *R.Pvu*II. As in the biochemical experiments, electrochemistry revealed that binding of native *M.Hha* I, the base-flipping enzyme that inserts a glutamine into the π -stack, significantly attenuated the

electrochemical response. Consistent with transport through a π -way, binding of the mutant protein, *M.Hha* I (Q237W), which inserts a tryptophan into the π -stack, showed little attenuation of the electrochemical response. A parallel series of experiments on DNA-modified electrodes containing an abasic site within the protein recognition site was also performed. In this case, only a small electrochemical signal was evident either without protein or with native protein. Interestingly, however, binding of the mutant here as well filled the π -stack and thus yielded a high electrochemical response. UDG, a base excision repair enzyme that extrudes uracil upon binding, was also probed utilizing this assay. Analogous to the results found upon binding of the native *M.Hha* I, UDG also showed a marked decrease in electrochemical response upon protein binding. Furthermore, introducing a gross structural distortion, as that found upon binding of TBP, which significantly kinks DNA, also led to attenuation of the electrochemical signal.

These data further illustrate the exquisite sensitivity of DNA electron transport to stacking perturbations and offer a novel assay through which to structurally probe how different proteins interact with DNA. This assay also offers a new opportunity to apply CT chemistry in directly probing DNA-protein interactions in real time.

Repair of Thymine Dimers

In addition to studies that probe oxidative damage to DNA from a distance, other reactions on DNA, promoted at long range through CT chemistry, have been demonstrated. It has been shown that DNA CT can also be utilized to promote the repair of thymine dimers in DNA [84]. Thymine dimers, the most common photochemical lesions in DNA, result from the photoinduced [2+2] cycloaddition reaction between adjacent thymines contained on the same polynucleotide strand to form the cyclobutane dimer [85]. This lesion is removed in eukaryotic cells by the excision of the dimer. However, in bacteria, the photolyase enzyme promotes repair using electron transfer chemistry; with irradiation in the visible region, a reduced flavin cofactor adds an electron to the cyclobutane dimer, triggering repair of the lesion and release of the electron back to the enzyme. In model systems, repair of the cyclobutane dimer has been triggered both oxidatively and reductively [86,87].

Upon irradiating duplexes, containing tethered $[\text{Rh}(\text{phi})_2\text{bpy}']^{3+}$ and a thymine dimer located 16 to 26 Å away from the metallointercalator, at 400 nm and after high performance liquid chromatography, a substantial amount of thymine dimer repair was revealed with increasing irradiation time [84].

Analogous to studies of oxidative damage, these investigations revealed that this repair was insensitive to increasing the distance between the metallointercalator

and the thymine dimer (16-26 Å). Furthermore, the repair efficiency was also found to be sensitive to π -stacking perturbations; a decrease in repair efficiency was seen with the introduction of base bulges between the site of rhodium intercalation and the thymine dimer. Hence, not only is DNA able to promote long-range oxidative damage to DNA from a remote site through CT chemistry, but CT chemistry with a similar sensitivity to the intervening base stack can also be harnessed to trigger thymine dimer repair from a distance.

Other potent photooxidants can also promote the repair of thymine dimers [88]. For example, analogous to $[\text{Rh}(\text{phi})_2\text{bpy}']^{3+}$, which has an oxidation potential of ~ 2.0 V vs. NHE, substantial repair from a distance was observed using the organic intercalator, naphthalene diimide, which has an oxidation potential of $+1.9$ V vs. NHE. However, repair was not observed using either ethidium or anthraquinone derivatives as noncovalently bound intercalators. In the case of ethidium, it is understandable that the organic intercalator cannot perform repair, since the reduction potential of the ethidium is sufficiently below that of the dimer. Surprisingly, however, the anthraquinone was also unable to repair the dimer [89]. The anthraquinone derivatives have a reduction potential of ~ 2.0 V vs. NHE from the excited triplet state and therefore should have sufficient driving force for repair. It has been suggested that the lack of repair with the anthraquinone moiety is due to the fact that its excited singlet state is

particularly short-lived [88]. In fact, anthraquinone derivatives that do not undergo rapid conversion to the excited triplet state can promote thymine dimer repair. Interaction with the singlet state may therefore be critical for effective repair.

Studies have also been performed that examine the competition between oxidative damage and thymine dimer repair, since oxidation of guanine sites should be thermodynamically favored [90]. Interestingly, the studies revealed that thymine dimer repair proceeds efficiently in the presence of potential thermodynamic traps provided by guanine doublets. Although it is thermodynamically favorable to perform guanine oxidation, it appears kinetically preferable to repair thymine dimers. This competition is useful to consider in the context of generally assessing reactions that may proceed within the cell based upon CT chemistry. Indeed other DNA-mediated CT reactions, perhaps initiated by proteins bound to DNA, could conceivably be carried out along the duplex without irreversible reaction at guanines, if, similarly, these reactions are kinetically favored.

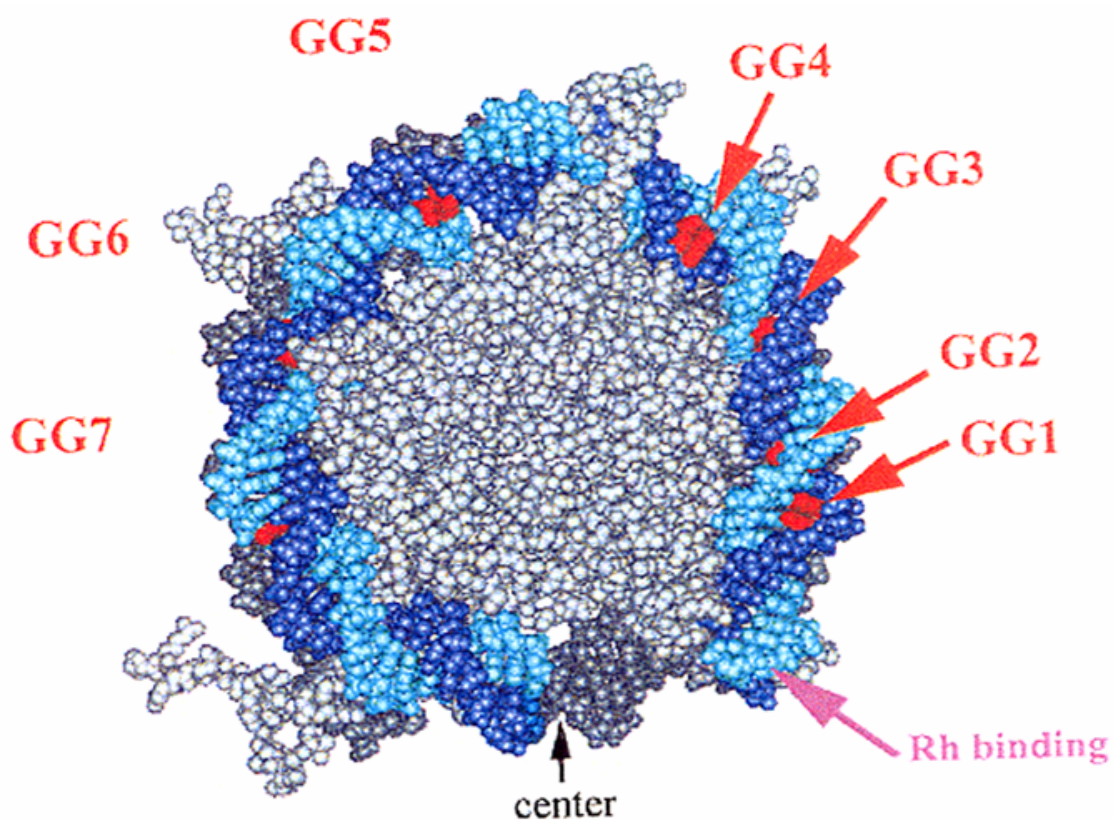
Oxidative Damage to DNA in Nucleosomes

In eukaryotic cells, DNA is packaged within nucleosome core particles [91]. In this unit, ~150 base pairs of DNA are wrapped around an octamer of

histone proteins, to which the DNA is associated by nonspecific, electrostatic interactions. It has been thought that this packaging of nucleosomal DNA serves to protect it from damage. The DNA is dynamically restricted and less accessible to solution-borne damaging agents. However, oxidative damage through CT chemistry does not require solution accessibility. On the other hand, the restricted motion and overall bending of the DNA within the nucleosome would not be expected to favor long-range CT. Notably, guanine oxidation was not observed at sites located further away from the site of rhodium intercalation either in the core particle or even in the absence of histones [Figure 1.9 and reference 92]; likely the highly bent DNA structure utilized to obtain consistent nucleosome phasing for these experiments also interfered with long-range CT. Nonetheless, over a significant distance regime ($> 75 \text{ \AA}$), long-range CT was established within the nucleosome core particle.

These data hold implications for damage to and repair of the genome *in vivo*, where much of the DNA is bound within nucleosome core particles. It has been considered that histones, in addition to packaging and regulating DNA, also function to protect DNA, since the histones reduce binding by a variety of potentially dangerous small molecules.

Figure 1.9. Schematic illustration of long-range charge transport in a nucleosome core particle. The nucleosome was assembled containing $[\text{Rh}(\text{phi})_2\text{bpy}']^{3+}$ covalently tethered to the terminus (indicated by the purple arrow). Efficacious charge transport leading to oxidative damage at a site 24 base pairs away (GG4) from the site of rhodium intercalation was evident [92]. The nucleosome structure shown here is based upon that determined crystallographically [91] and shows DNA in blue and histones in grey.



In fact, binding of DNA to histone proteins to form nucleosome core particles does reduce the ability even of the rhodium complex to intercalate into the DNA. However, packaging of DNA as nucleosomes does not protect it from long-range damage through CT through the base-pair stack. Indeed, such damage generated by long-range CT within the nucleosome may persist preferentially and lead to the formation of permanent mutations.

DNA Charge Transport within the Nucleus

Since DNA is the genetic material encoding all of the information within the cell, it becomes important to ask whether there exists cellular mechanisms to protect DNA from oxidative damage at a distance and perhaps that exploit DNA CT chemistry. A first step in exploring these issues involves establishing whether DNA CT can proceed within the cell nucleus.

Towards that end, studies, utilizing $[\text{Rh}(\text{phi})_2\text{DMB}]^{3+}$, were performed that probed exon 5 of the p53 gene as well as a transcriptionally active promoter within the phosphoglycerate kinase gene (PGK 1). Oxidative damage studies on exon 5 of the p53 gene revealed clearly the preferential damage at the 5'-G of 5'-GGG-3', 5'-GG-3', and 5'-GA-3' sites, a signature for electron transfer damage to DNA [93]. Thus the rhodium complex, with photoactivation, was shown to promote oxidative damage to DNA within the nucleus. More interesting still

were the experiments in which damage on the PGK promoter was probed. Here oxidative damage was found at protein-bound sites which are inaccessible to rhodium. Thus, on transcriptionally active DNA within the cell nucleus, DNA-mediated CT can promote base damage from a distance. Importantly, then, even within the nucleus, direct interaction of an oxidant is not necessary to generate a base lesion at a specific site. These observations set the stage for studies directed at probing *in vivo* applications of DNA CT. Certainly these data require consideration in understanding cellular mechanisms for DNA damage and repair.

DISSERTATION OVERVIEW

A great wealth of experimentation has demonstrated the importance of CT in a variety of contexts. The focus of this dissertation is to explore particular components of the CT process that are paramount for effective transport. Chapters 2 and 3 explore the effects of sequence and ionic distribution on the CT process, respectively, whereas Chapter 4 examines the effects of the photooxidant. Chapter 5 investigates how the overall bridge potential between oxidatively sensitive sites attenuate the charge transport process by the introduction of higher energy bases. A summary is outlined in Chapter 6.

REFERENCES

1. Kittel, C. *Introduction to Solid State Physics*, Wiley, New York, **1976**.
2. Marks, T. J. *Science* **1985**, 227, 881-889.
3. Watson, J. D.; Crick, F. H. C. *Nature* **1953**, 171, 737-738.
4. Szent-Györgi, A. *Nature* **1941**, 148, 157-159.
5. Eley, D. D.; Spivey, D. I. *J. Chem. Soc., Faraday Trans.* **1962**, 58, 411-415.
6. Warman, J. M.; de Haas, M. P.; Rupprecht, A. *Chem. Phys. Lett.* **1996**, 249, 319-322.
7. Snart, R. S. *Biopolymers* **1968**, 6, 293-297.
8. Liang, C. Y.; Scalco, E. G. *J. Chem. Phys.* **1964**, 40, 919-922.
9. Anderson, R. F.; Patel, K. B.; Wilson, W. R. *J. Chem. Soc., Faraday Trans.* **1991**, 87, 3739-3746.
10. Cullis, P. M.; McClymont, J. D.; Symons, M. C. R. *J. Chem. Soc., Faraday Trans.* **1990**, 86, 591-592.
11. Okahata, Y.; Kobayashi, T.; Tanaka, K.; Shimomura, M. *J. Am. Chem. Soc.* **1998**, 120, 6165-6166.
12. Fink, H.-W.; Schönenberger, C. *Nature* **1999**, 398, 407-410.
13. Porath, D.; Bezryadin, A.; de Vries, S.; Dekker, C. *Nature* **2000**, 403, 635-638.
14. Dekker, C.; Ratner, M. A. *Physics World* **2001**, 29-33.

15. Kasumov, A. Y.; Kociak, M.; Guéron, S.; Reulet, B.; Volkov, V. T.; Klinov, D. V.; Bouchiat, H. *Science* **2001**, *291*, 280-282.
16. Gray, H. B.; Winkler, J. R. *Annu. Rev. Biochem.* **1996**, *65*, 537-561.
17. Marcus, R. A.; Sutin, N. *Biochim. Biophys. Acta.* **1985**, *811*, 265-322.
18. Woitellier, S.; Launay, J. P.; Spangler, C. W. *Inorg. Chem.* **1989**, *28*, 758-762.
19. Murphy, C. J.; Arkin, M. R.; Jenkins, Y.; Ghatlia, N. D.; Bossmann, S. H.; Turro, N. J.; Barton, J. K. *Science* **1993**, *262*, 1025-1029.
20. Kelley, S. O.; Holmlin, R. E.; Stemp, E. D. A.; Barton, J. K. *J. Am. Chem. Soc.* **1997**, *119*, 9861-9870.
21. Lewis, F. D.; Wu, T.; Zhang, Y.; Letsinger, R. L.; Greenfield, S. R.; Wasielewski, M. R. *Science* **1997**, *277*, 673-676.
22. Fukui, K.; Tanaka, K. *Angew. Chem. Int. Ed.* **1998**, *37*, 158-161.
23. Wan, C.; Fiebig, T.; Kelley, S. O.; Treadway, C. R.; Barton, J. K.; Zewail, A. H. *Proc. Natl. Acad. Sci. USA* **1999**, *96*, 6014-6019.
24. Núñez, M. E.; Barton, J. K. *Curr. Opin. Chem. Biol.* **2000**, *4*, 199-206.
25. Erkkila, K. E.; Odom, D. T.; Barton, J. K. *Chem. Rev.* **1999**, *99*, 2777-2795.
26. Sitlani, A.; Barton, J.K. *Biochemistry* **1994**, *33*, 12100-12108.
27. Sitlani, A.; Long, E. C.; Pyle, A. M.; Barton, J. K. *J. Am. Chem. Soc.* **1992**, *114*, 2303-2312.
28. David, S. S.; Barton, J. K. *J. Am. Chem. Soc.* **1993**, *115*, 2984-2985.

29. Hudson, B. P.; Barton, J. K. *J. Am. Chem. Soc.* **1998**, *120*, 6877-6888.
30. Kielkopf, C. L.; Erkkila, K. E.; Hudson, B. P.; Barton, J. K.; Rees, D. C. *Nature Struc. Biol.* **2000**, *7*, 117-121.
31. Turro, C.; Hall, D. B.; Chen, W.; Zuilhof, H.; Barton, J. K.; Turro, N. J. *J. Phys. Chem. A* **1998**, *102*, 5708-5715.
32. Friedman, A. E.; Chambron, J.-C.; Sauvage, J.-P.; Turro, N. J.; Barton, J. K. *J. Am. Chem. Soc.* **1990**, *112*, 4960-4962.
33. Jenkins, Y.; Friedman, A. E.; Turro, N. J.; Barton, J. K. *Biochemistry* **1992**, *31*, 10809-10816.
34. Stemp, E. D. A.; Holmlin, R. E.; Barton, J. K. *Inorg. Chim. Acta.* **2000**, *297*, 88-97.
35. Olson, E. J. C.; Hu, D.; Hörmann, A.; Jonkman, A. M.; Arkin, M. R.; Stemp, E. D. A.; Barton, J. K.; Barbara, P. F. *J. Am. Chem. Soc.* **1997**, *119*, 11458-11467.
36. Hartshorn, R. M.; Barton, J. K. *J. Am. Chem. Soc.* **1992**, *114*, 5919-5925.
37. Dupureur, C. M.; Barton, J. K. *J. Am. Chem. Soc.* **1994**, *116*, 10286-10287.
38. Tuite, E.; Lincoln, P.; Nordén, B. *J. Am. Chem. Soc.* **1997**, *119*, 239-240.
39. Arkin, M. R.; Stemp, E. D. A.; Holmlin, R. E.; Barton, J. K.; Hörmann, A.; Olson, E. J. C.; Barbara, P. F. *Science* **1996**, *273*, 475-480.
40. Kelley, S. O.; Barton, J. K. *Chem. Biol.* **1998**, *5*, 413-425.

41. Kelley, S. O.; Barton, J. K. *Science* **1999**, *283*, 375-381.
42. Lewis, F. D.; Letsinger, R. L.; Wasielewski, M. R. *Acc. Chem. Res.* **2001**, *34*, 159-170.
43. Wan, C.; Fiebig, T.; Schiemann, O.; Barton, J. K.; Zewail, A. H. *Proc. Natl. Acad. Sci. USA* **2000**, *97*, 14052-14055.
44. Kelley, S. O.; Barton, J. K. *Metal ions in biological systems*, Vol. 36, Eds. A. Sigel and H. Sigel, pp 211-249, Dekker, New York, **1999**.
45. Sam, M.; Boon, E. M.; Barton, J. K.; Hill, M. G.; Spain, E. M. *Langmuir* **2001**, *17*, 5727-5730.
46. Kelley, S. O.; Barton, J. K.; Jackson, N. M.; Hill, M. G. *Bioconjugate Chem.* **1997**, *8*, 31-37.
47. Kelley, S. O.; Jackson, N. M.; Hill, M. G.; Barton, J. K. *Angew. Chem. Int. Ed.* **1999**, *38*, 941-945.
48. Leng, F. F.; Savkur, R.; Fokt, I.; Przewloka, T.; Priebe, W.; Chaires, J. B. *J. Am. Chem. Soc.* **1996**, *118*, 4731-4738.
49. Wang, A. H. J.; Gao, Y. G.; Liaw, Y. C.; Li, Y. K. *Biochemistry* **1991**, *30*, 3812-3815.
50. Kelley, S. O.; Boon, E. M.; Barton, J. K.; Jackson, N. M.; Hill, M. G. *Nucleic Acids Res.* **1999**, *27*, 4830-4837.

51. Boon, E. M.; Ceres, D. M.; Drummond, T. G.; Hill, M. G.; Barton, J. K.
Nature Biotech. **2000**, *18*, 1096-1100.
52. Boon, E. M. unpublished results.
53. Boon, E. M.; Barton, J. K.; Pradeepkumar, P. I.; Isaksson, J.; Petit, C.;
Chattopadhyaya, J. *Angew. Chem. Int. Ed.* **2002**, *41*, 3402-3405.
54. Steenken, S.; Jovanovic, S. V. *J. Am. Chem. Soc.* **1997**, *119*, 617-618.
55. Sugiyama, H.; Saito, I. *J. Am. Chem. Soc.* **1996**, *118*, 7063-7068.
56. Prat, F.; Houk, K. N.; Foote, C. S. *J. Am. Chem. Soc.* **1998**, *120*, 845-846.
57. Burrows, C. J.; Muller, J. G. *Chem. Rev.* **1998**, *98*, 1109-1151.
58. Hall, D. B.; Holmlin, R. E.; Barton, J. K. *Nature* **1996**, *382*, 731-735.
59. Núñez, M. E.; Hall, D. B.; Barton, J. K. *Chem. Biol.* **1999**, *6*, 85-97.
60. Hall, D. B.; Barton, J. K. *J. Am. Chem. Soc.* **1997**, *119*, 5045-5046.
61. Arkin, M. R.; Stemp, E. D. A.; Pulver, S. C.; Barton, J. K. *Chem. Biol.* **1997**, *4*,
389-400.
62. Hall, D. B.; Kelley, S. O.; Barton, J. K. *Biochemistry* **1998**, *37*, 15933-15940.
63. Nakatani, K.; Dohno, C.; Saito, I. *J. Am. Chem. Soc.* **1999**, *121*, 10854-10855.
64. Giese, B. *Acc. Chem. Res.* **2000**, *33*, 631-636.
65. Matsugo, S.; Kawanishi, S.; Yamamoto, K.; Sugiyama, H.; Matsuura, T.;
Saito, I. *Angew. Chem. Int. Ed.* **1991**, *30*, 1351-1353.

66. Núñez, M. E.; Noyes, K. T.; Gianolio, D. A.; McLaughlin, L. W.; Barton, J. K. *Biochemistry* **2000**, *39*, 6190-6199.
67. Gasper, S. M.; Schuster, G. B. *J. Am. Chem. Soc.* **1997**, *119*, 12762-12771.
68. Henderson, P. T.; Jones, D.; Hampikian, G.; Kan, Y.; Schuster, G. B. *Proc. Natl. Acad. Sci. USA* **1999**, *96*, 8353-8358.
69. Bixon, M.; Jortner, J. *J. Phys. Chem. B* **2000**, *104*, 3906-3913.
70. Berlin, Y. A.; Burin, A. L.; Ratner, M. A. *J. Am. Chem. Soc.* **2001**, *123*, 260-268.
71. Meggers, E.; Michel-Beyerle, M. E.; Giese, B. *J. Am. Chem. Soc.* **1998**, *120*, 12950-12955.
72. Ly, D.; Sanii, L.; Schuster, G. B. *J. Am. Chem. Soc.* **1999**, *121*, 9400-9410.
73. Hartwich, G.; Caruana, D. J.; de Lumley-Woodyear, T.; Wu, Y.; Campbell, C. N.; Heller, A. *J. Am. Chem. Soc.* **1999**, *121*, 10803-10812.
74. Bhattacharya, P. K.; Barton, J. K. *J. Am. Chem. Soc.* **2001**, *123*, 8649-8656.
75. Giese, B.; Wessely, S. *Angew. Chem. Int. Ed.* **2000**, *39*, 3490-3491.
76. Rajski, S. R.; Barton, J. K. *Biochemistry* **2001**, *40*, 5556-5564.
77. Rajski, S. R.; Kumar, S.; Roberts, R. J.; Barton, J. K. *J. Am. Chem. Soc.* **1999**, *121*, 5615-5616.
78. Cheng, X. D.; Kumar, S.; Posfai, J.; Pflugrath, J. W.; Roberts, R. J. *Cell* **1993**, *74*, 299-307.

79. Kim, Y. C.; Geiger, J. H.; Hahn S.; Sigler, P. B. *Nature* **1993**, *365*, 512-520.
80. Kim, J. L.; Nikolov, D. B.; Burley, S. K. *Nature* **1993**, *365*, 520-527.
81. Wagenknecht, H.-A; Rajsiki, S. R.; Pascaly, M.; Stemp, E. D. A.; Barton, J. K. *J. Am. Chem. Soc.* **2001**, *123*, 4400-4407.
82. Pascaly, M.; Yoo, J.; Barton, J. K. *J. Am. Chem. Soc.* **2002**, *124*, 9083-9092.
83. Boon, E. M.; Salas, J. E.; Barton, J. K. *Nature Biotech.* **2002**, *20*, 282-286.
84. Dandliker, P. J.; Holmlin, R. E.; Barton, J. K. *Science* **1997**, *275*, 1465-1468.
85. Sancar, A. *Annu. Rev. Biochem.* **1996**, *65*, 43-81.
86. Jacobsen J. R.; Cochran, A. G.; Stephans, J. C.; King, D. S.; Schultz, P. G. *J. Am. Chem. Soc.* **1995**, *117*, 5453-5461.
87. Young, T.; Nieman, R.; Rose, S. D. *Photochem. Photobiol.* **1990**, *52*, 661-668.
88. Vicic, D. A.; Odom, D. T.; Núñez, M. E.; Gianolio, D. A.; McLaughlin, L. W.; Barton, J. K. *J. Am. Chem. Soc.* **2000**, *122*, 8603-8611.
89. Dotse, A. K.; Boone, E. K.; Schuster, G. B. *J. Am. Chem. Soc.* **2000**, *122*, 6825-6833.
90. Dandliker, P. J.; Núñez, M. E.; Barton, J. K. *Biochemistry* **1998**, *37*, 6491-6502.
91. Luger, K.; Mader A. W.; Richmond, R. K.; Sargent, D. F.; Richmond, T. J. *Nature* **1997**, *389*, 251-260.
92. Núñez, M. E.; Noyes, K. T.; Barton, J. K. *Chem. Biol.* **2002**, *9*, 403-415.

93. Núñez, M. E.; Holmquist, G. P.; Barton, J. K. *Biochemistry* **2001**, *40*, 12465-12471.

CHAPTER 2

Variations in DNA Charge Transport with Nucleotide Composition and Sequence

* Adapted from Williams, T. T., Odom, D. T., and Barton, J. K. *J. Am. Chem. Soc.* **2000**, *122*, 9048-9049.

** Duncan Odom synthesized the complementary strands whereas Tashica Williams synthesized the rhodium conjugates. Both performed the sequence experiments.

INTRODUCTION

Long-range oxidative damage to DNA (DNA CT) has been demonstrated in experiments using a variety of remotely bound oxidants [1-5]. However, the mechanism(s) by which charge is transported through the base-pair stack still needs to be established. Recent theoretical proposals bring together tunneling and hopping mechanisms to describe charge transport over various distance and energetic regimes [6]. Based upon measurements of oxidative damage yield, it has been proposed that charge transport occurs by hopping between guanine sites and tunneling through TA steps [7]. In accord with the notion that low energy guanine “stepping stones” are required for efficient long-range charge transport, oxidative damage over a long distance was not observed when 5'-TATATA-3' intervened between G sites [8]. Phonon-assisted polaron hopping has been suggested as an alternative mechanism by which charge propagates through DNA [9]. In this model, the sequence-dependent conformational dynamics of DNA upon hole injection are expected to aid in charge transport, but no sequence-dependent effects have been documented.

These different proposals have led us to investigate systematically the effect of intervening base composition and sequence on long-range oxidative DNA damage. Here, we vary the intervening sequence between two oxidatively sensitive sites without varying overall base composition. Previous experiments

have shown that oxidative damage can occur up to 200 Å from the site of hole injection; the sequence-dependent effects we observed were attributed to variations in sequence-dependent structure and flexibility [10]. Recent ultrafast spectroscopic studies have shown that base dynamics may gate charge transport [11], and fluorescence studies on DNA assemblies containing bound donors and acceptors have underscored the sensitivity of fluorescence quenching to the stacking of the donor, acceptor, and intervening bases [12].

EXPERIMENTAL

Oligonucleotide Synthesis. Oligonucleotides were synthesized utilizing standard phosphoramidite chemistry on an ABI 392 DNA/RNA synthesizer. DNA was synthesized with a 5'-dimethoxy trityl (DMT) protecting group and purified on a Dynamax 300 Å C₄ reverse phased column (Rainin) (100% 50 mM NH₄OAc, pH 7, to 70% 50 mM NH₄OAc/ 30% Acetonitrile over 35 minutes) on a Hewlett-Packard 1100 HPLC. The isolated strands were treated with 80% acetic acid and HPLC was performed once more. All strands were quantified using UV-visible spectroscopy on a Beckman DU 7400 Spectrophotometer using the following extinction coefficients: ϵ (260 nm M⁻¹ cm⁻¹) adenine = 15,400, guanine = 11,500, cytosine = 7,400, thymine = 8,700. The preparation of oligonucleotides appended with rhodium have been described elsewhere [15] and were purified

on a Dynamax C₄ column by reverse phase HPLC (95% 50 mM NH₄OAc (pH 7)/5% Acetonitrile to 85% 50 mM NH₄OAc/ 15% Acetonitrile over 45 minutes).

DNA strands containing the Δ diastereomer of rhodium was utilized, established by circular dichroism (AVIV CD spectrophotometer).

Assay of Oxidative DNA Damage. The oligonucleotides were labeled at the 5'-end utilizing γ -³²P ATP and T4 polynucleotide kinase. After desalting, the reaction mixture was purified on a 20% denaturing polyacrylamide gel. The desired band was excised from the gel, soaked in 1 mL of 10 mM Tris-Cl and 1 mM EDTA (pH 7.5), dried in vacuo, and isolated by use of Micro Bio-Spin columns. Duplexes were prepared by mixing equimolar amounts of modified and unmodified strands to a final concentration of 4 μ M and annealed in 20 mM Tris-Cl (pH 8) and 10 mM NaCl by heating to 90 °C for 5 min and gradually cooling to ambient temperature over 2 h. For direct strand cleavage experiments, samples (30 μ L) were irradiated at 313 nm for 10 min using a 1000 W Hg/Xe lamp equipped with a monochromator and immediately dried following irradiation. For oxidative damage experiments, parallel samples were irradiated at 365 nm for 1 h, treated with 10% piperidine (v/v), heated for 30 min at 90 °C, and dried in vacuo. Samples were resuspended into formamide loading dye and electrophoresed through a 20% denaturing polyacrylamide gel. The extent of oxidative damage was determined by phosphorimagery (ImageQuant).

RESULTS AND DISCUSSION

Assembly Design

Table 2.1 shows substrates that were designed to examine long-range charge transport through sequences rich in AT base pairs. Each sequence contains two 5'-GG-3' doublets [13], one proximal and one distal to the tethered intercalating photooxidant, $[\text{Rh}(\text{phi})_2\text{bpy}]^{3+}$ (phi = phenanthrenequinone diimine) [15]; the rhodium complex promotes damage to the 5'-G of the guanine doublet by photoinduced electron transfer. Irreversible trapping of the guanine radical by H_2O and O_2 , once generated, is assumed to be independent of the global DNA sequence, since each 5'-CGGC-3' site is identical in its local sequence context; we also normalize distal oxidation to oxidative damage at the proximal site. The ratio in yield of damage at the 5'-G of the 5'-GG-3' site for the distal versus proximal sites provides a measure of relative transport efficiency through the intervening sequence [16]. The damage yield can be determined by treatment of the 5'- ^{32}P labeled oligonucleotide with piperidine, followed by polyacrylamide gel electrophoresis and phosphorimager analysis [1,17,18].

Table 2.1. Long-range oxidative damage in DNA assemblies functionalized with the tethered photooxidant $[\text{Rh}(\text{phi})_2\text{bpy}']^{3+}$.

Sequence ^a	Assembly ^b	Distal/Proximal Oxidation Ratio ^c
 AC ^{Rh} GAGCCGAAAAGCCGTAT-3' 3'-TG CTCGGCTTTTCGGCATA-5'*	TT-2	0.9 ± 0.1
 AC ^{Rh} GAGCCGTTTGCCGTAT-3' 3'-TG CTCGGCAAACGGCATA-5'*	AA-2	2.5 ± 0.2
 AC ^{Rh} GAGCCGTATAGCCGTAT-3' 3'-TG CTCGGCATATCGGCATA-5'*	AT-2	0.6 ± 0.2
 AC ^{Rh} GAGCCGAAAAAGCCGTAT-3' 3'-TG CTCGGCTTTTTTCGGCATA-5'*	TT-3	1.2 ± 0.3
 AC ^{Rh} GAGCCGTTTTTGCCGTAT-3' 3'-TG CTCGGCAAACGGCATA-5'*	AA-3	3.5 ± 0.5
 AC ^{Rh} GAGCCGTATATAGCCGTAT-3' 3'-TG CTCGGCATATATCGGCATA-5'*	AT-3	1.0 ± 0.2
 AC ^{Rh} GAGCCGAAAAAAAAAGCCGTAT-3' 3'-TG CTCGGCTTTTTTTCGGCATA-5'*	TT-4	2.2 ± 0.4
 AC ^{Rh} GAGCCGTTTTTTTGCCGTAT-3' 3'-TG CTCGGCAAACGGCATA-5'*	AA-4	2.3 ± 0.1
 AC ^{Rh} GAGCCGTATATATAGCCGTAT-3' 3'-TG CTCGGCATATATATCGGCATA-5'*	AT-4	1.8 ± 0.2
 AC ^{Rh} GAGCCGAAAAAAAAAGCCGTAT-3' 3'-TG CTCGGCTTTTTTTCGGCATA-5'*	TT-5	0.4 ± 0.3
 AC ^{Rh} GAGCCGTTTTTTTGCCGTAT-3' 3'-TG CTCGGCAAACGGCATA-5'*	AA-5	1.2 ± 0.1
 AC ^{Rh} GAGCCGTATATATATAGCCGTAT-3' 3'-TG CTCGGCATATATATCGGCATA-5'*	AT-5	1.3 ± 0.1
 AC ^{Rh} GAGCCGTATAGCTATAGCCGTAT-3' 3'-TG CTCGGCATATCGATATCGGCATA-5'*	TAGC	0.6 ± 0.1

^a Only the Δ diastereomer was used in these studies. * denotes the site of ^{32}P labeling.

^b Abbreviations are based on the identity and repetition of the two base-pair units spanning the distal and proximal guanine doublets on the strand complementary to the metallointercalator bearing strand.

^c Intensity ratios of the oxidative DNA damage at the 5'-G of the guanine doublets proximal and distal to the rhodium complex were measured after photooxidation. Values represent averages of three trials.

Long-Range Guanine Oxidation: Sequence Composition and Bridge Length

Figure 2.1 shows the phosphorimagery after photooxidation of AA-2, TT-2, and AT-2. For these assemblies, the base-pair composition between proximal and distal guanine doublets is constant, although the sequence of bases varies (Table 2.1). If the mechanism of charge transport were strictly a function of hopping between guanine sites [6,7], one would expect the distal/proximal ratio of oxidative damage for these assemblies to be equal. In fact, based upon data obtained by others for charge transport across 5'-ATAT-3' [7], little distal oxidation might be expected for all assemblies [20]. As is evident in Figure 2.1 and quantitated in Table 2.1, this is not the case. Instead, we find significant distal oxidation, and in particular, the ratio to be consistently higher for the AA assemblies and lower for the TT and AT assemblies. Based upon energetic considerations [21] as well as poor stacking overlap, the TT sequences might be expected to be the poorest conduits for charge transport [22]. Similar considerations dictate that adenine tracts should yield efficacious charge transport, and duplexes containing AT tracts might be expected to show damage in the intermediate range. Additionally, temperature investigations were also performed to delineate whether the difference in oxidative damage yields were due to denaturation of the highly repetitive tracts.

Figure 2.1. Phosphorimager of a denaturing 20% polyacrylamide gel showing the sequence dependence of long-range oxidative damage in assemblies containing tethered Δ -[Rh(phi)₂bpy']³⁺. Shown are the results from sequences containing 4 base pairs intervening between distal and proximal guanine doublets, AA-2, TT-2, and AT-2. Sequence designations are as in Table 2.1, where the strand containing guanine doublets is 5'-³²P end-labeled. For each assembly, lanes are as follows: A+G, C+T, and C show Maxam-Gilbert sequencing reactions [35]; 313 shows the fragment after direct photocleavage by the photoexcited metallointercalator at 313 nm for 10 min without piperidine treatment; 365 nm shows the fragment after irradiation at 365 nm for 1 h at 23 °C, followed by piperidine treatment; DC (dark control) shows samples not irradiated but treated with piperidine. All samples contained 4 μM metal complex-tethered duplex, 20 mM Tris-HCl, pH 8, and 10 mM NaCl. Sites of proximal and distal 5'-GG-3' damage are indicated.

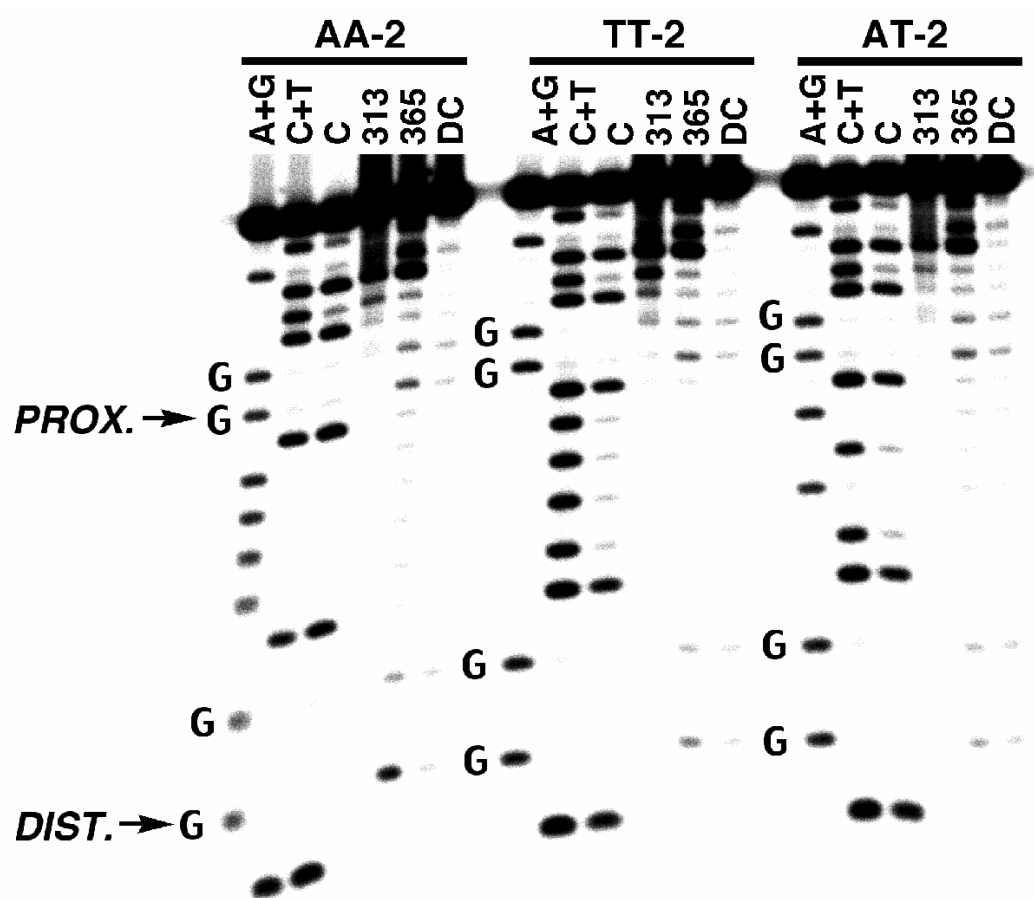
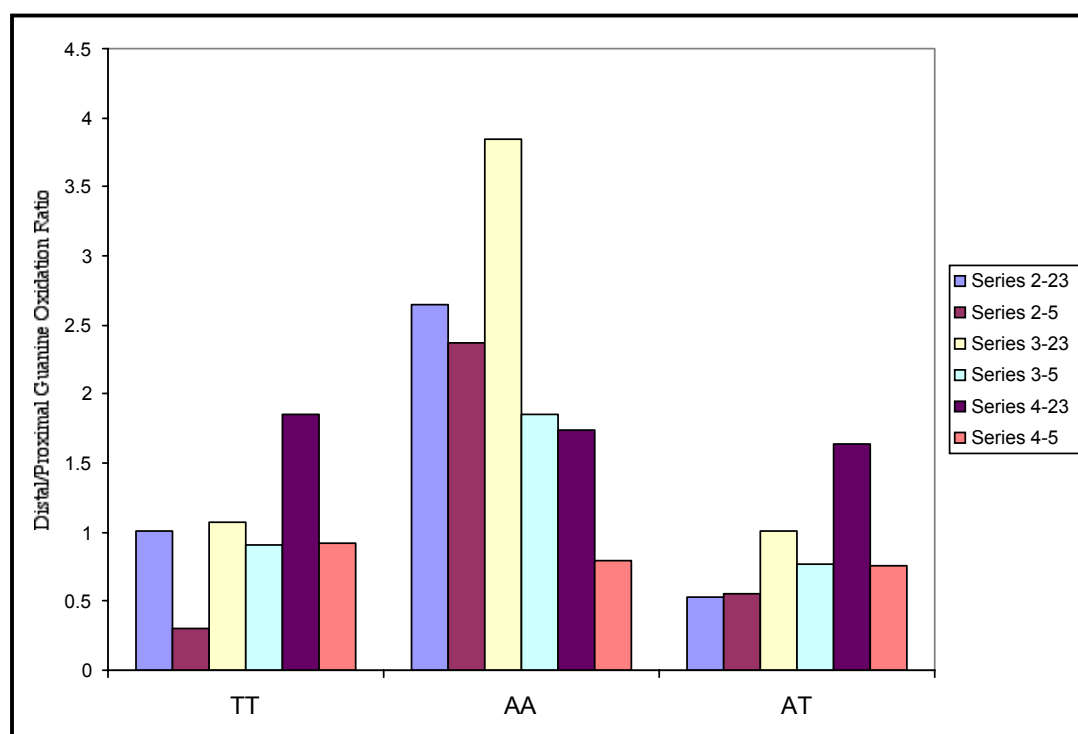


Figure 2.2. Temperature dependence of sequence composition. Note that comparable trend in the yield of oxidative damage for the respective assemblies at 23 °C and 5 °C.



As shown in Figure 2.2, this certainly is not the case and, in fact, reiterates that the efficiency of the charge transport is attenuated by characteristics of the A-tract assemblies. Additionally, the lower oxidative guanine yield at 5 °C is expected because of decreased DNA dynamics at this temperature and the increased probability of destacking, which is known to attenuate DNA CT.

Table 2.1 and Figures 2.3 through 2.5 also show the effect of increasing the length of the intervening segment. Based upon a guanine hopping model [6,7], increasing the number of adenines or thymines between the guanine doublets should result in marked decreases in long-range guanine oxidation; indeed, if the sole mechanism for charge transport through TA sequences were tunneling, as proposed [7], one would expect negligible oxidative damage at the distal site. However, as is evident in Figure 2.5, it is the *sequence* of bases that is critical. Increasing the length of the AA sequence only slightly decreases the guanine oxidation ratio, consistent with the shallow distance dependence expected for hole hopping through *all* the bases. Remarkably, in the case of the TT and AT assemblies, there appears to be an *increase* in oxidation ratios with increasing oligonucleotide length from 4 to 8 intervening base pairs (Figure 2.5) [24]. Furthermore, in contrast to that predicted by a guanine-hopping model, insertion of a GC step into the otherwise A•T bridge actually *decreases* the efficiency of charge transport (Table 2.1, TAGC).

Figure 2.3. Phosphorimager of a denaturing 20% polyacrylamide gel showing the sequence dependence of long-range oxidative damage in assemblies containing tethered Δ -[Rh(phi)₂bpy']³⁺. Shown are the results from sequences containing 6 base pairs intervening between distal and proximal guanine doublets, TT-3, AA-3, and AT-3. Sequence designations are as in Table 2.1, where the strand containing guanine doublets is 5'-³²P end-labeled. For each assembly, lanes are as follows: A+G and C+T show Maxam-Gilbert sequencing reactions [35]; 313 shows the fragment after direct photocleavage by the photoexcited metallointercalator at 313 nm for 10 min without piperidine treatment; 365 nm shows the fragment after irradiation at 365 nm for 1 h at 23 °C, followed by piperidine treatment; DC (dark control) shows samples not irradiated but treated with piperidine. All samples contained 4 μM metal complex-tethered duplex, 20 mM Tris-HCl, pH 8, and 10 mM NaCl. Sites of proximal and distal 5'-GG-3' damage are indicated.

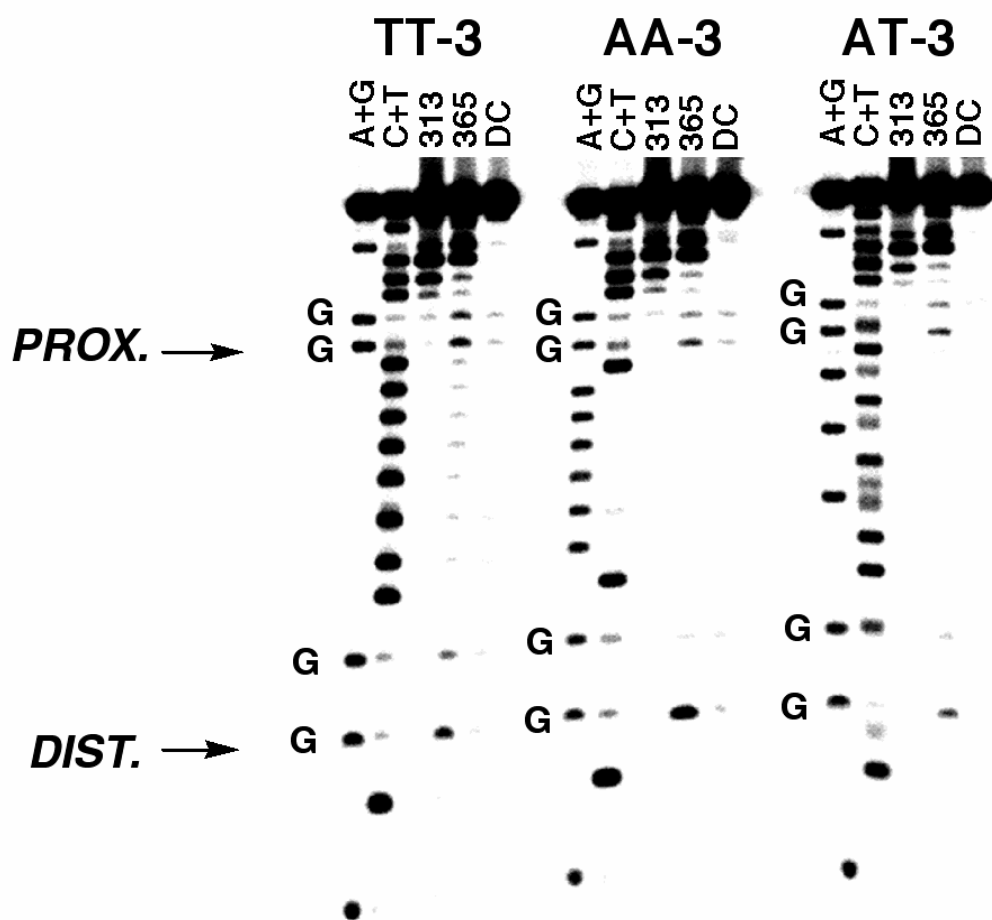


Figure 2.4. Phosphorimager of a denaturing 20% polyacrylamide gel showing the sequence dependence of long-range oxidative damage in assemblies containing tethered Δ -[Rh(phi)₂bpy']³⁺. Shown are the results from sequences containing 8 base pairs intervening between distal and proximal guanine doublets, TT-4, AA-4, and AT-4. Sequence designations are as in Table 2.1, where the strand containing guanine doublets is 5'-³²P end-labeled. For each assembly, lanes are as follows: A+G and C+T show Maxam-Gilbert sequencing reactions [35]; 313 shows the fragment after direct photocleavage by the photoexcited metallointercalator at 313 nm for 10 min without piperidine treatment; 365 nm shows the fragment after irradiation at 365 nm for 1 h at 23 °C, followed by piperidine treatment; DC (dark control) shows samples not irradiated but treated with piperidine. All samples contained 4 μM metal complex-tethered duplex, 20 mM Tris-HCl, pH 8, and 10 mM NaCl. Sites of proximal and distal 5'-GG-3' damage are indicated.

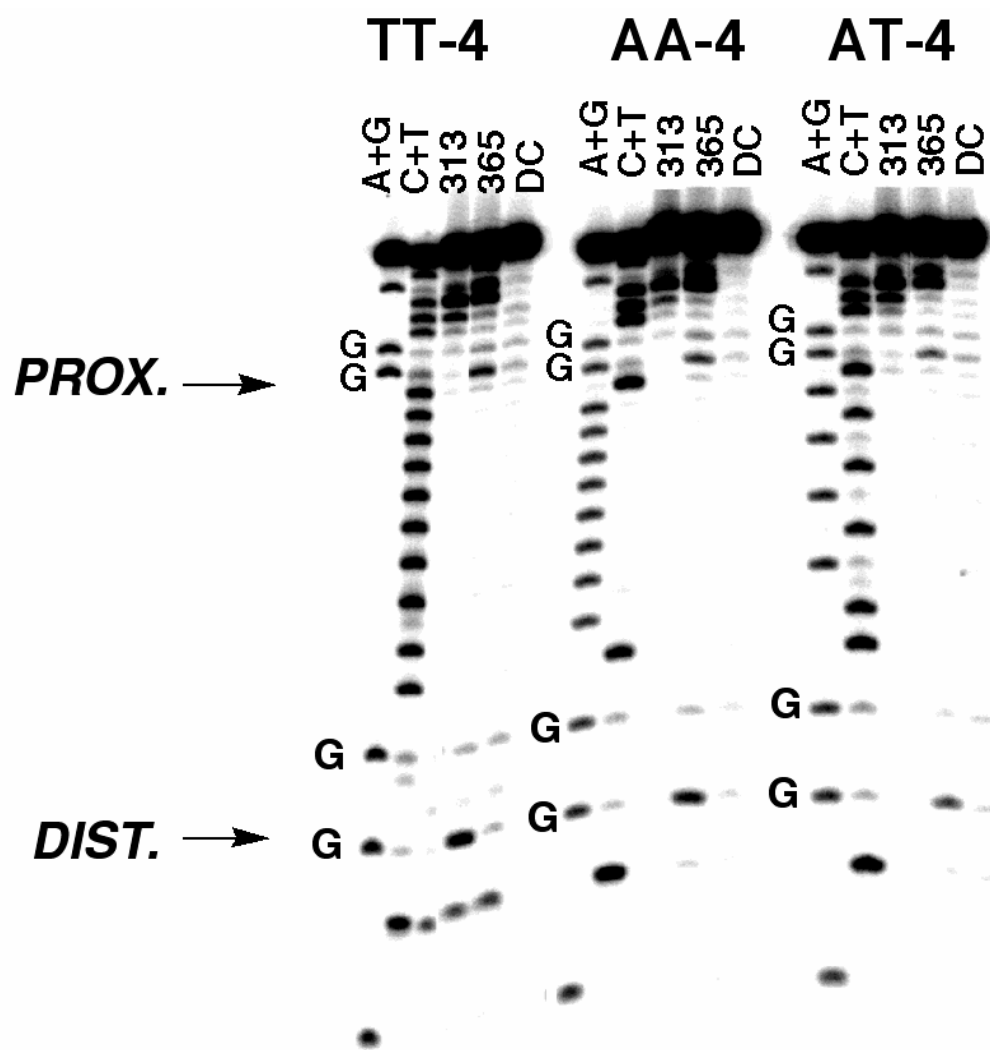
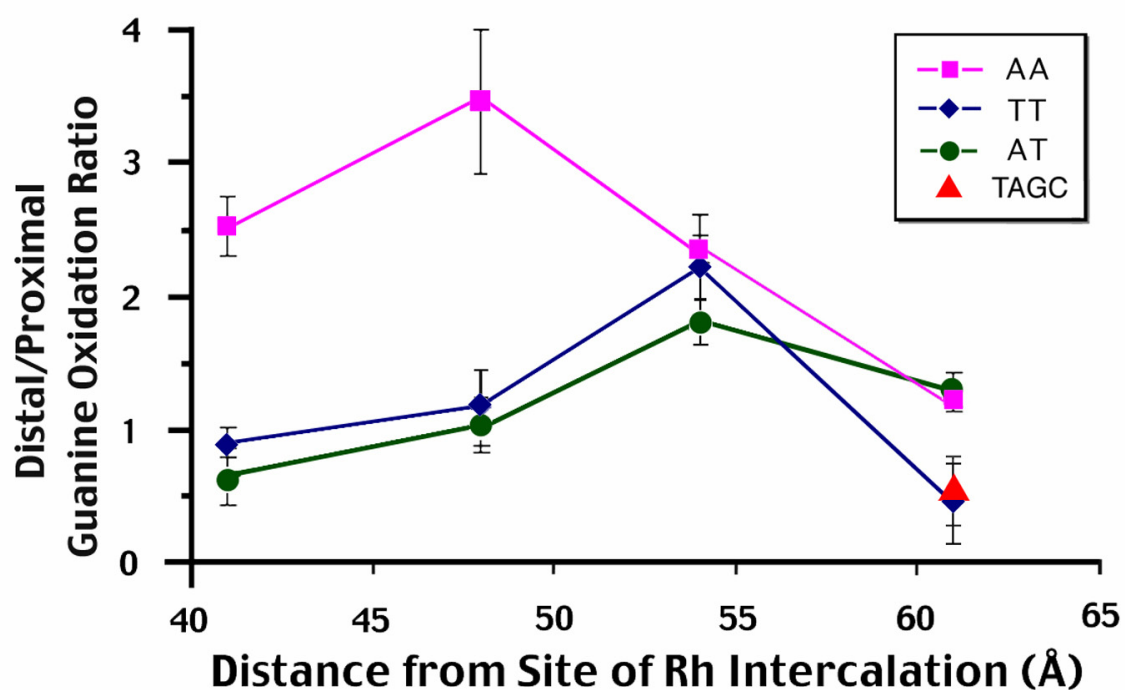


Figure 2.5. A plot of the 5'-G distal/proximal guanine oxidation ratio versus the distance from the intercalation site, based upon data given for the assemblies in Table 2.1. Distances are estimated from the primary intercalation site, established by direct photocleavage at 313 nm, and assuming 3.4 Å stacking.



This result provides clear evidence that strict guanine hopping cannot describe long-range DNA-mediated charge transport in this system [25]. Alternative mechanisms which involve hopping also among other bases are required [28].

DNA-Mediated Charge Transport: Domain Hopping

We propose that the variations observed with sequence and length must depend also upon the conformational dynamics associated with these sequences. In contrast to hole hopping models developed primarily for aromatic crystals [29], here electronic coupling between bases is dynamic and sequence-dependent. For the AA oligonucleotides, the efficiency of charge transport may depend upon the extensive overlap of the stacked purines [30]. Moreover, A-tracts are well known to adopt conformations that differ from that of canonical B-form DNA [31]. The increase in damage ratios with increasing length for TT sequences is consistent with the cooperative formation of conformational domains in longer A-tract DNA structures; generation of structures that introduce bends into DNA seems to require a nucleating core of five adenines before the A-tract stabilizes into a bend [32]. In our system, convergence of the oxidation ratios occurs in the duplexes containing six or more A•T base pairs between the guanine doublets. Critically, however, the result we obtain with 5'-TATA-3', which may contrast previous reports [7], can now be viewed in a

systematic context [33]. Furthermore, a report utilizing an anthraquinone derivative also did not find a steep oxidative dependence upon increasing A/T bridge length [36]. As with the A-tracts, the increase in transport efficiency with lengthening of this segment may also reflect some conformational transition associated with the longer, ordered sequence, but no precedence for such a finding is available. Rather than considering hopping from guanine to guanine within a DNA segment, then, we might consider hopping between domains.

Giese and coworkers have since deviated from the strict guanine hopping model [37]. A subsequent study did substantiate their previous report in which a steep oxidative dependence was observed when the bridge consisted of one to three A/T steps [7]; however, upon increasing the number of A/T steps from four to sixteen, long-range guanine oxidation was *also* observed. To elucidate this apparent disparity from their previous investigations, they propose that a mechanistic shift occurs from that of coherent tunneling to thermally-induced hopping, which will have a weak distance dependence. Thus, they have modified their original hypothesis to include adenine hopping.

To experimentally explore the possibility of charge injection into adenines, Saito and coworkers utilized an end-capped anthraquinone moiety as the oxidant and a modified adenine that contained a cyclopropyl group (^{CP}A) [38], which had been found in previous studies with guanine (Chapter 4) to be a

kinetically faster trap. The studies revealed rapid consumption of the $^{\text{CP}}\text{A}$ through a bridge containing six A/T steps. Additionally, their report revealed that using a cyanobenzophenone-substituted uridine as the oxidant resulted in a markedly slower rate of $^{\text{CP}}\text{A}$ consumption. Hence, the weak distance dependence across A/T bridges also appears to depend on the identity of the oxidant and hence the ability to chemically form transient adenine species (Chapter 4).

Takada and coworkers also experimentally probed adenine hopping in their spectroscopic investigation of charge recombination using DNA hairpins in which naphthaldiimide (NDI) served as the electron acceptor and phenothiazine as the electron donor, separated by a series of adenine bridges (4-8) [39]. They found that the formation of $\text{NDI}^{\bullet-}$ was extremely rapid across the A-tract and that the quantum yield of charge transport only slightly decreased with increasing the number of adenine steps. However, the charge recombination rate was strongly dependent on distance across this series of adenine bridges, an issue discussed in Chapter 4.

Although Giese, Saito, and others provide evidence for a transient species formed during charge transport, they do not detail a mechanism for the process. Furthermore, the idea of *any* single nucleotide hopping model is hard to realize for it fails to elucidate the ability of the fluorescent base analog, 2-aminopurine

(Ap), to sense different hole acceptors upon charge injection [41] in addition to the fast, unchanged rate of indole radical formation, which was located 17 Å to 37 Å away from the intercalation site, found for charge transport over a series of adenine bridges [40]. Our mechanistic proposal of “domain hopping” has been substantiated by additional studies that have been performed utilizing aminopurine. These studies investigated the temperature dependence of the yield of DNA-mediated charge transport through A_n -bridges, where $n=1-9$ [41]. In all cases, a temperature regime was observed where quenching of the aminopurine excited state by guanine in duplex DNA increased with increasing temperature, indicating that enhanced base dynamics can enhance the yield of DNA-mediated CT. Modeling of the distance dependence of CT resulted in a sinusoidal periodicity that suggested the formation of charge transport domains that delocalized the charge over four to five base pairs.

Hence, our studies here and the aminopurine investigation(s) underscore the need to consider the impact on DNA charge transport of sequence-dependent conformational domains and their dynamics and to repudiate the simplistic, *single* nucleotide hopping model previously proposed.

REFERENCES

1. Hall, D. B.; Holmlin, R. E.; Barton, J. K. *Nature* **1996**, *382*, 731-735.
2. Gasper, S. M.; Schuster, G. B. *J. Am. Chem. Soc.* **1997**, *119*, 12762-12771.
3. a) Hall, D. B.; Kelley, S. O.; Barton, J. K. *Biochemistry* **1998**, *37*, 15933-15940. b) Arkin, M. R.; Stemp E. D. A.; Barton, J. K. *Chem. Biol.* **1997**, *4*, 389-400.
4. Meggers, E.; Kusch, D.; Spichy, M.; Wille, U.; Giese, B. *Angew. Chem. Int. Engl. Ed.* **1998**, *37*, 460-462.
5. Saito, I; Nakamura, T.; Nakatani, K.; Yoshioka, Y.; Yamaguchi, K.; Sugiyama, H. *J. Am. Chem. Soc.* **1998**, *120*, 12686-12687.
6. a) Bixon, M.; Jortner, J. *J. Phys. Chem. B* **2000**, *104*, 3906-3913. b) Bixon, M.; Giese, B.; Wessely, S.; Langenbacher, T.; Michel-Beyerle, M. E.; Jortner, J. *Proc. Natl. Acad. Sci. USA* **1999**, *96*, 11713-11716. c) Berlin, Y. A.; Burin, A. L.; Ratner, M. A. *J. Phys. Chem. A* **2000**, *104*, 443-445. d) see also Felts, A. K.; Pollard, W. T.; Friesner, R. A. *J. Phys. Chem.* **1995**, *99*, 2929-2940.
7. a) Meggers, E.; Michel-Beyerle, M. E.; Giese, B. *J. Am Chem. Soc.* **1998**, *120*, 12950-12955. b) Giese, B.; Wessely, S.; Spormann, M.; Lindemann, U.; Meggers, E.; Michel-Beyerle, M. E. *Angew Chem. Int. Ed. Engl.* **1999**, *38*, 996-998.

8. Nakatani, K.; Dohno, C.; Saito, I. *J. Am. Chem. Soc.* **1999**, *121*, 10854-10855.
9. a) Henderson, P. T.; Jones, D.; Hampikian, G.; Kan, Y.; Schuster, G. B. *Proc. Natl. Acad. Sci. USA* **1999**, *96*, 8353-8358. b) Ly, D.; Sani, L.; Schuster, G. B. *J. Am. Chem. Soc.* **1999**, *121*, 9400-9410. c) Conwell, E. M.; Rakhmanova, S. V. *Proc. Natl. Acad. Sci. USA* **2000**, *97*, 4556-4560.
10. Núñez, M. E.; Hall, D. B.; Barton, J. K. *Chem. Biol.* **1998**, *6*, 85-97.
11. Wan, C.; Fiebig, T.; Kelley, S. O.; Treadway, C. R.; Barton, J. K.; Zewail, A. H. *Proc. Natl. Acad. Sci. USA* **1999**, *96*, 6014-6019.
12. a) Kelley, S. O.; Barton, J. K. *Science* **1999**, *283*, 375-381. b) Kelley, S. O.; Holmlin, R. E.; Stemp, E. D. A.; Barton, J. K. *J. Am. Chem. Soc.* **1997**, *119*, 9861-9870. c) Kelley, S. O.; Barton, J. K. *Chem. Biol.* **1998**, *5*, 413-425.
13. Both empirical and theoretical studies have shown that the 5'-G of 5'-GG-3' sites are preferentially oxidized [1,14].
14. Sugiyama, H.; Saito, I. *J. Am. Chem. Soc.* **1996**, *118*, 7063-7068.
15. Holmlin, R. E.; Dandliker, P. J.; Barton, J. K. *Bioconjugate Chem.* **1999**, *10*, 1122-1130.
16. a) Hall, D. B.; Barton, J. K. *J. Am. Chem. Soc.* **1997**, *119*, 5045-5046. b) Rajski, S. R.; Kumar, S.; Roberts, R. J.; Barton, J. K. *J. Am. Chem. Soc.* **1999**, *121*, 5615-5616.

17. a) Chung, M.-H.; Kiyosawa, H.; Ohtsuka, E.; Nishimura, S.; Kasai, H. *Biochem. Biophys. Res. Commun.* **1992**, *188*, 1-7. b) Cullis, P. M.; Malone, M. E.; Merson-Davies, L. A. *J. Am. Chem. Soc.* **1996**, *118*, 2775-2781.
18. These piperidine labile lesions correlate linearly with oxidative damage as revealed by enzymatic treatment [19].
19. Rajski, S. personal communication.
20. Sequence contexts, oxidants, and reaction conditions may affect the comparison. However, in those studies, no systematic variation in sequence was made [7,8].
21. a) Steenken, S.; Jovanovic, S. V. *J. Am. Chem. Soc.* **1997**, *119*, 617-618. b) Seidel, C. A. M.; Schultz, A.; Sauer, M. H. M. *J. Phys. Chem.* **1996**, *100*, 5541-5553.
22. We assay charge transport to the strand containing the 5'-GG-3' doublet. However, phi complexes of rhodium intercalate over both strands [23], and thus, some hole injection may occur into both strands; interstrand charge transfer is also possible [12a].
23. Kielkopf, C. L.; Erkkila, K. E.; Hudson, B. P.; Barton, J. K.; Rees, D. C. *Nat. Struct. Biol.* **2000**, *7*, 117-121.
24. Some interstrand electron transfer may be responsible in part for the convergence of results seen with the longer oligonucleotides.

25. The rhodium excited state appears to be sufficiently potent to oxidize all of the bases [26]. Nonetheless, hole hopping must be fast relative to thermal relaxation at a site to account for oxidative damage at a distal guanine [27].
26. Turro, C.; Evenzahav, A.; Bossman, S. H.; Barton, J. K.; Turro, N. J. *Inorg. Chim. Acta* **1996**, *243*, 101-108.
27. Dee, D.; Baur, M. E. *J. Chem. Phys.* **1974**, *60*, 541-560.
28. Our data provides neither support nor refutation of the phonon-assisted polaron hopping model.
29. a) Le Blanc, O. H. *J. Chem. Phys.* **1961**, *35*, 1275-1279. b) Katz, J. L.; Rice, S. A.; Choi, S. I.; Jortner, J. *J. Chem. Phys.* **1963**, *39*, 1683-1688.
30. Saenger, W. *Principles of Nucleic Acid Structure*, Springer-Verlag, New York, **1984**.
31. a) Crothers, D. M.; Drak, J.; Kahn, J. D.; Levene, S. D. *Meth. Enzym.* **1992**, *212*, 3-29. b) Koo, H. S.; Drak, J.; Rice, J. A.; Crothers, D. M. *Biochemistry* **1990**, *29*, 4227-4234.
32. a) Crothers, D. M. personal communication. b) Price, M. A.; Tullius, T. D. *Biochemistry* **1993**, *32*, 127-136. c) Nadeau, J. G.; Crothers, D. M. *Proc. Natl. Acad. Sci. USA* **1989**, *86*, 2622-2626.

33. The low charge transport efficiency for AT-2 seen here, on a relative basis, may actually be consistent with earlier reports [7,8]. However, the explanation may rest not on tunneling through AT segments but instead upon the increased flexibility and poor overlap associated with the 5'-TATA-3' sequence [34].
34. Dickerson, R. E. *Structure, Motion, Interaction, and Expression of Biological Macromolecules.*, pp. 17-36, **1998** b) Dickerson, R. E. *Nucleic Acids Res.* **1998**, *26*, 1906-1926. c) Kim, J. L.; Nikolov, D. B.; Burley, S. K. *Nature* **1993**, *365*, 520-527. d) Kim, Y. C.; Geiger, J. H.; Hahn S.; Sigler, P. B. *Nature* **1993**, *365*, 512-520.
35. Maxam A. M.; Gilbert, W. *Mol. Biol.* **1986**, *20*, 461-509.
36. Sartor, V.; Boone, E.; Schuster, G. B. *J. Phys. Chem. B* **2001**, *105*, 11057-11059.
37. Giese, B.; Amaudrut, J.; Köhler, A.-K.; Spormann, M.; Wessely, S. *Nature* **2001**, *412*, 318-320.
38. Dohno, C.; Ogawa, A.; Nakatani, K.; Saito, I. *J. Am. Chem. Soc.* **2003**, *125*, 10154-10155.
39. Takada, T.; Kawai, K.; Cai, X.; Sugimoto, A.; Fujitsuka, M.; Majima, T. *J. Am. Chem. Soc.* **2004**, *126*, 1125-1129.
40. Pascaly, M.; Yoo, J.; Barton, J. K. *J. Am. Chem. Soc.* **2002**, *124*, 9083-9092.

41. O'Neill, M. A.; Barton, J. K. submitted.

CHAPTER 3

The Effect of Varied Ion Distributions on Long-Range Charge Transport in DNA

* Adapted from Williams, T. T. and Barton, J. K. *J. Amer. Chem. Soc.* **2002**, *124*, 1840-1841.

INTRODUCTION

Oxidative damage to DNA from a distance has been demonstrated in a variety of systems using a range of photooxidants [1-4]. These studies have been useful not only in delineating new routes to biochemical damage but also in exploring mechanisms for DNA charge transport (CT). Our laboratory has employed metallointercalators to demonstrate oxidative damage over a distance of 200 Å [5], to explore the effects on CT of intervening DNA sequence [6], of DNA structure [7,8] and of protein-binding to DNA [9], and to examine DNA CT within the cell nucleus [10]. Typically, DNA assemblies are constructed containing the tethered metallointercalator $[\text{Rh}(\text{phi})_2\text{bpy}]^{3+}$ as the photooxidant, which is spatially separated from two 5'-GG-3' sites. The extent of charge transport is assessed through measurements of the ratio of yields of damage at the guanine doublet distal versus that proximal to the metal binding site. Theoretical [11] and experimental studies [1-4] have shown that the 5'-G of 5'-GG-3' sequences in DNA are preferentially oxidized, and this 5'-G reactivity has become a hallmark for electron transfer damage to DNA. Oxidative damage in these studies is quantitated by measuring strand breaks after piperidine treatment of 5'-³²P end-labeled DNA and gel electrophoresis [12].

Since CT through well-stacked DNA duplexes appears to be much faster than trapping of the resultant guanine radical by O₂ and H₂O [13], one might

expect that the ratio of the damage at the distal versus proximal guanine doublets would be ≤ 1 , assuming that the thermodynamic potentials and the trapping rates at the two sites are equal. Yet, in many of our experiments using Rh^{3+} and Ru^{3+} intercalators, we have observed distal/proximal damage ratios significantly higher than one [14]. Ratios closer to one were observed using organic photooxidants [2,4,17,18]. One explanation that we considered was that the cationic charge on the metallointercalator bound near the duplex terminus might be sufficient to increase the oxidation potential of the proximal GG doublet in comparison to the distal site [19]. Thus, we decided to study this possibility utilizing $[\text{Rh}(\text{phi})_2\text{bpy}]^{3+}$ as the photooxidant and modifying the end-label of various DNA assemblies.

EXPERIMENTAL

Oligonucleotide Synthesis. Oligonucleotides were synthesized utilizing standard phosphoramidite chemistry on an ABI 392 DNA/RNA synthesizer. DNA was synthesized with a 5'-dimethoxy trityl (DMT) protecting group and purified on a Dynamax 300 Å C_4 reverse phased column (Rainin) (100% 50 mM NH_4OAc , pH 7, to 70% 50 mM NH_4OAc /30% Acetonitrile over 35 minutes) on a Hewlett-Packard 1100 HPLC. The isolated strands were treated with 80% acetic acid and HPLC was performed once more. All strands were quantified using

UV-visible spectroscopy on a Beckman DU 7400 Spectrophotometer using the following extinction coefficients: ϵ (260 nm $M^{-1} cm^{-1}$) adenine = 15,400, guanine = 11,500, cytosine = 7,400, thymine = 8,700. The preparation of oligonucleotides appended with rhodium have been described elsewhere [32] and were purified on a Dynamax C₄ column by reverse phase HPLC (95% 50 mM NH₄OAc (pH 7)/5% Acetonitrile to 85% 50 mM NH₄OAc/15% Acetonitrile over 45 minutes). The Δ isomer of rhodium was utilized, established by circular dichroism (AVIV CD spectrophotometer).

Assay of Oxidative DNA Damage. The oligonucleotides were labeled at the 5'-end utilizing γ -³²P ATP and T4 polynucleotide kinase; they were labeled at the 3'-end utilizing α -³²P ATP and terminal transferase. After desalting, the reaction mixture was purified on a 20% denaturing polyacrylamide gel. The desired band was excised from the gel, soaked in 1 mL of 10 mM Tris-Cl and 1 mM EDTA (pH 7.5), dried in vacuo, and isolated by use of Micro Bio-Spin columns. Duplexes were prepared by mixing equimolar amounts of modified and unmodified strands to a final concentration of 4 μ M and annealed in 20 mM Tris-Cl (pH 8) and 10 mM NaCl by heating to 90 °C for 5 min and gradually cooling to ambient temperature over 2 h. For direct strand cleavage experiments, samples (20 μ L) were irradiated at 313 nm for 10 min using a 1000 W Hg/Xe lamp equipped with a monochromator and immediately dried following irradiation.

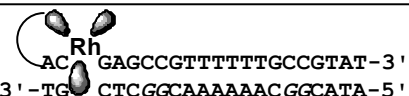
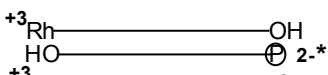
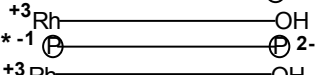
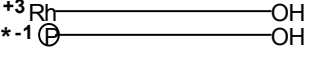
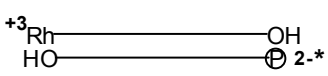
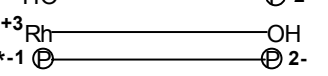
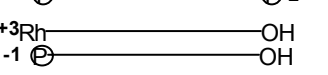
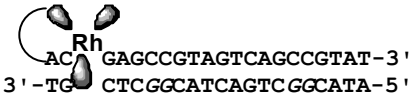
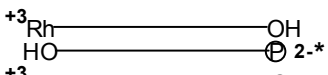
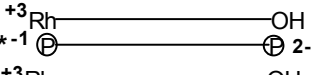
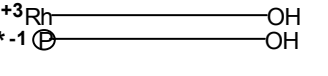
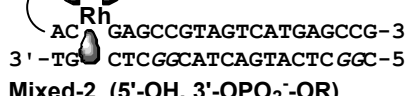
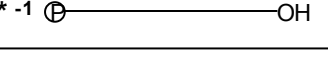
For oxidative damage experiments (20 μ L), parallel samples were irradiated at 365 nm for 20 minutes, treated with 10% piperidine (v/v), heated for 30 min at 90 $^{\circ}$ C, and dried in vacuo. Samples were resuspended into formamide loading dye and electrophoresed through a 20% denaturing polyacrylamide gel. The extent of oxidative damage was determined by phosphorimagery (ImageQuant).

RESULTS AND DISCUSSION

Assembly Design

To examine how the charge distribution on the DNA helix affects charge transport, we simply compared distal/proximal damage ratios after photooxidation of otherwise identical Rh-tethered assemblies, except for 32 P-labeling either at the 5'- or 3'-end (Figure 3.1). Since the unlabeled end of the oligonucleotide is a hydroxyl moiety, while the labeled end is a phosphate, this labeling difference corresponds, in the absence of charge neutralization by condensed counterions, to an increase in one negative charge on the proximal side of the oligomer and a decrease in two negative charges on the distal side of the oligomer.

Table 3.1. The long-range oxidative damage obtained in the presence of various charge distributions utilizing the tethered photooxidant [Rh(phi)₂bpy'³⁺].

Sequence ^a	Charge Distribution ^{b,c}	Distal/Proximal Guanine ^d Oxidation Ratio
 AA (5'-OPO ₃ ²⁻ , 3'-OH)		5.2 (±0.4)
AA (5'-OPO ₃ ²⁻ , 3'-OPO ₂ ⁻ -OR)		0.8 (±0.1)
AA (5'-OH, 3'-OPO ₂ ⁻ -OR)		0.4 (±0.1)
 AA* (5'-OPO ₃ ²⁻ , 3'-OH)		3.6 (±0.2)
AA* (5'-OPO ₃ ²⁻ , 3'-OPO ₂ ⁻ -OR)		0.9 (±0.3)
AA* (5'-OH, 3'-OPO ₂ ⁻ -OR)		0.8 (±0.5)
 Mixed (5'-OPO ₃ ²⁻ , 3'-OH)		1.1 (±0.3)
Mixed (5'-OPO ₃ ²⁻ , 3'-OPO ₂ ⁻ -OR)		0.5 (±0.02) ^e
Mixed (5'-OH, 3'-OPO ₂ ⁻ -OR)		0.6 (±0.2)
 Mixed-2 (5'-OH, 3'-OPO ₂ ⁻ -OR)		0.1 (±0.04)

^a The Δ diastereomer of the [Rh(phi)₂bpy'³⁺] (phi = 9,10 phenanthrenequinone diimine; bpy' = 4'-methylbipyridine-4-butyric acid) was utilized in these studies.

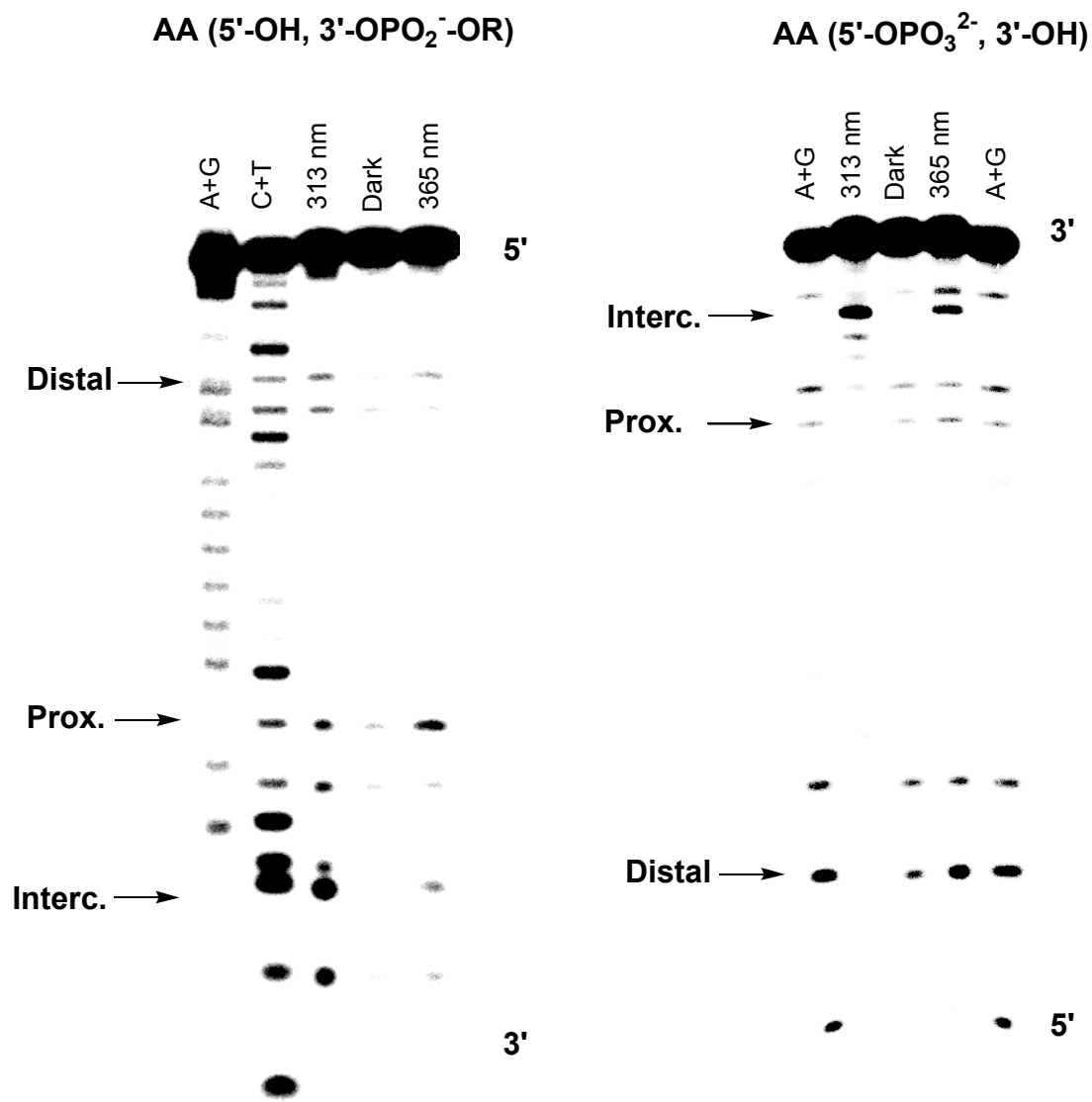
^b A pictorial representation of the charge distribution around the oligomers. * denotes the ³²P-end labeling

^c The 5'-labeling procedures were performed using γ -³²P ATP and T4 PNK (polynucleotide kinase) and the 3'-labeling procedures were performed using α -³²P ATP and terminal transferase.

^d Ratio of the oxidative DNA damage observed at the 5'-G of guanine doublets that were located proximal and distal to the rhodium complex upon photooxidation. The ratios represent an average of two to four trials.

^e The mixed sequence studies did not always represent single hit conditions, given the lower levels of damage but the correction would be < 10%.

Figure 3.1. Phosphorimager of a denaturing 20% polyacrylamide gel that delineates the effect of different labeling on long-range charge transport for assemblies AA (5'-OH, 3'-OPO₂-OR) and AA (5'-OPO₃²⁻, 3'-OH), using tethered Δ -[Rh(phi)₂bpy']³⁺. The sequence designations are shown in Table 3.1, where the strand containing the guanine doublets are either 5' or 3' ³²P end-labeled. For each assembly, the lanes are as follows: A+G, C+T show Maxam-Gilbert sequencing reactions; 313 nm shows the DNA fragment after direct photocleavage by the photoexcited metallointercalator at 313 nm for 10 min without piperidine treatment; 365 nm shows the DNA fragment after irradiation at 365 nm for 20 min at ambient temperature followed by 10% piperidine treatment for thirty minutes at 90 °C; Dark shows samples not irradiated but treated with piperidine. All samples contained 4 μ M metal complex-tethered duplex, 20 mM Tris-Cl, pH 8, 10 mM NaCl. Sites of distal and proximal 5'-GG-3' damage as well as the intercalation site are indicated.



Ionic Distribution and Charge Transport

Table 3.1 summarizes the results of end-labeling on the charge transport process. The highest distal/proximal damage ratio we observed was 5.2 with the 5'-³²P end-labeled assembly containing an intervening A₆ tract (AA (5'-OPO₃²⁻, 3'-OH)). 3'-end-labeling resulted in a ratio of 0.4 (AA (5'-OH, 3'-OPO₂⁻-OR)). Thus, moving the negative charges to the proximal end of the duplex dramatically decreased hole transport to the distal end.

Assemblies containing intermediate charge distributions were also examined. In assembly AA (5'-OPO₃²⁻, 3'-OPO₂⁻-OR), we added an unlabeled phosphate to the 5'- end but maintained the 3'-³²P end-label (Figure 3.2). In this case, where some negative charge was now returned to the distal side of the oligomer, the ratio increased to the intermediate value of 0.8. We also introduced a single base overhang, effectively adding one negative charge to the 3'-end of the Rh-tethered strand. With 3'- ³²P end-labeling of the complementary strand, and no phosphate on the 5'-end, the damage ratio was also 0.8 (AA* (5'-OH, 3'-OPO₂⁻-OR) Figure 3.3); an added phosphate on the distal side of the oligomer, through 5'-labeling, increased the ratio to 3.6 (AA* (5'-OPO₃²⁻, 3'-OH)) (Figure 3.3).

Figure 3.2. Phosphorimagery of a denaturing 20% polyacrylamide gel that delineates the effect of different labeling on long-range charge transport for AA (5'-OPO₃²⁻, 3'-OPO₂-OR) assembly using tethered Δ -[Rh(phi)₂bpy']³⁺. The sequence designation is shown in Table 3.1, where the strand containing the guanine doublets is 3' ³²P end-labeled and a non-radioactive ³²P group has been added to the 5' end. For each assembly, the lanes are as follows: A+G, C+T show Maxam-Gilbert sequencing reactions; 313 nm shows the DNA fragment after direct photocleavage by the photoexcited metallointercalator at 313 nm for 10 min without piperidine treatment; 365 nm shows the DNA fragment after irradiation at 365 nm for 20 min at ambient temperature followed by 10% piperidine treatment for thirty minutes at 90 °C; Dark shows sample not irradiated but treated with piperidine. All samples contained 4 μ M metal complex-tethered duplex, 20 mM Tris-Cl, pH 8, 10 mM NaCl. Sites of distal and proximal 5'-GG-3' damage are indicated.

AA (5'-OPO₃²⁻, 3'-OPO₂⁻-OR)

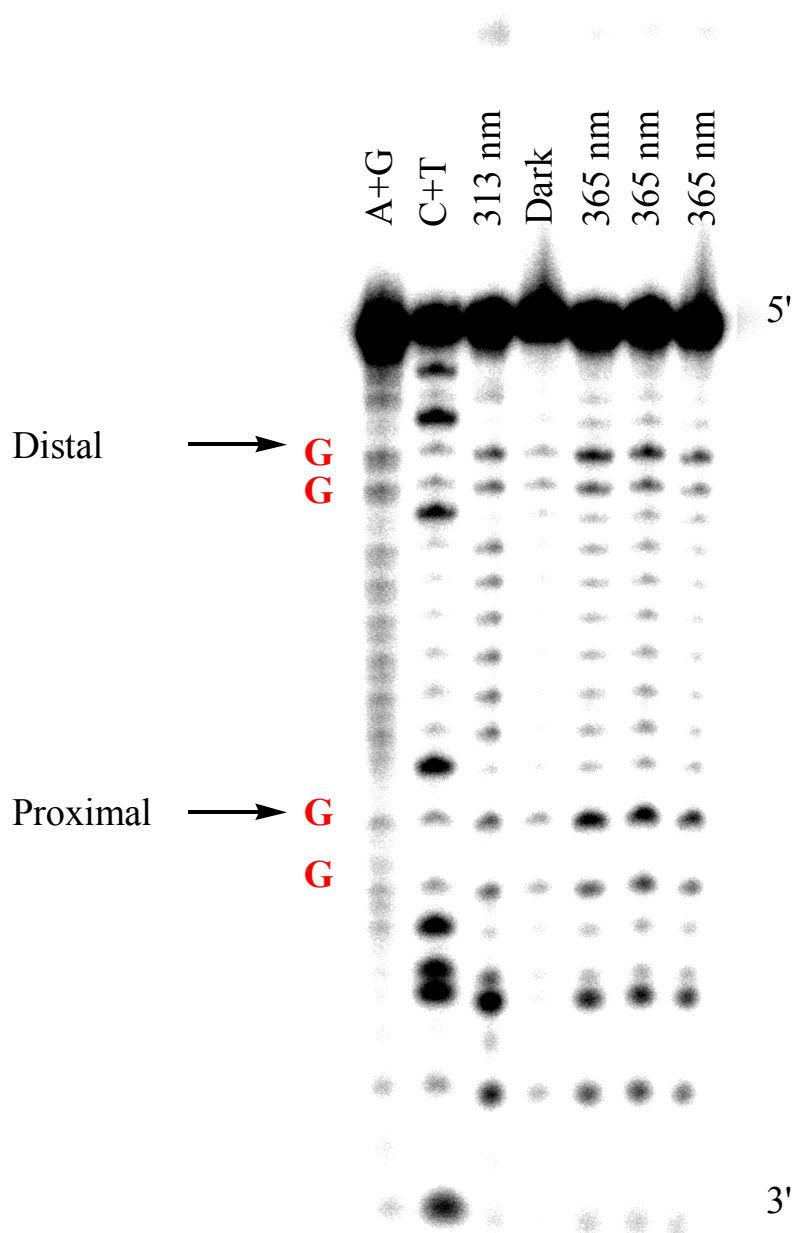
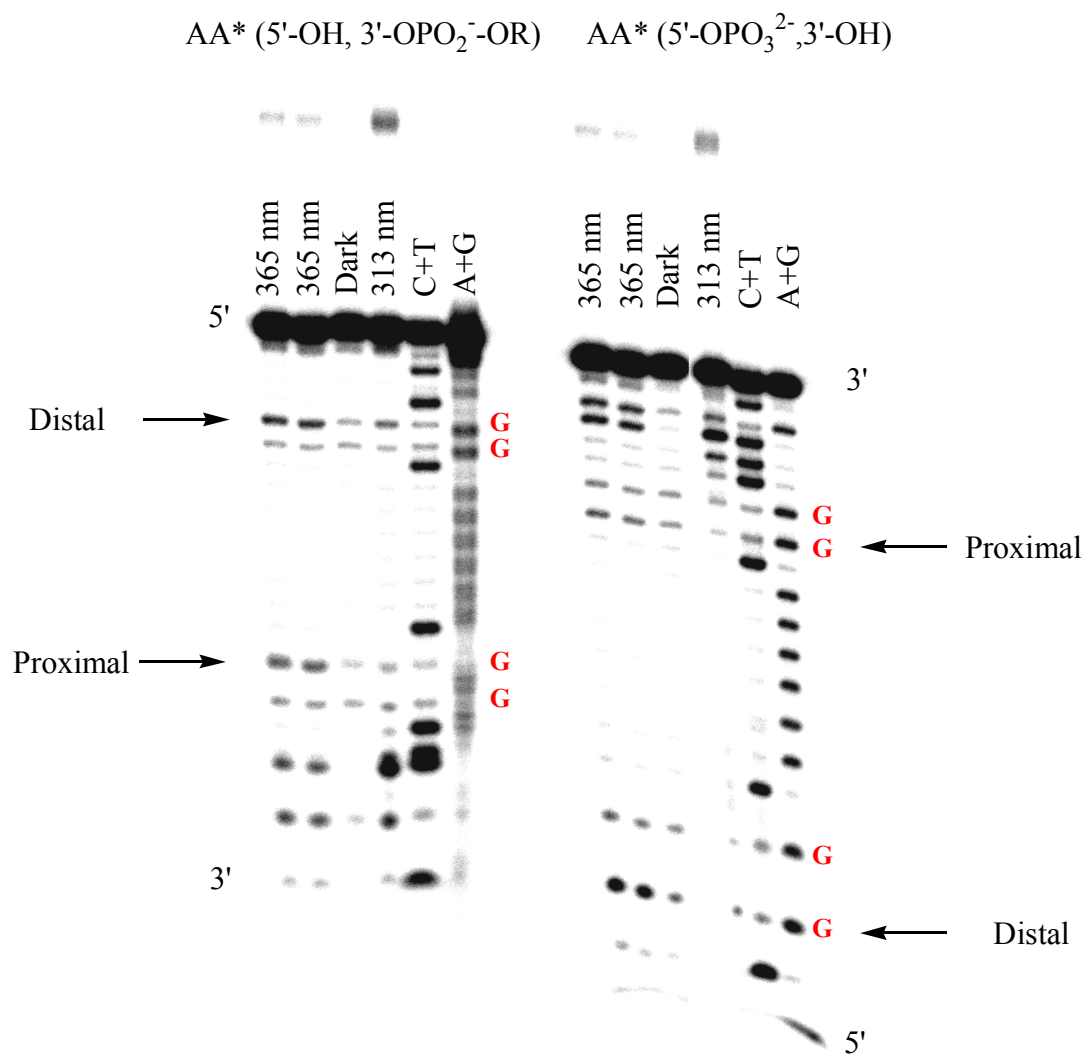


Figure 3.3. Phosphorimagery of a denaturing 20% polyacrylamide gel that delineates the effect of different labeling on long-range charge transport for AA* (5'-OH, 3'-OPO₂-OR) and AA* (5'-OPO₃²⁻, 3'-OH) assemblies using tethered Δ -[Rh(phi)₂bpy']³⁺. The sequence designation is shown in Table 3.1, where the strand containing the guanine doublets is 3' ³²P end-labeled and a non-radioactive ³²P group has been added to the 5' end. For each assembly, the lanes are as follows: A+G, C+T show Maxam-Gilbert sequencing reactions; 313 nm shows the DNA fragment after direct photocleavage by the photoexcited metallointercalator at 313 nm for 10 min without piperidine treatment; 365 nm shows the DNA fragment after irradiation at 365 nm for 20 min at ambient temperature followed by 10% piperidine treatment for thirty minutes at 90 °C; Dark shows sample not irradiated but treated with piperidine. All samples contained 4 μ M metal complex-tethered duplex, 20 mM Tris-Cl, pH 8, 10 mM NaCl. Sites of distal and proximal 5'-GG-3' damage are indicated.

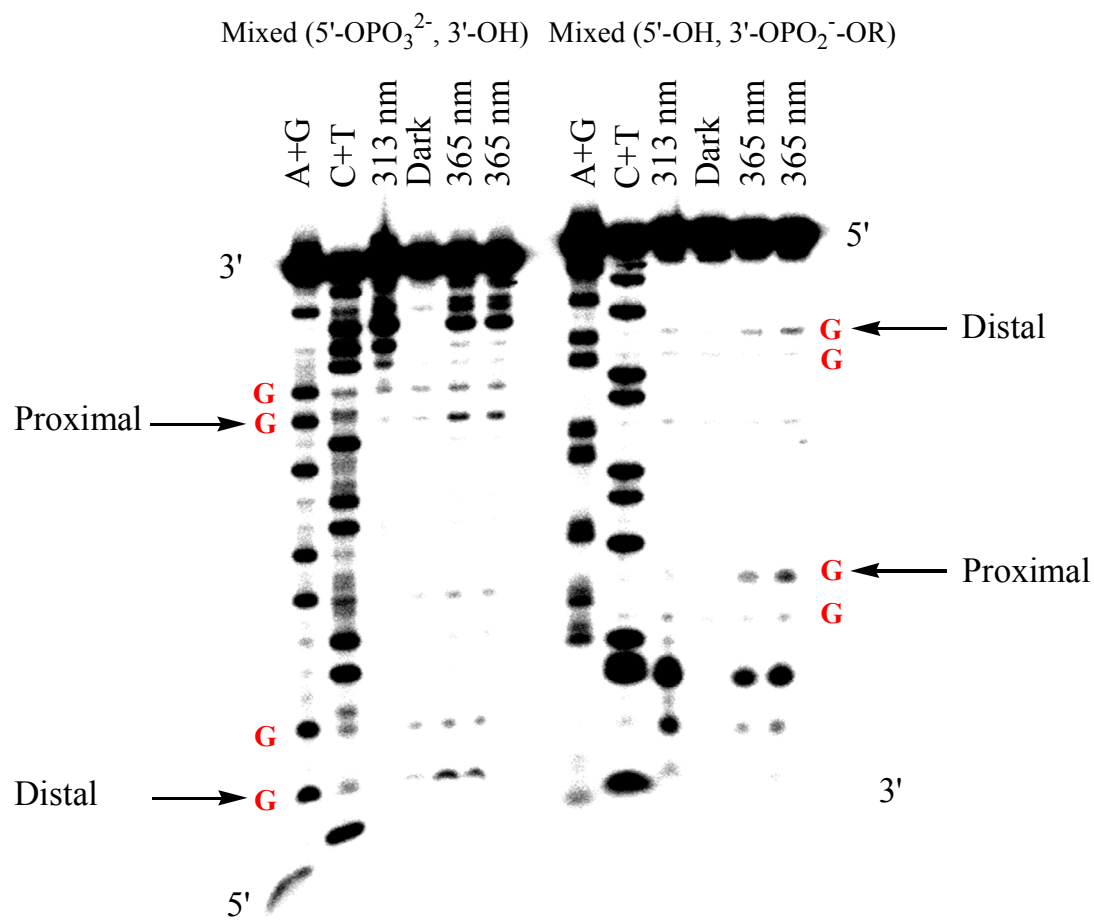


It is important to note that these oxidation experiments were conducted under single-hit conditions (at most one strand break per labeled strand [21]). Thus the differences seen in ratios with the different labeling cannot be the result of multiple breaks on a given strand, counted differently depending upon the position of the label. Our results must instead reflect how the different charge distributions affect DNA hole transport.

We also carried out experiments using a range of ionic strengths (10-500 mM NaCl). Increasing the ionic strength did not alter the observed oxidative damage ratios. This result is consistent with models for condensed counterion atmosphere distributions, which do not appear to vary appreciably with ionic strength over this range [22]. We also found that changing the associated counterion to Mg^{2+} had no significant effect on the damage ratios [23].

The possibility that the difference in the amount of guanine oxidative damage observed with changes in ion distributions was a consequence of a conformational change in the A_6 -tract [25; Chapter 2] was also considered. Mixed sequences were designed to address this issue. The results were found to parallel those using the AA sequences. Interestingly, with these mixed sequences, the distal/proximal ratio was at most only 1.1 compared to 5.2 for the AA-sequences (Figure 3.4). Thus the effect of changing the charges at the termini was smaller; 3'-labeling of the mixed sequence yielded a distal/proximal damage

Figure 3.4. Phosphorimagery of a denaturing 20% polyacrylamide gel that delineates the effect of different labeling on long-range charge transport for Mixed (5'-OPO₃²⁻, 3'-OH) and Mixed (5'-OH, 3'-OPO₂-OR) assemblies using tethered Δ -[Rh(phi)₂bpy']³⁺. The sequence designation is shown in Table 3.1, where the strand containing the guanine doublets is 3' ³²P end-labeled and a non-radioactive ³²P group has been added to the 5' end. For each assembly, the lanes are as follows: A+G, C+T show Maxam-Gilbert sequencing reactions; 313 nm shows the DNA fragment after direct photocleavage by the photoexcited metallointercalator at 313 nm for 10 min without piperidine treatment; 365 nm shows the DNA fragment after irradiation at 365 nm for 20 min at ambient temperature followed by 10% piperidine treatment for thirty minutes at 90 °C; Dark shows sample not irradiated but treated with piperidine. All samples contained 4 μ M metal complex-tethered duplex, 20 mM Tris-Cl, pH 8, 10 mM NaCl. Sites of distal and proximal 5'-GG-3' damage are indicated.



ratio of 0.6. With these sequences, we also tested the effect of moving the end-label away from the distal site; in this case, a further decrease in oxidative yield is obtained (Mixed-2 (5'-OH, 3'-OPO₂-OR)). However, this result could arise from fraying at the ends of the duplex.

Potential Differences and Long-Range Charge Transport

We propose that these results reflect a change in oxidation potential at the distal site relative to the proximal site due to the change in charges at the termini of the oligomer. Changes in the thermodynamic potential of a metalloprotein as a function of pendant charges have been seen previously [26]. Since DNA is a polyanion, with an atmosphere of condensed counterions surrounding it, one might have expected only a minor perturbation in the net charge distribution around the oligomer, but our results indicate that this is not the case. We also considered that the primary effects might be the result of changes in rates of charge injection into the helix, but analogous fluorescence measurements of base-base electron transfer [27] showed no significant modulations in fluorescence with changes in the charge distributions at the termini [28].

If the results reflect a change in thermodynamic potential at the guanine doublets, then, based upon these data, one can make a coarse calculation of the internal longitudinal dielectric constant of DNA. Given a one dimensional point model,

$$\phi_i = \frac{qe}{4\pi\epsilon_0\epsilon_r r_i} \quad (1)$$

where ϵ_0 is the permittivity in a vacuum, ϵ_r is the dielectric constant, q is the magnitude of the charge, e is the elementary charge, and r is the distance from the charge to the 5'-G, one considers that the pendant charges alter the potentials, ϕ_i , of the two sites, so that one can relate the relative permittivity, ϵ_r , to the yield of oxidative damage:

$$\phi_2 - \phi_1 = \kappa T \ln (\text{distal 5'-G damage} / \text{proximal 5'-G damage}) \quad (2)$$

where κ is Boltzmann's constant and T is 298 K.

Particularly high values of 10^2 for the dielectric constant, ϵ_r , are obtained using this model, assuming no screening of the pendant charges by counterions; partial screening yielded somewhat lower values (30–300). Since charge transport is through the base-pair stack, these calculations reflect the dielectric constant *within* the base stack and not the *average* dielectric of DNA. Electronic structure calculations have included values for the internal dielectric of DNA ranging from 2 to 100 [29]. Importantly, a high longitudinal polarizability has been proposed [30] as a factor in DNA conductivity in electrochemical measurements on DNA films [31]. The high dielectric values obtained here are consistent with such a proposal. Certainly these results suggest that further consideration be given to the longitudinal polarizability of DNA as a factor in mechanisms for charge transport.

REFERENCES

1. a) Hall, D. B.; Holmlin, R. E.; Barton, J. K. *Nature* **1996**, *382*, 731-735. b) Núñez, M. E.; Barton, J. K. *Curr. Opin. Chem. Biol.* **2000**, *4*, 199-206.
2. Schuster, G. B. *Acc. Chem. Res.* **2000**, *33*, 253-260.
3. Giese, B. *Acc. Chem. Res.* **2000**, *33*, 631-636.
4. Nakatani, K.; Dohno, C.; Saito, I. *J. Am. Chem. Soc.* **1999**, *121*, 10854-10855.
5. Núñez, M. E.; Hall, D. B.; Barton, J. K. *Chem. Biol.* **1998**, *6*, 85-97.
6. Williams, T. T.; Odom, D. T.; Barton, J. K. *J. Am. Chem. Soc.* **2000**, *122*, 9048-9049.
7. a) Bhattacharya, P. K.; Barton, J. K. *J. Am. Chem. Soc.* **2001**, *123*, 8649-8656. b) Hall, D. B.; Barton, J. K. *J. Am. Chem. Soc.* **1997**, *119*, 5045-5046.
8. a) Odom, D. T.; Barton, J. K. *Biochemistry* **2001**, *40*, 8727-8737. b) Odom, D. T.; Dill, E. A.; Barton, J. K. *Chem. Biol.* **2000**, *7*, 475-481.
9. a) Rajski, S. R.; Barton, J. K. *Biochemistry* **2001**, *40*, 5556-5564. b) Rajski, S. R.; Kumar, S.; Roberts, R. J.; Barton, J. K. *J. Am. Chem. Soc.* **1999**, *121*, 5615-5616.
10. Núñez, M. E.; Holmquist, G. P.; Barton, J. K. *Biochemistry* **2001**, *40*, 12465-12471.
11. a) Sugiyama, H.; Saito, I. *J. Am. Chem. Soc.* **1996**, *118*, 7063-7068. b) Prat, F.; Houk, K. N.; Foote, C. S. *J. Am. Chem. Soc.* **1998**, *120*, 845-846.

12. The yield of piperidine labile strand cleavage correlates linearly with oxidative damage as revealed by enzymatic treatment. Rajski, S. unpublished results in our laboratory.
13. Wagenknecht, H.-A.; Rajski, S. R.; Pascaly, M.; Stemp, E. D. A.; Barton, J. K. *J. Am. Chem. Soc.* **2001**, *123*, 4400-4407.
14. In reactions where radicals were generated first on the sugar [15], damage ratios were less than one. In our studies, where intercalating photooxidants are used, the damage ratio appear primarily to reflect thermodynamic potentials of the sites, with hole equilibration across the duplex on a timescale fast compared to the trapping reaction [16].
15. Giese, B.; Amaudrut, J.; Köhler, A.-K.; Spormann, M.; Wessely, S. *Nature* **2001**, *412*, 318-320.
16. Arkin, M. R.; Stemp, E. D. A.; Pulver, S. C.; Barton, J. K. *Chem. Biol.* **1997**, *4*, 389-400.
17. Hall, D. B.; Kelley, S. O.; Barton, J. K. *Biochemistry* **1998**, *37*, 15933-15940.
18. Gasper, S. M.; Schuster, G. B. *J. Am. Chem. Soc.* **1997**, *119*, 12762-12771.
19. It was also proposed that the steric bulk of the intercalator might be important [20], but since the intercalation is at least 17 Å from the closest guanine site, this is difficult to understand.
20. Giese, B.; Spichty, M. *Chem. Phys. Chem.* **2000**, *1*, 195-198.

21. Lutter, L. C. *J. Mol. Biol.* **1978**, *124*, 391-420.
22. Manning, G. S. *Macromolecules* **2001**, *34*, 4650-4655.
23. The gating of charge transport through DNA by bound counterions has been proposed [24]. Our experiments provide no evidence in support of such modulation, since, on the timescale of the charge transport, the ion distributions, although varied in the different assemblies, should be constant.
24. Barnett, R. N.; Cleveland, C. L.; Joy, A.; Landmann, U.; Schuster, G. B. *Science* **2001**, *294*, 567-571.
25. Nadeau, J. G.; Crothers, D. M. *Proc. Natl. Acad. Sci. USA* **1989**, *86*, 2622-2626.
26. Bashford, D.; Karplus, M.; Canters, G. W. *J. Mol. Biol.* **1988**, *203*, 507-516.
27. Kelley, S. O.; Barton, J. K. *Science* **1999**, *283*, 375-381.
28. O'Neill, M. unpublished results in our laboratory.
29. Jayaram, B.; Sharp, K. A.; Honig, B. *Biopolymers* **1989**, *28*, 975-993.
30. Hartwich, G.; Caruana, D. J.; Lumley-Woodyear, T.; Wu, Y.; Campbell, C. N.; Heller, A. *J. Am. Chem. Soc.* **1999**, *121*, 10803-10812.
31. a) Boon, E. M.; Ceres, D. M.; Drummond, T. G.; Hill, M. G.; Barton, J. K. *Nature Biotech.* **2000**, *18*, 1096-1100. b) Kelley, S. O.; Jackson, N. M.; Hill, M. G.; Barton, J. K.; *Angew. Chem. Int. Ed. Engl.* **1999**, *38*, 941-947.

32. Holmlin, R. E.; Dandliker, P. J.; Barton, J. K. *Bioconjugate Chem.* **1999**, *10*, 1122-1130.

CHAPTER 4

Effects of the Photooxidant on DNA-Mediated Charge Transport

* Adapted from Williams, T. T. Dohno, C., Stemp, E. D. A., and Barton, J. K. submitted.

** Dr. Chikara Dohno synthesized the anthraquinone conjugates and performed the thionine experiments and all of the ^{CPG} photooxidant experiments.

INTRODUCTION

Oxidative damage to DNA promoted from a distance through DNA-mediated charge transport (CT) from a remotely bound photooxidant has, by now, been demonstrated and confirmed using a variety of photooxidants [1-10]. Hole transport from DNA-bound photooxidants can lead to oxidative damage at guanine sites, in particular at the 5'-G of 5'-GG-3' doublets [11]. Indeed, reaction at the 5'-G of guanine doublets has become the signature for long-range oxidation by CT. DNA-mediated oxidative damage has been demonstrated over a distance of 200 Å [12,13]. While the reaction can, therefore, occur over long molecular distances, it is exquisitely sensitive to intervening sequence-dependent DNA structure. Intervening mismatches can attenuate oxidative damage through long-range CT [14], as can protein binding [15,16] that perturb the intervening base-pair stack. In fact, the sensitivity of long-range CT to perturbations in base-pair stacking has led to the development of electrochemical sensors for mutations, lesions, and protein binding [17-20]. Oxidative damage to DNA from a distance has been demonstrated within cell nuclei [21] and within DNA packaged in nucleosomes [22]. The sensitivity of DNA CT chemistry to mismatches and lesions has furthermore prompted the proposal that DNA repair enzymes may exploit DNA CT in detecting their targets within the cell [23].

Oxidative damage from a distance through DNA CT was first demonstrated using a phenanthrenequinone diimine (phi) complex of rhodium(III) as the tethered intercalating photooxidant in DNA assemblies, where the metallointercalator was spatially separated from two 5'-GG-3' doublets [1]. Thereafter, organic intercalators such as naphthalene diimide (NDI) [2], ethidium [3] and modified anthraquinones [4] were also used to promote long-range oxidative DNA damage. Modified nucleotides such as 5-cyano-benzene deoxyuridine [5] and 4'-pivaloyl deoxythymine [6] have, in addition, been photolysed to generate hot base and sugar radicals, respectively, that lead to oxidative damage at guanine sites from a remote position. A ground state ruthenium(III) oxidant, containing the dipyrrophenazine (dppz) ligand as the intercalating ligand, and generated *in situ* in a flash-quench reaction has, in addition to oxidative studies, been particularly valuable in spectroscopic measurements of the formation of radical intermediates at long-range through DNA CT [7-10].

These studies of oxidative damage have been utilized in developing mechanistic proposals for how DNA CT proceeds. The chemistry is currently viewed as involving a mixture of hopping and tunneling [12,24,25]. Owing to the sensitivity of DNA CT to the dynamical structure of DNA, we have considered DNA CT in terms of domain hopping, that is, hopping among DNA

domains defined dynamically as stacked regions within the duplex through which charge is delocalized [25c,26].

Given this mechanistic perspective, DNA CT is expected to be a characteristic of the DNA helix. Hence, while differences in oxidative damage may arise as a function of variations in intervening sequence and structure, results were expected to be similar irrespective of the oxidant employed. To account for differences in the efficiency of photoreaction, studies employed measurements of oxidative damage at distal versus proximal guanine sites as a means of normalization. Within such a framework, distal/proximal damage ratios were considered to be independent of the remotely bound oxidant employed. Moreover, these distal/proximal ratios were expected to have values of ≤ 1 . Studies of oxidative damage using the rhodium photooxidant, however, revealed damage ratios consistently higher than 1; in the case of CT across an adenine tract particularly high damage ratios of 3.5 were obtained [26; Chapter 2]. As described in Chapter 3, these high damage ratios were explained in part to the high longitudinal polarizability of DNA, and the resultant effect of the high charge of the pendant Rh(III) photooxidant on the relative oxidation potentials of proximal versus distal 5'-GG-3' sites [27].

In multiply stranded DNA crossover assemblies, Sen and coworkers reported differing oxidation patterns using the rhodium intercalator versus

anthraquinone as the photooxidant [28]. They accounted for these differences by arguing that the rhodium intercalators, once tethered, promote DNA aggregation, and hence oxidative damage yields were not wholly the result of oxidation by a remotely bound intercalator within one assembly but also arose owing to inter-assembly reactions. In support of this aggregation, non-denaturing gels were utilized to show a small percentage of a lower mobility band in the rhodium crossover assemblies. Importantly, conditions differed considerably from those utilized in earlier tests of oxidative damage using rhodium intercalators owing to the need for large concentrations of Mg^{2+} to maintain the crossover structures. Controls for intermolecularity were not carried out in these crossover studies, also in contrast to all earlier studies of DNA CT in our laboratory. Moreover, the slow mobility band was neither characterized nor systematically examined as a function of concentration or incubation time. Schuster and coworkers then examined oxidative damage in a duplex assembly containing the repetitive adenine tract using the modified anthraquinone as the photooxidant and they reported a distal/proximal oxidative damage ratio of 0.1 [29]. Based on that data point, they have now proposed that all oxidative damage studies with all metallointercalators be considered difficult to interpret and problematic at best. How they rationalize such aggregation as

mismatch-dependent [14], protein-binding dependent [15], and not revealed in detailed control measurements of intermolecularity is not made clear.

These rationalizations and extrapolations concerning our studies of long-range oxidative damage with metallointercalators prompted us to examine in detail the possibility of aggregation by metallointercalators. It is noteworthy that detailed NMR studies had already been conducted that showed the anticooperative binding of metallointercalators to DNA [30]. Additionally, these proposals prompted us to carry out a direct comparison of oxidative damage using various photooxidants for the first time. Here, therefore, we directly compare reactions with different photooxidants. Indeed, we do find clear differences in oxidative damage ratios depending upon the photooxidant employed. We provide additional data that demonstrate the absence of any DNA aggregation by the DNA-bound metallointercalators under the conditions used for photooxidation studies. Furthermore, using guanine derivatives that allow hole-trapping to form irreversible oxidation products on a fast timescale, we provide evidence that the differences in oxidative damage ratios may depend upon differences in rates of back electron transfer (BET) for different photooxidants. Such differences are important to consider in interpreting past and developing future models for DNA CT.

EXPERIMENTAL

Oligonucleotide Synthesis. Oligonucleotides were synthesized utilizing standard phosphoramidite chemistry on an ABI 392 DNA/RNA synthesizer [31]. DNA was synthesized with a 5'-dimethoxy trityl (DMT) protecting group and purified on a Dynamax 300 Å C₄ reverse phased column (Rainin) (100% 50 mM NH₄OAc, pH 7, to 70% 50 mM NH₄OAc/ 30% Acetonitrile over 35 minutes) on a Hewlett-Packard 1100 HPLC. 2-fluoro-O⁶-nitrophenyldeoxyinosine containing strands, also containing a 5'-dimethoxy group, on solid support were treated with a 0.5 M DBU solution in acetonitrile for 20 minutes at ambient temperature, washed with additional acetonitrile, and treated with a 1% solution of triethylamine in acetonitrile. The strands were then treated with 6 M aqueous cyclopropylamine and heated at 60 °C for 16 hours to generate the ^{CP}G containing DNA strands. The solution was filtered and concentrated to dryness. The isolated strands were then further treated with 80% glacial acetic acid and purified by reverse phase HPLC on a Microsorb C₁₈ column (10 x 250 mm; elution with 98% 50 mM NH₄OAc/2% Acetonitrile to 88% 50 mM NH₄OAc/12 % Acetonitrile over 30 minutes). Those strands not containing 2-fluoro-O⁶-nitrophenyldeoxyinosine were also treated with 80% acetic acid and HPLC was performed once more. All strands were quantified using UV-visible

spectroscopy on a Beckman DU 7400 Spectrophotometer; ϵ_{260} ($M^{-1} \text{ cm}^{-1}$) adenine = 15,400, guanine = 11,500, cytosine = 7,400, thymine = 8,700.

Preparation of oligonucleotides appended with rhodium, ruthenium, ethidium, and anthraquinone have been described elsewhere [4,32-33] and were purified on a Dynamax C₄ column by reverse phase HPLC (95% 50 mM NH₄OAc (pH 7)/5% Acetonitrile to 85% 50 mM NH₄OAc/15% Acetonitrile over 45 minutes). In the case of the ruthenium and rhodium appended oligonucleotides, the Δ stereoisomer, established by circular dichroism (AVIV CD spectrophotometer) was used. All strands were characterized by either MALDI-TOF or ESI mass spectrometry and UV visible spectroscopy.

Synthesis of Thionine-Modified DNA. *Preparation of N³-Octanoic acid modified thionine (1).* A mixture of thionine (1.31 g, 4.54 mmol) and 8-bromooctanoic acid (1.51 g, 6.76 mmol) in DMF (20 mL) was refluxed for 6 h. The reaction mixture was concentrated *in vacuo*, and the residue was dissolved in methanol and filtered through celite. The crude product was purified by column chromatography on silica gel (chloroform: methanol: acetic acid = 100: 12: 1.2) to give **1** (148.1 mg, 9%): ¹H NMR (CD₃OD, 300 MHz) δ 1.38–1.73 (10H), 2.23 (m, 2H), 3.45 (m, 2H), 7.10-7.23 (4H), 7.86-7.89 (2H); ESI MS m/z 370.2 (M⁺).

Preparation of N-Hydroxysuccinimidyl ester of 1 (2). To a mixture of DCC (18.4 mg, 0.089 mmol) and the hydrogen chloride salt of **1** (17.5 mg, 0.043 mmol)

in dry DMF (1 mL) was added *N*-hydroxysuccinimide (10.1 mg, 0.088 mmol). The mixture was stirred at ambient temperature for 2 days under nitrogen. The solvent was removed *in vacuo*, and the crude product was purified by column chromatography on silica gel (chloroform: methanol : acetic acid = 100: 12: 1.2) to give **2** (14.0 mg, 0.028 mmol, 65%): ^1H NMR (CD_3OD , 300 MHz) δ 1.36–1.74 (10H), 2.63 (t, 2H, $J = 7.1$ Hz), 2.81 (s, 4H), 3.44 (m, 2H), 7.06–7.20 (4H), 7.82–7.85 (2H); ESI MS m/z 467.2 (M^+); UV-Vis (50 mM NaCl, 10 mM sodium phosphate (pH 7.0)) 619 nm, 286 nm.

Preparation of Thionine-DNA Conjugates. The synthesis of thionine-DNA conjugates was accomplished by the coupling of the succinimidyl ester of modified thionine (**2**) with 5'-alkylamino DNA. The 5'-alkylamino DNA was prepared by standard phosphoramidite synthesis followed by functionalization with hexamethylene diamine. To a DMF solution of activated ester (**2**) was added the 5'-alkylamino DNA in sodium phosphate buffer (pH 8.0) and the solution was kept at an ambient temperature for 2 h. The reaction mixture was purified on Sep-Pack cartridge followed by reverse phase HPLC. All strands were confirmed by MALDI-TOF mass spectrometry and were all within 2 mass units of the calculated values.

Assay of Oxidative DNA Damage. The oligonucleotides were labeled at the 5'-end utilizing γ - ^{32}P ATP and polynucleotide kinase [34]. After desalting, the

reaction mixture was purified on a 20% denaturing polyacrylamide gel. The desired band was excised from the gel, soaked in 1 mL of 10 mM Tris-Cl and 1 mM EDTA (pH 7.5), dried in vacuo, and isolated by use of Micro Bio-Spin columns. Duplexes were prepared by mixing equimolar amounts of modified and unmodified strands to a final concentration of 2 μ M and annealed in 20 mM Tris-Cl (pH 8.1) and 10 mM NaCl by heating to 90 °C for 5 min and gradually cooling to ambient temperature over 2 h. For direct strand cleavage experiments, samples (30 μ L) were irradiated at 313 nm for 10 min using a 1000 W Hg/Xe lamp equipped with a monochromator and immediately dried following irradiation. For oxidative damage experiments, parallel samples were irradiated at 365 nm for 1 h, treated with 10% piperidine (v/v), heated for 30 min at 90 °C, and dried in vacuo. For the ruthenium-modified oligonucleotides (30 μ L), irradiations were performed at 436 nm for either 1 h (without $[\text{Co}(\text{NH}_3)_5\text{Cl}]^{2+}$) or 10 min (with $[\text{Co}(\text{NH}_3)_5\text{Cl}]^{2+}$ (Aldrich)) and subsequently treated with 10% piperidine, heated to 90 °C for 30 min, and dried. The ethidium and anthraquinone-modified oligonucleotides were irradiated at 340 nm and 350 nm, respectively, for 1 h, and treated with piperidine as previously described. All samples were resuspended into formamide loading dye and electrophoresed through a 20% denaturing polyacrylamide gel. The extent of oxidative damage was determined by phosphorimagery (ImageQuant).

In determining the quantum yields, the extinction coefficients ($M^{-1} \text{ cm}^{-1}$) were estimated to be the following for the respective oxidants: Rh, $\epsilon_{365} = 15,600$; AQ-2, $\epsilon_{350} = 3000$; Et, $\epsilon_{340} = 11,000$; Ru-4, $\epsilon_{436} = 19,000$. The lamp power was estimated to be 7 mW to 20 mW over the irradiation wavelengths of the oxidants. Sample volumes were 30 μL and duplex concentrations were 2 μM .

Gel Electrophoresis under Non-Denaturing Conditions. Parallel samples being used to test for oxidative damage were electrophoresed at 4 °C and 500 V for 24 h through a 20% non-denaturing gel containing 0.045 M Tris-Borate (pH 8.3), 1 mM EDTA, and running dye. Subsequent analysis was performed utilizing phosphorimagery (ImageQuant).

Assay of Oxidative Damage with the ^{CPG} Containing Duplexes.

Duplexes were prepared by mixing equimolar amounts of modified and ^{CPG} containing strands to a final concentration of either 2 μM or 5 μM and annealed in 20 mM Tris-Cl (pH 8.1) and 10 mM NaCl. Samples were irradiated for up to 60 min at the following wavelengths: AQ-2 at 350 nm; Rh at 365 nm; Ru at 436 nm; Et at 340 nm. After irradiation (20 μL), samples were fully digested with alkaline phosphatase (33 units/mL), snake venom phosphodiesterase (3 units/mL), and nuclease P1 (33 units/mL) at 37 °C for 2 h. Digested solutions were analyzed by HPLC (C_{18} , 4.6 x 150 mm; elution with 98% 50 mM

NH₄OAc/2% acetonitrile to 86% 50 mM NH₄OAc/14% acetonitrile over 30 min with a flow rate of 1 mL/min).

RESULTS

Photooxidants and DNA Assembly. The photooxidants and DNA assembly examined are illustrated in Figure 4.1. Photooxidants tested include the two metallointercalators, [Rh(phi)₂bpy']³⁺ and [Ru(phen)(dppz)(bpy')]²⁺, and three organic intercalators, ethidium (Et), thionine (Th), and anthraquinone (AQ), which was tethered in two ways (AQ-2 (end-capped) and AQ-5 (intercalated)). We focused primarily on CT through a DNA duplex composed of an A₆-tract and two 5'-GG-3' sites, since this sequence has been examined extensively and was found to be an effective medium for CT [26]. To provide a systematic comparison, all of the photooxidants were covalently tethered to one end of the DNA duplex. CT was assayed both through determination of the yield of oxidative damage by PAGE analysis and by HPLC analysis of the yield of ring-opening of *N*²-cyclopropylguanine (^{CP}G) within the DNA duplex. In the case of thionine, additional DNA duplexes were tested using the *N*²-isopropylguanine (^{iPr}G) trapping reaction.

Figure 4.1. Photooxidants, modified nucleosides, and DNA assembly utilized in this work. (A) Clockwise from upper left: Anthraquinone, $[\text{Rh}(\text{phen})_2\text{bpy}']^{3+}$, $[\text{Ru}(\text{phen})(\text{dppz})(\text{bpy}')^{2+}$, Ethidium and Thionine. (B) The modified nucleoside *N*²-cyclopropylguanosine (left) and ring-opened product *N*²-(3-hydroxypropanoyl)dG (right). (C) DNA assembly and functionalized linkers to the assembly.

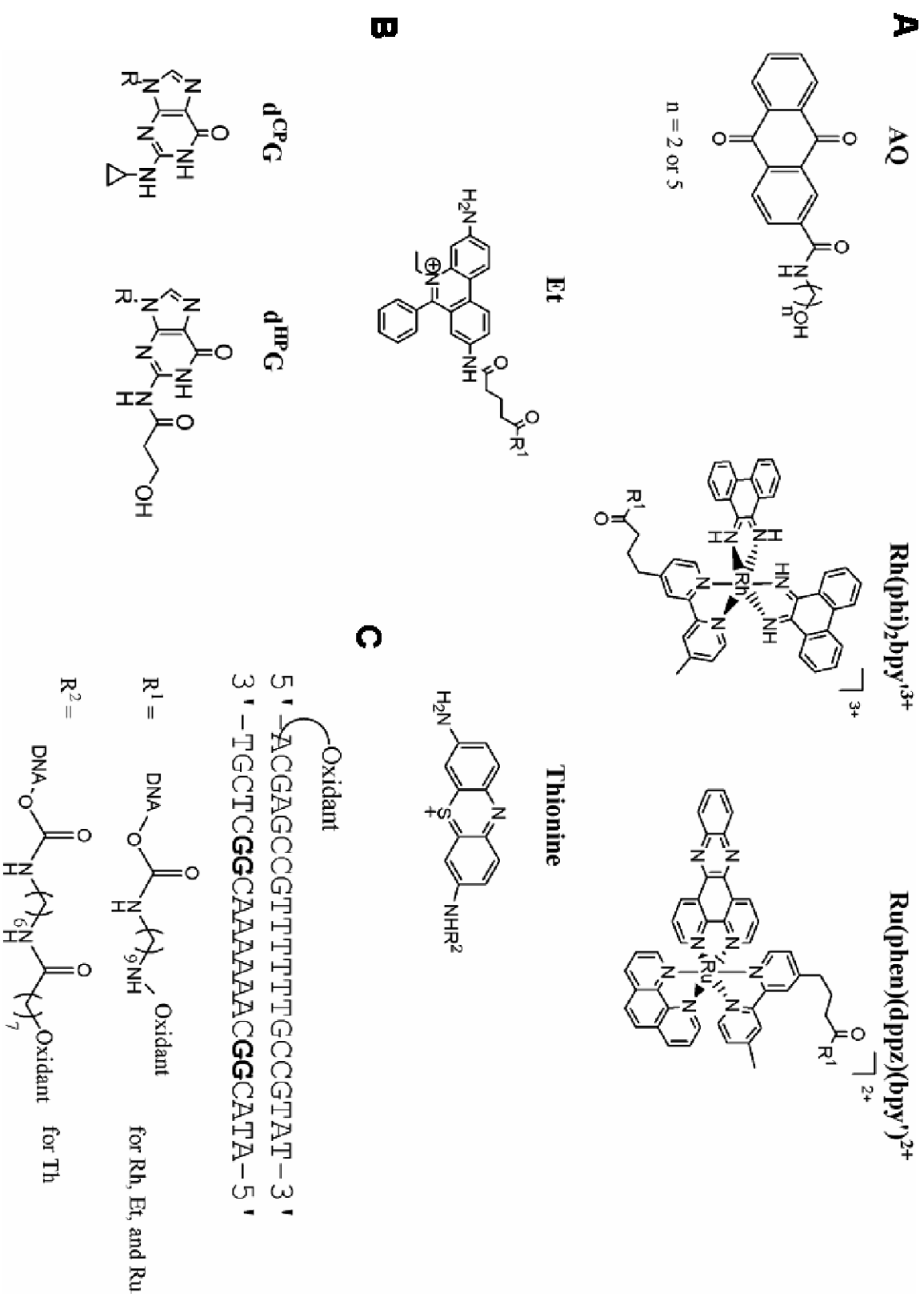


Figure 4.2. Oxidative damage with different photooxidants. 20% PAGE after irradiation of functionalized 5'-³²P-labelled DNA assemblies containing (A) Δ -[Rh(phi)₂bpy']³⁺, AQ-2, AQ-5 and the Δ -1 and Δ -4 isomers (order of elution from HPLC) of [Ru(phen)(dppz)(bpy')]²⁺ and (B) Et, respectively. The numbers above the lanes indicate the wavelength of irradiation. A+G and C+T are Maxam-Gilbert sequencing lanes. In A, following irradiation, samples were treated with 10% piperidine (v/v), heated for 30 min at 90 °C and dried; the 313 lane was not treated with piperidine. The 313 nm lane shows direct strand cleavage by Δ -[Rh(phi)₂bpy']³⁺ after 10 minutes of irradiation at 313 nm; the arrow to the left indicates the site of direct cleavage marking the Rh intercalation. In all cases, lane DC indicates the dark control, which is the functionalized assembly without irradiation but with subsequent piperidine treatment. Lane 365 shows oxidative damage after irradiation of DNA functionalized with Δ -[Rh(phi)₂bpy']³⁺ at 365 nm for one hour. Lane 350 shows the oxidative damage yield after irradiation of both AQ-2 and AQ-5 assemblies for one hour at 350 nm. Lanes 436-Q and 436+Q show oxidative damage after irradiation of DNA-tethered [Ru(phen)(dppz)(bpy')]²⁺ at 436 nm for one hour without [Co(NH₃)₅Cl]²⁺ and for ten minutes with [Co(NH₃)₅Cl]²⁺ (25 μ M), respectively. In B, Et-functionalized assemblies are shown upon irradiation at 340 nm for one hour with or without piperidine treatment. Here, direct crosslinking of the Et near the duplex terminus is indicated by the arrow. The concentrations for all of the assemblies were 2 μ M duplex in 20 mM Tris-HCl (pH 8.1) and 10 mM NaCl.

Oxidative Damage Patterns of the Various Oxidants. Figure 4.2 shows the oxidative guanine damage that is revealed after 20% PAGE analysis of the photooxidant-tethered duplexes after irradiation and treatment of the DNA with piperidine. For all of the photooxidants tested here, damage is found at 5'-GG-3' sites both proximal and distal to the tethered oxidant. However both the extent of damage and relative damage at the proximal versus distal sites vary among the oxidants. Consistent with earlier reports [26,29], a high distal/proximal guanine damage ratio is evident with Rh whereas a very low distal/proximal guanine damage ratio is found with AQ-2 and AQ-5. PAGE analysis of Ru-tethered duplexes (two Δ configurational isomers) show oxidative damage patterns that resemble those of the anthraquinone derivatives; appreciable damage is observed at the 5'-GG-3' site that is proximal to the photooxidant, but little damage is seen at the distal 5'-GG-3' site. Not shown is reaction with tethered thionine; we had earlier demonstrated that, despite the large driving force for photoreaction, no oxidative guanine damage is evident with thionine covalently or non-covalently bound to DNA [35].

Also noteworthy is the direct strand photocleavage of DNA by tethered Rh upon irradiation at 313 nm. This direct strand cleavage chemistry marks the site of rhodium intercalation near the end of the duplex [1]. This direct cleavage chemistry has been utilized by us in all tests of oxidative reaction with Rh as a

control to mark the rhodium binding site. Under the conditions in which we probe long-range oxidative damage, no cleavage is observed at sites other than near the duplex terminus where the Rh is tethered (Figure 4.2). Hence, these observations stand in contrast to a model of interduplex aggregation promoted by Rh under the conditions where long-range CT is probed [28].

Ethidium, once tethered and irradiated at 340 nm, shows an oxidative damage pattern resembling that of Rh (Figure 4.2B). An appreciable amount of long-range oxidative guanine damage is observed at the distal 5'-GG-3' site compared to the proximal site. Damage is also observed at the guanine located near the duplex terminus where the Et is tethered. We have attributed this reaction to covalent crosslinking by the ethidium moiety [3a,36]. Also noteworthy here and consistent with earlier studies [3], a high preference for the 5'-G of the guanine doublet is not found with Et; hole-trapping studies with CPG nonetheless confirm one-electron chemistry (*vide infra*).

Table 4.1 summarizes the distal/proximal DNA oxidation ratios for these tethered photooxidants on DNA assemblies of identical sequence. It is clear that different distal/proximal oxidation ratios are found depending upon the photooxidant employed. Notably Et, like Rh, yields high distal/proximal ratios whereas for Ru or AQ, greater reaction is found at the proximal 5'-GG-3' site compared to the distal site.

Also shown in Table 4.1 are estimates of the quantum yield for oxidative guanine damage, $\Phi(G_{ox})$, on these DNA assemblies. For all photooxidants, these values are low. These low yields are understandable given (i) irreversible oxidative guanine damage is at least two steps removed from guanine radical formation, and (ii) the gel assay measures only the portion of that reaction that is piperidine sensitive. The yields decrease with photooxidants as follows: Ru > AQ > Rh > Et. Notably, the highest efficiency reaction is obtained with the ruthenium oxidant, and in fact, if calculated versus Ru(III) oxidant generated *in situ* rather than per Ru(II), the value would be still higher. For Rh, the yield is approximately one order of magnitude lower than for AQ, measured on DNAs of identical sequence using identical conditions. For Et a still lower yield is obtained. These differences can certainly be understood based upon a difference in rates of BET among the photooxidants (*vide infra*).

Native Gel Analysis of Photooxidant-Tethered Assemblies. As another test of possible aggregation of assemblies, we examined the mobility of the oxidant-tethered DNA using non-denaturing gel electrophoresis. As shown in Figure 4.3, under conditions and using samples tested also for oxidative damage, two duplex bands of similar mobility are found with the Rh-tethered assemblies

Table 4.1. A summary of the oxidative guanine damage by biochemical analysis and ^{CP}G consumption.

Photooxidant ^a	5'-GG-3' D/P ^b	5'-G D/P ^g	$\Phi_{G_{ox}} \times 10^4$	5' ^{CP} G D/P ^j
[Rh(phi) ₂ bpy'] ³⁺	1.4 (±0.2)	1.8 (±0.3)	0.02	0.12
[Ru(phen)(dppz)(bpy')] ²⁺	0.08 (±0.03) ^c 0.08 (±0.05) ^d	0.04 (±0.01) ^c 0.04 (±0.02) ^d	0.9 ^h	0.03
AQ	0.07 (±0.02) ^e 0.09 (±0.06) ^f	0.06 (±0.01) ^e 0.08 (±0.07) ^f	0.2 ⁱ	0.03 ⁱ
Et'	1.5 (±0.3)	N.D. ^l	0.01	0.4 ^k

^a Photooxidants tethered to assemblies as shown in Figure 4.1.

^b Total amount of 5'-G and 3'-G oxidative guanine damage as observed by PAGE analysis at the distal (D) versus proximal (P) sites. The results reflect three to five trials for each.

^{c,d} (5'+3') GG oxidative damage yields for Ru-1 and Ru-4 Δ isomers, respectively.

^{e,f} (5'+3') GG oxidative damage yields for AQ modified DNA with n=2 and n=5 methylene spacers, respectively.

^g Total amount of 5'-G oxidative guanine damage as observed by PAGE analysis at the distal (D) versus proximal (P) sites. The results reflect three to five trials for each.

^h This yield is determined per Ru(II) and is an underestimate versus Ru(III) oxidant generated using 25 μ M [Co(NH₃)₅Cl²⁺] as the quencher.

ⁱ AQ-2 was utilized.

^j Consumption of the distal ^{CP}G versus 40% consumption of the ^{CP}G at the proximal site.

^k Consumption of the distal ^{CP}G versus 30% consumption of the ^{CP}G at the proximal site.

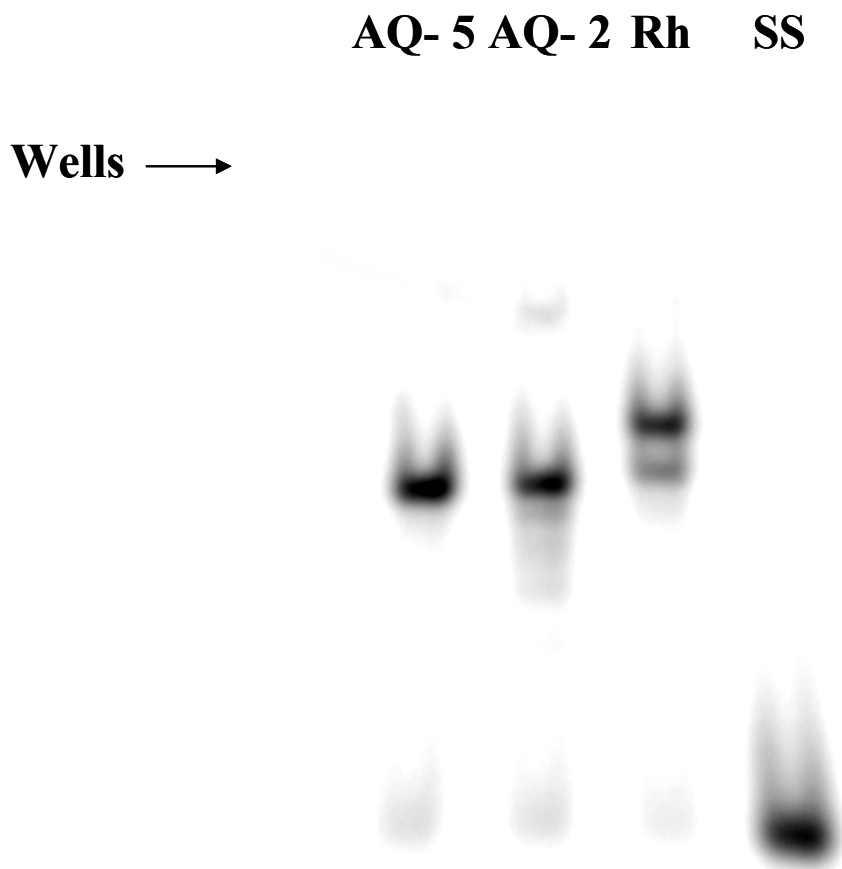
^l The 5'-G distal to proximal ratio was not determined for Et because of the lack of 5' specificity with this oxidant.

and primarily one band of comparable mobility is evident with the AQ-modified duplexes. The two bands found with Rh, only distinguishable with very slow gel electrophoresis, are assigned to the two configurational isomers of the tethered complex. Both have mobilities slightly less than the AQ-functionalized DNA, consistent with the high positive charge on the Rh. Importantly, no significantly slow-moving band, as might be expected if two duplexes aggregated together, is evident with the Rh-tethered DNA. In fact, a very small intensity of a slow migrating band is observed only in the end-capped AQ-2 sample.

We also examined Et and Ru-tethered assemblies by non-denaturing gel electrophoresis. For these assemblies as well, no slow moving bands are evident. None of these modifications led to aggregation of DNA under conditions where long-range DNA CT is probed.

These results differ from those reported by Sen and coworkers in their studies of DNA crossover assemblies with tethered Rh. In an effort to understand the basis for their observations, we examined Rh-modified duplexes also under the high ionic strength conditions used to stabilize the DNA crossovers (0.04 M Tris-Borate, 0.1 mM EDTA, 2 mM Mg^{2+}). There, too, no low mobility bands are evident. We also tested the assemblies by non-denaturing electrophoresis with 2 mM Mg^{2+} within the gel.

Figure 4.3. 20% non-denaturing polyacrylamide gel electrophoresis of 5'-³²P-labelled DNA duplexes functionalized with AQ-2 (end-capped), AQ-5 (intercalated), or Δ -[Rh(phi)₂bpy']³⁺. Also shown is the single strand control (SS) for the 5'-³²P-labelled DNA, without annealing to a functionalized complement. All samples were 2 μ M duplex in 20 mM Tris-Cl (pH 8.1) and 10 mM NaCl. Note in the Rh lane the presence of two bands assigned to the two bound isomers of the Rh-functionalized DNA. In the AQ-2 lane, there is also a small percentage of a much slower mobility band.



In this case, we sometimes observed a small percentage of a slow moving band, but this was not reproducible; we believe this result to be an artifact associated with loading the samples onto gels with high $[Mg^{2+}]$. Besides the high $[Mg^{2+}]$ in solution samples and in the gels, another difference between our conditions and those utilized by Sen is that they appear to have first precipitated samples and carried out the electrophoresis experiments on a subsequent day. In our experiments, samples are not first precipitated and resuspended, and samples are never stored overnight before completing the experiment. For there to be a direct extrapolation of our studies, experiments clearly need to be performed under the same conditions.

Long-Range CT Studies with Thionine. Since we had earlier determined that photolysis of thionine yielded no detectable oxidative damage to DNA, we sought chemical evidence of long-range CT with this intercalating photooxidant. Toward that end, we synthesized d^{CPG} as described previously [37,38] and first examined the photooxidation of the d^{CPG} nucleoside by thionine. Irradiation was carried out at 599 nm aerobically in the presence of thionine, and the oxidation products were analyzed by HPLC. Upon irradiation, d^{CPG} was rapidly consumed producing two major products. These two products were identified as dG and N^2 -(3-hydroxypropanoyl)dG (d^{HPG}) by mass spectrometry and HPLC

retention times, and are fully consistent with previously observed one-electron oxidation products of d^{CPG} (Figure 4.4, Figure 4.5). The rapid consumption and the identical oxidation products indicate that the excited thionine surely produces d^{CPG} radical cation.

For further confirmation of one-electron oxidation chemistry, we also examined the effect of oxygen, since thionine is known to be a singlet oxygen generator [39,40]. Under anaerobic conditions, d^{CPG} was consumed with similar kinetics as in the presence of oxygen, but different products were generated. Since oxygen is considered to be involved in the mechanism of the formation of d^{HPG} under aerobic conditions, different products are expected in the absence of oxygen. Significantly, the similar consumption rate indicates that singlet oxygen is not responsible for the rapid consumption of d^{CPG} .

In contrast to the rapid decomposition of d^{CPG} , dG remains unchanged under the same reaction conditions (Figure 4.5). Although dG loses an electron to generate the dG radical cation in the presence of photoexcited thionine, we have recently shown that fast BET suppresses the decomposition of dG [35]. In that case, fast BET conceals the evidence of electron transfer, such as the formation of the oxidation products. Reaction of d^{CPG} reveals the occurrence of electron transfer since rapid ring-opening traps the hole on a timescale that is competitive with BET.

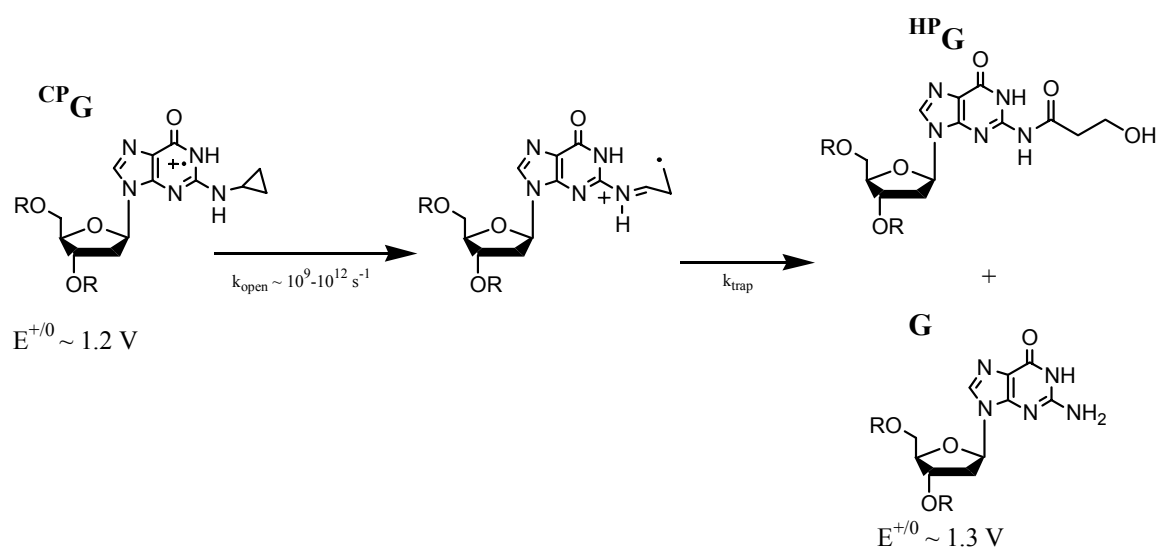
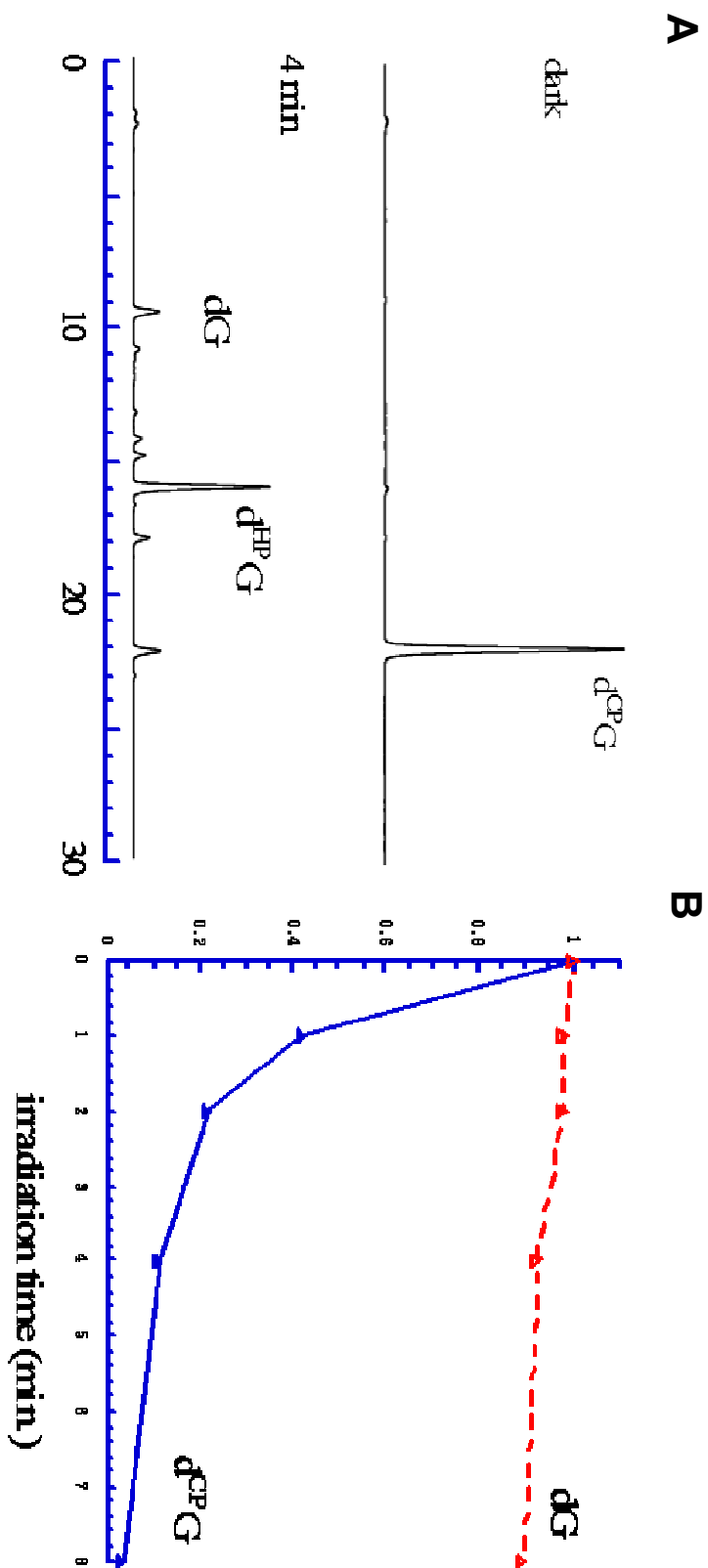
Figure 4.4. The ring-opening reaction of ^{CP}G and products.

Figure 4.5. (A) HPLC profiles of d^{CP}G oxidation by photoexcited thionine. A solution of d^{CP}G (250 μ M) and thionine (25 μ M) in 10 mM sodium phosphate (pH 7.6), 50 mM NaCl, was irradiated at 599 nm for 4 min under aerobic conditions. (B) Time course of the amount of dG and d^{CP}G remaining upon irradiation of each in the presence of thionine (25 μ M).



In order to establish CT between excited thionine and ^{CP}G embedded in duplex DNA, we have also examined trapping of the radical cation by d^{CP}G-containing DNA. The d^{CP}G-containing DNA strands are hybridized with complementary thionine-DNA conjugates in which thionine is covalently tethered at the 5'-terminus of the DNA (Figure 4.1). The DNA duplexes were irradiated at 599 nm followed by enzymatic digestion to the nucleosides. HPLC traces (Figure 4.6A) of the nucleosides clearly show the consumption of d^{CP}G accompanied by the formation of d^{HP}G. In contrast, when isopropylguanosine (d^{iPr}G) is incorporated instead of ^{CP}G, the amount of d^{iPr}G does not vary-even after 60 min irradiation (Figure 4.6B). This indicates that hole-trapping is based on the rapid ring-opening of the attached cyclopropyl group, not the lowered oxidation potential of d^{CP}G (-0.14 V compared to dG) [37,38]. These results clearly demonstrate that excited thionine produces G radical cation from a distance via electron transfer through π -stacked DNA, even though no evidence [35] of oxidative DNA damage is observed by gel electrophoresis.

To provide a comparison to our studies of distal/proximal oxidation ratios with other photooxidants, we were interested also in determining how the yield of the ring-opening trapping reaction varies as a function of distance from the tethered thionine. Figure 4.7 includes several assemblies prepared with tethered thionine as well as the distance dependence of the ^{CP}G consumption in these

assemblies. Overall, the consumption decreases with increasing distance between thionine and ^{CP}G. For example, in contrast to the rapid consumption of ^{CP}G in assembly **P**, the amount of ^{CP}G in assembly **6** remained almost unchanged even after 60 minutes of irradiation. This is also the case for DNAs with a shorter distance between two GG sites. These results indicate that BET from the proximal GG site is much faster than the rate of hole transport to the distal GG site [41,42]. Also notable is the observation that the ^{CP}G consumption rate is lowered if a mismatched base pair (**M**) is introduced at the 3'-side of the ^{CP}G. Interestingly, however, we also observe a slower consumption rate in assembly **T** than in assembly **P**, where ^{CP}G is located very close to the tethered thionine. This can be understood if the ^{CP}G ring-opening rate is slower than the rate of BET in **T**, since it is known that BET between thionine and dG in poly d(GC) occurs on the femtosecond timescale [39,43]. An analogous inverse distance dependence was observed for short distances in hole-trapping studies using photoexcited 2-aminopurine [44] and in photooxidation studies using NDI [45].

Hole-Trapping by ^{CP}G with other Photooxidants. We also examined hole-trapping of 5'-^{CP}G containing DNA by the full family of photooxidants shown in Figure 4.1.

Figure 4.6. HPLC profiles of nucleoside mixtures obtained from the enzymatic digestion of the irradiated (A) d^{CP}G-containing DNA/Th-conjugate and (B) d^{iPr}G-containing/ Th-conjugate. The duplex (5 μ M) in 10 mM sodium phosphate (pH 7.6), 50 mM NaCl was irradiated for 10 min at 599 nm under aerobic conditions, followed by enzymatic digestion.

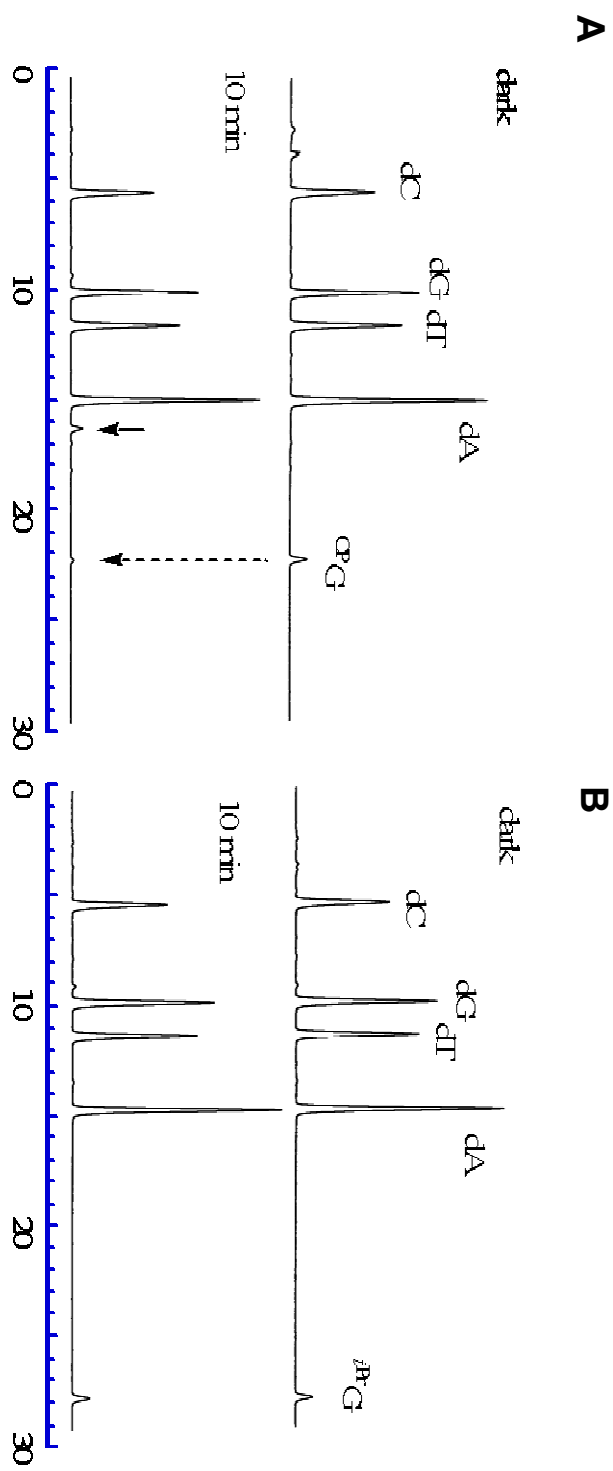
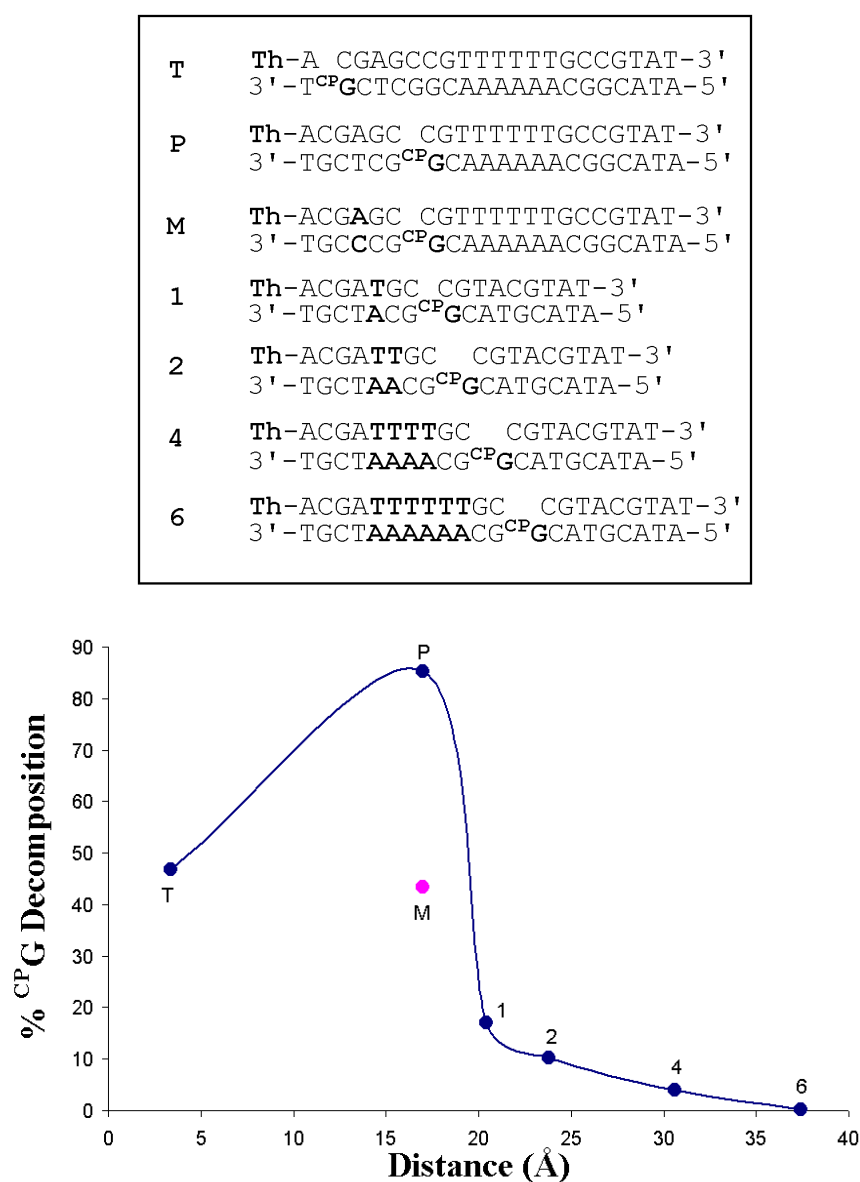


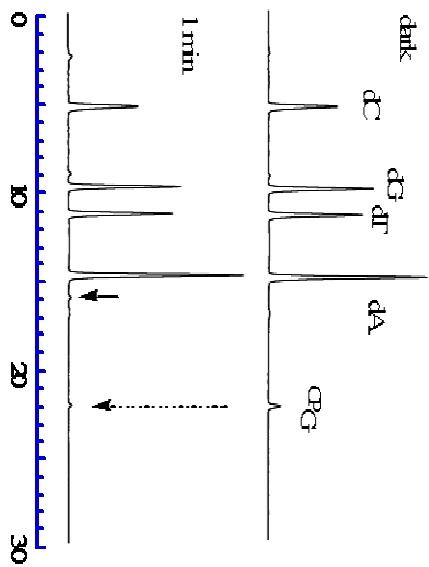
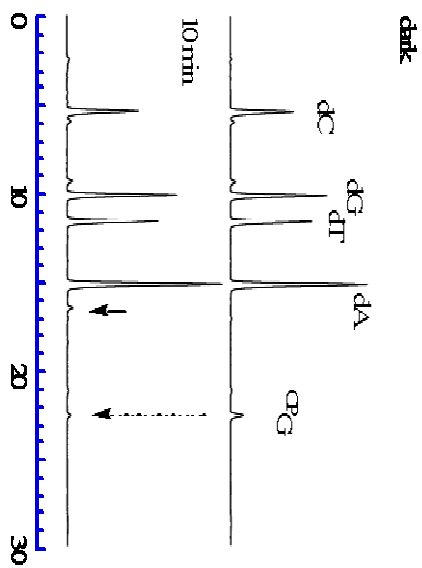
Figure 4.7. Consumption of CPG in CPG -containing DNA/Th-conjugates as a function of distance separating CPG and thionine. The sequences for the assemblies examined (top) and the plot of % CPG decomposition versus distance (bottom) are shown. In all cases, samples (5 μ M) were irradiated for 20 min at 599 nm under aerobic conditions, followed by enzymatic digestion and HPLC analysis. Note that the presence of an intervening mismatch (M) attenuates the long-range CT reaction. Also note the complex distance dependence.



As with bound thionine, the ^{CP}G-DNAs contained two 5'-GG-3' sites with an intervening A₆-tract, where one of the 5'-GG-3' sites is replaced by 5'-^{CP}GG-3'. The consumption of ^{CP}G in each strand was analyzed by HPLC after enzymatic digestion to nucleosides. Typical HPLC profiles after photooxidation are shown in Figure 4.8 for AQ-2 and Rh. With all of the photooxidants utilized, oxidation at the proximal 5'-^{CP}GG-3' site produces the known product, d^{HP}G (Figure 4.1). In contrast to rapid consumption of the proximal ^{CP}G, the distal ^{CP}G is consumed more slowly under the same reaction conditions, but yields the same product, d^{HP}G. A study under anaerobic conditions was also performed utilizing AQ-2, since oxygen has been proposed to be a key participant in the long-range chemistry of AQ [46]. Deoxygenation does not significantly attenuate trapping by ^{CP}G at the proximal site, although a slight decrease in trapping of the ^{CP}G at the distal site is observed.

Table 4.1 also summarizes the distal/proximal ratio of reaction at 5'-^{CP}GG-3' sites. Once again, Rh and Et yield higher 5'-^{CP}G distal/proximal ratios than observed for Ru or AQ. All values, however, reflect ratios that are < 1. Furthermore, for all photooxidants, the yield of this trapping reaction is two orders of magnitude higher than oxidative damage yields. Moreover, as with measurements of oxidative damage, the yields decrease with photooxidants as follows: Ru ≥ AQ > Rh > Et.

Figure 4.8. HPLC profiles of nucleoside mixtures obtained from enzymatic digestion of irradiated ^{CPG}-containing DNA assemblies functionalized with Rh and AQ. Results are shown for the assembly derivatized with ^{CPG} at the proximal site. (A) The ^{CPG}-DNA/AQ-2 duplex (5 μ M) in 10 mM sodium phosphate (pH 7) was irradiated for one minute at 350 nm followed by enzymatic digestion. (B) The ^{CPG}/Rh assembly (5 μ M) in 20 mM Tris-Cl (pH 8.1), 10 mM NaCl was irradiated at 365 nm for ten minutes followed by enzymatic digestion.

A**B**

DISCUSSION

Tethered Metallointercalators Do Not Aggregate under Assay

Conditions for DNA CT. The application of metallointercalators generally and rhodium intercalators specifically to probe long-range CT in DNA was called into question owing to the possibility of metal-promoted aggregation of DNA assemblies in solution [28]. Our experiments provide evidence against aggregation of metal-tethered DNA assemblies under the conditions where DNA CT studies are measured. We find no evidence of a slow-moving species in non-denaturing gels as would be expected if aggregation were occurring.

Additionally, direct strand cleavage controls on Rh-tethered assemblies are always performed in our laboratory in each DNA CT investigation to mark the site of Rh binding on the assembly and to establish that the reaction is intraduplex. In our experiments, these data always reveal direct strand cleavage near the duplex terminus, the tethered intercalator binding site.

The suggestion that non-denaturing gels be included as another assay of the modified DNA assemblies is nonetheless a reasonable one, especially for DNA assemblies where the binding site cannot be marked discretely as it can with the Rh photochemistry. In more recent investigations, we have been incorporating this additional control; studies of DNA CT in a DNA duplex/quadruplex assembly utilizing $[\text{Rh}(\text{phi})_2\text{bpy}']^{3+}$ as the photooxidant also

show no evidence of aggregating species in non-denaturing gels and clearly reveal one band due to the DNA duplex/quadruplex conjugate [47]. The aggregation studies performed by Sen and coworkers on DNA crossover assemblies [28] were not carried out under conditions we utilize to promote DNA CT generally nor were they carried out in a systematic fashion. In fact, the yield of the slow moving band reported cannot even account for the oxidative DNA damage yields obtained in the DNA crossovers. How aggregation models can account for differences found in oxidative damage as a function of protein binding [15,16] or with intervening mismatches [14] is also difficult to understand.

Therefore, the difference in oxidative damage yields and distal/proximal damage ratios using the photooxidants presented here is certainly not the result of the aggregation of the metallointercalators. There are, nonetheless, significant differences among photooxidants and this issue needs to be addressed. We propose that differing extents of BET can account for the differing extents of oxidative guanine damage that we observe here.

Differences in Both Yield and Distal/Proximal Damage Ratios are Found to Depend upon the Tethered Photooxidant. While differences seen with assemblies containing various photooxidants cannot be attributed to

differential aggregation, there are clear differences among them. In fact, remarkably, these studies represent the first time where various photooxidants have been compared directly with respect to long-range DNA CT. In the series examined, the lowest distal/proximal ratios are obtained with Ru and AQ, while for both Rh and Et high distal/proximal damage ratios are found. In the case of thionine, calculation of the damage ratio is moot since no oxidative damage is detected. Consistent with this finding, a correlation is seen between absolute yield of oxidative damage and distal/proximal ratio; photooxidants that produce higher damage yields overall give lower distal/proximal ratios (Table 4.1). Certainly these results establish that the use of distal/proximal damage ratios as a means of characterizing a given assembly with respect to efficiency of CT is valid only with a constant photooxidant. Comparisons in assemblies using different photooxidants reveal characteristics of the photooxidant as well as characteristics of the DNA assembly.

We first proposed that differences in the oxidative damage ratios may be based in part upon the high charge of the photooxidant affecting potentials at the proximal versus distal 5'-GG-3' sites to a differing extent [27]. Here, however, the differing ratios do not correlate with different charges on the photooxidants. Aggregation has also been eliminated as a possible explanation for the differences. Additional factors must therefore govern these dissimilar results.

Back Electron Transfer as a Distinguishing Characteristic of the

Photooxidant. Another explanation rests in the differing rates of back electron transfer (BET) for the different photooxidants. It is known that trapping of the guanine radical cation to produce irreversible products is relatively slow compared to CT. Measurements of guanine radical decay by transient absorption spectroscopy reveal a decay time on the order of milliseconds [8]. Since oxidative damage measurements by gel electrophoresis only provide a static picture of the net product yield, certainly these yield measurements may be expected to differ based upon rates of BET.

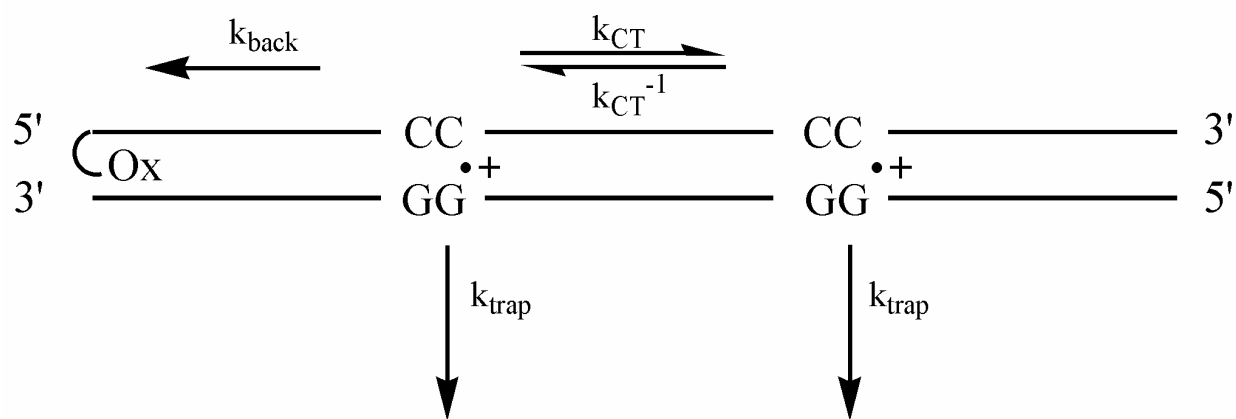
Figure 4.9 shows the full scheme for hole equilibration across a DNA assembly. Several limiting conditions should be considered. First, if the trapping reaction is much slower than the rate of CT and the potentials on the distal and proximal 5'-GG-3' guanine sites are the same, one would expect equal yield at distal and proximal sites, e.g., a distal/proximal damage ratio of 1. Conversely, if the rate of CT is limiting compared to the rate of trapping, reaction would be expected to be much greater at the proximal site, e.g., approaching a distal/proximal damage ratio of 0. As the rate of CT and rate of trapping become competitive, an intermediate distal/proximal ratio is expected.

These limiting cases, however, assume no contribution of BET. If the rate of BET is competitive with the rate of trapping but slower than CT, equilibration

across the two sites would still hold. However, as the rate of BET increases compared to trapping, indeed as it approaches the rate of CT, reaction at the proximal site should be depleted. Hence high values of the distal/proximal damage ratio exceeding values of 1 would be expected. Indeed, with Rh and Et as photooxidants, this is what we observe. In that context, thionine provides an example of an extreme. Despite a large driving force and evidence for reaction by CT chemistry, no oxidative DNA damage at either proximal or distal sites is detectable with photoexcited thionine [35]. However, fast BET in poly d(GC) by photoexcited thionine has been seen to proceed on the femtosecond timescale [39,43-44]. This rapid BET accounts for the absence of any detectable yield of oxidative DNA damage. If we examine reactions using a faster trap, however, as in the ring-opening reaction, now oxidation at a distance is evident. The overall yield of reaction necessarily depends upon the rate of BET relative to the rate of trapping.

Perhaps more interesting is the distance dependence for this oxidation reaction viewed with the fast trap as illustrated in Figure 4.7. At long distances, where BET is slow, there is an understandable decrease in reaction with increasing distance; the slope of the efficiency of reaction with distance is negative and any measure of a “distal/proximal” ratio would be < 1 .

Figure 4.9. Schematic illustrating pathways for CT in oxidant-tethered assemblies.



At short distance, however, the opposite is seen. BET over this shorter distance range becomes comparable to CT and trapping; the slope of the efficiency of reaction with distance is positive and a measure of a “distal/proximal” ratio in this regime would be > 1 . It should be noted that photoexcited 2-aminopurine similarly shows no yield in oxidative DNA damage, reflecting a high rate of BET, and with this photooxidant as well, an inverse distance dependence in cyclopropyl guanosine ring-opening is found at short distances [44]. Furthermore, photooxidation experiments with NDI show guanine oxidation to correlate with the lifetime of the charge separated state and not the distance separating the oxidant and its substrate [45].

The other photooxidants surely have BET rates slower than that of thionine since oxidative DNA damage can be seen. Nonetheless, as one would expect if BET is a dominating factor in comparing these photooxidants, their quantum yields for oxidative DNA damage vary in the order $Ru > AQ > Rh > Et$, and similarly the distal/proximal guanine damage ratios vary $Ru = AQ < Rh < Et$. Just as the quantum yields for oxidative damage for Rh and Et are lower than for Ru and AQ, the distal/proximal ratios are higher for Rh and Et versus Ru and AQ. Importantly, then, if rates of BET for the Rh and Et photooxidants approach rates of CT, then reaction with these oxidants at the proximal site is expected to be depleted, and distal/proximal damage ratios are expected to increase. Indeed,

this is what we observe. Hence, faster rates of BET for Rh and Et relative to those for Ru and AQ account well for the differing ratios and quantum yields we observe.

It is worth noting that the energetics of the redox reactions for formation and disappearance of the guanine radical also support the idea that the kinetics of BET are fundamental in determining the yield of guanine damage at a distance. For Rh and AQ, oxidation of G is accomplished from the excited states, which have energies of +2.0 eV and +2.7 eV for photoexcited Rh [48] and AQ (triplet state) [49], respectively. The driving forces for photooxidation of G (1.3 V) [50] are 0.7 eV for Rh and 0.6 eV for AQ [51]. In the case of the reduction of one-electron oxidized guanine by the reduced intercalator (i.e., the back reaction), the driving force would be 1.3 eV for Rh and 2.1 eV for AQ. Estimates of the reorganization energy for DNA systems vary, but assuming a reorganizational energy of ~ 1 eV for these through-DNA ET processes [25] the forward CT reaction (charge injection) for both AQ and Rh will lie in the normal region, while BET will lie in the inverted region [52]. However, BET should be more inverted for AQ. Additionally, formation of a triplet ion pair with AQ will further slow BET. Thus inspection of the energetics suggests that BET should be considerably slower for AQ than for Rh.

Implications and Conclusions. These studies provide the first direct comparison of DNA CT reactions using a variety of DNA-bound photooxidants. Significant differences are apparent using the different photooxidants. These differences cannot be attributed to artifacts associated with aggregation of intercalators. Instead, comparisons in assemblies using different photooxidants reveal CT characteristics of the photooxidant as well as CT characteristics of the DNA assembly. A dominating feature of the photooxidant may be its efficiency in carrying out BET. Complementary studies examining long-range CT utilizing a significantly faster trap than oxidative DNA damage highlight the importance of BET in attenuating yields of oxidative damage and relative yields at distal versus proximal sites. Results with thionine are perhaps most illustrative, where no oxidative DNA damage is observed using the slow guanine radical trap, and a complex distance dependence is observed in the oxidative reaction using a fast radical trap. The results presented here underscore that oxidative damage yields cannot be utilized alone to estimate the forward rate of DNA CT. BET should be considered as a critical parameter in characterizing long-range CT through DNA.

REFERENCES

1. Hall, D. B.; Holmlin, R. E.; Barton, J. K. *Nature* **1996**, *382*, 731-735.
2. Saito, I.; Takayama, M.; Sugiyama, H.; Nakatani, K.; Tsuchida, A.; Yamamoto, M. *J. Am. Chem. Soc.* **1995**, *117*, 6406-6407.
3. a) Hall, D. B.; Kelley, S. O.; Barton, J. K. *Biochemistry* **1998**, *37*, 15933-15940.
b) Kurbanyan, K.; Nguyen, K. L.; To, P.; Rivas, E. V.; Lueras, A. M. K.; Kosinski, C.; Steryo, M.; González, A.; Mah, D. A.; Stemp, E. D. A. *Biochemistry* **2003**, *42*, 10269-10281.
4. Gasper, S. M.; Schuster, G. B. *J. Am. Chem. Soc.* **1997**, *119*, 12762-12771.
5. Nakatani, K.; Dohno, C.; Saito, I. *J. Am. Chem. Soc.* **1999**, *121*, 10854-10855.
6. Giese, B. *Acc. Chem. Res.* **2000**, *33*, 631-636.
7. Arkin, M. R.; Stemp, E. D. A.; Pulver, S. C.; Barton, J. K. *Chem. Biol.* **1997**, *4*, 389-400.
8. a) Stemp, E. D. A.; Arkin, M. R.; Barton, J. K. *J. Am. Chem. Soc.* **1997**, *119*, 2921-2925. b) Nguyen, K. L.; Steryo, M.; Kurbanyan, K.; Nowitzki, K. M.; Butterfield, S. M.; Ward, S. R.; Stemp, E. D. A. *J. Am. Chem. Soc.* **2000**, *122*, 3585-3594.
9. Wagenknecht, H.-A.; Rajski, S. R.; Pascaly, M.; Stemp, E. D. A.; Barton, J. K. *J. Am. Chem. Soc.* **2001**, *123*, 4400-4407.
10. Pascaly, M.; Yoo, J.; Barton, J. K. *J. Am. Chem. Soc.* **2002**, *124*, 9083-9092.

11. Sugiyama, H.; Saito, I. *J. Am. Chem. Soc.* **1996**, *118*, 7063-7068.
12. Nùñez, M. E.; Hall, D. B.; Barton, J. K. *Chem Biol.* **1999**, *6*, 85-97.
13. Henderson, P. T.; Jones, D.; Hampikian, G.; Kan, Y.; Schuster, G. B. *Proc. Natl. Acad. Sci. USA* **1999**, *96*, 8353-8358.
14. Bhattacharya, P. K.; Barton, J. K. *J. Am. Chem. Soc.* **2001**, *123*, 8649-8656.
15. Rajski, S. R.; Kumar, S.; Roberts, R. J.; Barton, J. K. *J. Am. Chem. Soc.* **1999**, *121*, 5615-5616.
16. Rajski, S. R.; Barton, J. K. *Biochemistry* **2001**, *40*, 5556-5564.
17. Kelley, S. O.; Boon, E. M.; Barton, J. K.; Jackson, N. M.; Hill, M. G. *Nucleic Acids Res.* **1999**, *27*, 4830-4837.
18. Boon, E. M.; Ceres, D. M.; Drummond, T. G.; Hill, M. G.; Barton, J. K. *Nature Biotech.* **2000**, *18*, 1096-1100.
19. Boon, E. M.; Salas, J. E.; Barton, J. K. *Nature Biotech.* **2002**, *20*, 282-286.
20. Drummond, T. G.; Hill, M. G.; Barton, J. K. *Nature Biotech.* **2003**, *21*, 1192-1199.
21. Nùñez, M. E.; Holmquist, G. P.; Barton, J. K. *Biochemistry* **2001**, *40*, 12465-12471.
22. Nùñez, M. E.; Noyes, K. T.; Barton, J. K. *Chem. Biol.* **2002**, *9*, 403-415.
23. Boon, E. M.; Livingston, A. L.; Chmiel, N. H.; David, S. S.; Barton, J. K. *Proc. Natl. Acad. Sci. USA* **2003**, *100*, 12543-12547.

24. a) Giese, B. *Annu. Rev. Biochem.* **2002**, *71*, 51-70. b) Schuster, G. B. *Acc. Chem. Res.* **2000**, *33*, 253-260. c) Delaney, S.; Barton J. K. *J. Org. Chem.* **2003**, *68*, 6475-6483.
25. a) Renger, T.; Marcus, R. A. *J. Phys. Chem. A* **2003**, *107*, 8404-8419. b) Bixon, M.; Jortner, J. *Chem. Phys.* **2002**, *281*, 393-408. c) Grozema, F. C.; Berlin, Y. A.; Siebbeles, L. D. A. *J. Am. Chem. Soc.* **2000**, *122*, 10903-10909.
26. Williams, T. T.; Odom, D. T.; Barton, J. K. *J. Am. Chem. Soc.* **2000**, *122*, 9048-9049.
27. Williams, T. T.; Barton, J. K. *J. Am. Chem. Soc.* **2002**, *124*, 1840-1841.
28. Fahlman, R. P.; Sharma, R. D.; Sen, D. *J. Am. Chem. Soc.* **2002**, *124*, 12477-12485.
29. Santhosh, U.; Schuster, G. B. *J. Am. Chem. Soc.* **2002**, *124*, 10986-10987.
30. Franklin, S. J.; Treadway, C. R.; Barton, J. K. *Inorg. Chem.* **1998**, *37*, 5198-5210.
31. Beaucage, S. L.; Caruthers, M. H. *Tetrahedron Lett.* **1981**, *22*, 1859-1862.
32. Holmlin, R. E.; Dandliker, P. J.; Barton, J. K. *Bioconjugate Chem.* **1999**, *10*, 1122-1130.
33. Kelley, S. O.; Holmlin, R. E.; Stemp, E. D. A.; Barton, J. K. *J. Am. Chem. Soc.* **1997**, *119*, 9861-9870.

34. Sambrook, J.; Fritsch, E. F.; Maniatis, T. *Molecular Cloning: A Laboratory Manual*, 2nd ed., Cold Spring Harbor Laboratory, New York, **1989**.
35. Dohno, C.; Stemp, E. D. A.; Barton, J. K. *J. Am. Chem. Soc.* **2003**, *125*, 9586-9587.
36. Wan, C.; Fiebig, T.; Kelley, S. O.; Treadway, C. R.; Barton, J. K.; Zewail, A. *H. Proc. Natl. Acad. Sci. USA* **1999**, *96*, 6014-6019.
37. Nakatani, K.; Dohno, C.; Saito I. *J. Am. Chem. Soc.* **2001**, *123*, 9681-9682.
38. Dohno, C.; Ogawa, A.; Nakatani, K.; Saito I. *J. Am. Chem. Soc.* **2003**, *125*, 10154-10155.
39. a) Tuite, E. M.; Kelly, J. M. *J. Photochem. Photobiol. B Biol.* **1993**, *21*, 103-124.
b) Tuite, E. M.; Kelly, J. M.; Beddard, G. S.; Reid, G. S. *Chem. Phys. Lett.* **1994**, *226*, 517-524.
40. Saito, I.; Inoue, K.; Matsuura, T. *Photochem. Photobiol.* **1975**, *21*, 27-30.
41. Lewis F. D.; Wu, T.; Letsinger, R. L.; Wasielewski, M. R. *Acc. Chem. Res.* **2001**, *34*, 159-170.
42. The rate for hole hopping between two single Gs separated by two AT base pairs was estimated to be $\geq 10^6 \text{ s}^{-1}$ [24].
43. Reid, G. D.; Whittaker, D. J.; Day, M. A.; Turton, D. A.; Kayser, V.; Kelly, J. M.; Beddard, G. S. *J. Am. Chem. Soc.* **2002**, *124*, 5518-5527.

44. O'Neill, M. A.; Dohno, C.; Barton, J. K. *J. Am. Chem. Soc.* **2004**, *126*, 1316-1317.
45. Kawai, K.; Takada, T.; Nagai, T.; Cai, X.; Sugimoto, A.; Fujitsuka, M.; Majima, T. *J. Am. Chem. Soc.* **2003**, *125*, 16198-16199.
46. Ly, D.; Kan, Y.; Armitage, B.; Schuster, G. B. *J. Am. Chem. Soc.* **1996**, *118*, 8747-8748.
47. Delaney, S.; Barton, J. K. *Biochemistry* **2003**, *42*, 14159-14165.
48. Turro, C.; Evenzhav, A.; Bossmann, S. H.; Barton, J. K.; Turro, N. J. *Inorg. Chim. Acta* **1996**, *243*, 101-108.
49. Armitage, B.; Yu, C.; Devadoss, C.; Schuster, G. B. *J. Am. Chem. Soc.* **1994**, *116*, 9847-9859.
50. Steenken, S.; Jovanovic, S. V. *J. Am. Chem. Soc.* **1997**, *119*, 617-618.
51. Driving force values for redox processes with AQ are based on calculations from reference 49, but utilize the oxidation potential of G reported [50] by Steenken and Jovanovic.
52. Marcus, R. A.; Sutin, N. *Biochim. Biophys. Acta* **1985**, *811*, 265-322.

CHAPTER 5

Probing the Effects of Bridge Energetics on Long-Range Charge Transport in DNA

INTRODUCTION

At the heart of the DNA double helix is the aromatic, heterocyclic array of stacked base pairs. As elucidated in Chapter 1, since the delineation of the structure of DNA in 1953 [1], its π -stack has piqued the interest of scientists who wanted to explore the possibility of DNA conductivity, and who have since performed extensive measurements in attempts to delineate the molecule's conductivity; it is now generally believed that DNA possesses conductivity comparable to that of a large band gap semiconductor (Chapter 1, reference [2]).

A variety of experimental systems in which DNA served as the bridge between intercalated donor-acceptor moieties demonstrated that electron transfer could occur over distances greater than 40 Å [3,4]. Additional studies in which DNA was both the bridge and reactant have shown that charge transport (CT) can proceed long molecular distances (i.e., over 200 Å) and is sensitive to the π -stacking of the bases [5,6]. Although numerous reports have since substantiated the ability of DNA to support charge transport (Chapters 1 and 4 and references [7-11]), the data are conflicting, hence leading to varied conclusions about the mechanism of DNA-mediated charge transport.

Superexchange is a mechanism in which electron transfer occurs *via* the high-lying empty orbitals of a bridge (e.g. DNA) [12,13]. It is a nonadiabatic process in which the electron/hole simply "tunnels" through the barrier (i.e., the

DNA bases; the bridge elements), to the acceptor molecule. The electron transfer rate, described in (1), in such a system decays exponentially with increasing distance between donor and acceptor [14]. Moreover, the energy gap that exists between the donor orbitals and those bridge elements involved in the electron transfer process is fairly substantial compared to the *direct* coupling between the bridge and the donor [15]. There is no occupation of the bridge and hence no transient species formed during the charge transport from donor to acceptor.

$$k_{ET} = k_0 e^{-\beta r} \quad (1)$$

where k_{ET} is the rate of electron transfer, k_0 is a constant that is characteristic of the donor/acceptor pair and r is the distance separating the donor and acceptor.

A contentious parameter from (1) in regards to DNA CT is the value of β , which provides a measurement of the weakening of electronic coupling with increasing donor-acceptor distance. β values ranging from 1.0 \AA^{-1} to 1.4 \AA^{-1} have been observed in proteins [16], and thus superexchange has been successfully utilized to describe the electron transfer process in proteins. However, in DNA-mediated CT studies, measurements of β have ranged from $\leq 0.1 \text{ \AA}^{-1}$ to $> 1.4 \text{ \AA}^{-1}$ [17-19]. Therefore, an exclusive superexchange mechanism has not been able to adequately delineate DNA-mediated charge transport observations in which the rate of charge transport appears to have a shallow distance dependence and has been found to be unchanged over a range of distances [4,20,21]. It appears that

lower values of β (e.g., 0.2 \AA^{-1}) will be expected for those systems in which the oxidant is well-coupled into the π -stack [4,5,20].

A corollary to the superexchange mechanism proffered by Felts *et al.* to elucidate the shallow distance dependencies observed by Barton *et al.* is multi-level Redfield theory [22]. This theory incorporates a high-frequency oscillator into the DNA CT proposal and couples the system to a thermal bath. These incorporated elements lead to a thermal population of the bridge, which opens an adiabatic channel for distance independent electron transfer.

Hopping is yet another mechanism proposed for long-range charge transport. In this mechanism, the electron/hole *does* occupy the bridge, discreetly hopping from the molecular orbitals localized on the bases; thus, the donor and the acceptor do not need to be well coupled. If the rate of charge migration is faster than trapping, the charge would be able to migrate long distances before it is trapped in a site of low oxidation potential [5].

Most proposals combine, to varying extents, the ideas of superexchange and hopping. For example, Giese *et al.* proposed that the mechanism of charge transport occurs via tunneling through AT steps and hopping from G sites [23]. This initial conclusion was drawn because of the ease of guanine oxidation [24-26]. Although they have since modified this proposal to include hopping

amongst adenines, they still are proponents of a single nucleotide hopping process (Chapter 2).

Schuster *et al.* has provided another theoretical proposition in regards to charge transport. They propose that the mechanism of DNA CT is by phonon-assisted polaron hopping [27]. They contend that the introduction of a hole into the DNA induces structural distortions that lead to self-trapping of the charge. These deformations consist of the reduction in the intra-base distance, the unwinding of DNA, hence leading to more efficacious π -overlap of the bases and radical cation stabilization, and the change in the position of the hydrogen bonding between the bases. These are the elements of the polaron. The hopping portion comes from thermal fluctuations, in which bases enter and leave the polaron (i.e. phonon-assisted hopping). However, we contend that charge injection into inherent, dynamically defined DNA domains better characterize DNA-mediated charge transport, in which the charge is injected into domains that are sequence-dependent (Chapter 2).

Although these models attempt to form a comprehensive view of the mechanism of DNA CT, further investigations of the innate characteristics of various DNA sequences (e.g., dynamics) and oxidants must be performed so that these influential features are incorporated into mechanistic proposals. In moving towards this goal, here we study the effects of intervening bridge energetics on

DNA CT using the excited state photooxidant $[\text{Rh}(\text{phi})_2\text{bpy}']^{3+}$. Charge transport using rhodium conjugates involves charge injection from an oxidant whose excited state has the ability to oxidize all of the DNA bases.

EXPERIMENTAL

Preparation of the Oligonucleotides

The DNA oligonucleotides were prepared using standard phosphoramidite chemistry. Utilizing an Applied Biosystems 392 DNA/RNA synthesizer, the oligonucleotides were synthesized using 1000 Å columns and with a dimethoxy trityl-protecting group on the 5' end of the strand. The oligonucleotides were then purified on a RAININ Dynamax (300 Å) C₁₈ column using reverse phase HPLC (40 mM NH₄OAc, pH 7.6, 5-30% acetonitrile over 30 minutes). The purified strands were deprotected by incubation in 80% acetic acid for exactly 15 minutes, followed by an addition of 3 volumes of 100% ethanol (absolute). The solvent was then removed *in vacuo*. Upon lyophilization, the oligonucleotides were purified once more utilizing the same column and conditions as stated previously. The quantification of the oligonucleotides was performed using UV-visible absorption spectroscopy on a Beckman DI 7400 Spectrophotometer. The phosphoramidite chemicals and columns were purchased from Glen Research.

Synthesis of the Metal Complex, [Rh(phi)₂bpy']³⁺

[Rh(phi)₂bpy']³⁺ (phi = phenanthrenequinone diimine; bpy' = 4-butyric acid-4-methylbipyridine) was synthesized in accordance with published procedures [28].

Preparation of Metal-Conjugated Oligonucleotides

The metal-conjugated assemblies were prepared in accordance to published procedures [29]. The resulting rhodium-conjugated oligonucleotides were purified on a RAININ Dynamax (300 Å) C₁₈ column using reverse phase HPLC (40 mM NH₄OAc, pH 7.6, 5-35% acetonitrile over 35 minutes). The absolute stereochemical configurations of the metal-conjugated oligonucleotides were determined by circular dichroism. The rhodium-conjugates were quantified using UV-visible spectroscopy using the following extinction coefficient: ϵ (350 nm, M⁻¹ cm⁻¹) = 23,500.

Irradiation of the Metal-Conjugated Oligonucleotides

The complementary oligonucleotides were radioactively labeled using γ -³²P ATP and T4 polynucleotide kinase. The salts were removed using P-6 Tris chromatography columns. The strands were subsequently treated with a 10% piperidine solution (v/v) and heated to 90 °C for exactly 30 minutes. The resulting radioactive oligonucleotides were dried under vacuum. The strands

were purified using gel electrophoresis in a 20% denaturing polyacrylamide gel. The bands were exposed by autoradiography, excised, and crushed. The radioactive labels were then extracted 3 times with 400 μ l of 50 mM NH_4OAc (heating to 37°C for 20 minutes each) and purified once more with P-6 Tris chromatography columns. The amount of radioactivity for each strand was determined using a Beckman liquid scintillation counter.

The labeled strands were annealed to the rhodium-modified oligonucleotides (1 μ M) in the presence of cold complementary strands (1 μ M), in 20 mM Tris-Cl buffer (pH 8) and 10 mM NaCl. For irradiation of the rhodium conjugates, 30 μ l samples were irradiated at 313 nm for ten minutes and 365 nm for one hour using a 1000 W Hanovia Hg-Xe arc lamp, which had a monochromator. Dark control samples were kept in the dark and were not irradiated. The resulting 365 nm and dark control samples were treated with a 10% piperidine solution (v/v) for 30 minutes at 90 °C. All of the irradiated samples were subsequently dried and analyzed by 20% PAGE analysis. The amount of cleavage was determined by phosphorimager using ImageQuant. The distal 5'-G was normalized to that of the proximal 5'-G. The amount of background damage was subtracted from the normalized value for each of the duplexes.

RESULTS AND DISCUSSION

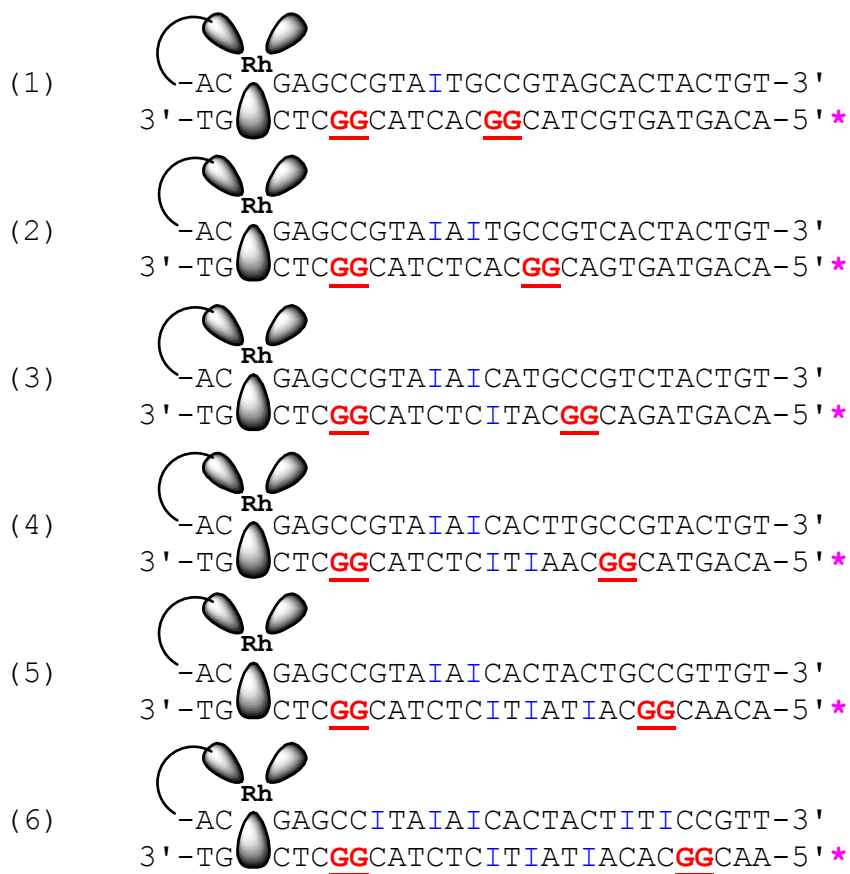
Design of assemblies

Figure 5.1 illustrates the duplexes investigated in this study utilizing $[\text{Rh}(\text{phi})_2\text{bpy}']^{3+}$ as the photooxidant. Each duplex contains identical 5'-CGGC-3' sites both proximal and distal to the photooxidant. The proximal site remains a constant 14 Å from the rhodium intercalation site, whereas the distal site is marched out in two base pair increments up to a distance of 75 Å. The sequences were modeled after those found in a previous investigation in which a shallow distance dependence was observed [5].

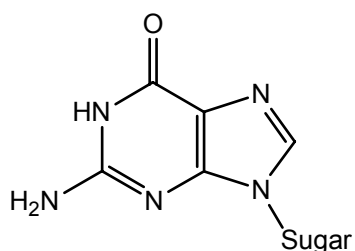
Bridge energetics using the $[\text{Rh}(\text{phi})_2\text{bpy}']^{3+}$ photooxidant

With an estimated redox potential of ~2.0 V vs. NHE [31], the $[\text{Rh}(\text{phi})_2\text{bpy}']^{3+}$ photooxidant has the ability to oxidize all of the DNA bases. Initial thoughts in regards to charge transport presumed that, upon charge injection and regardless of the oxidant, the hole relaxes to the average ionization potential of the bridge and thus the yield of charge transport would be dependent upon distance and sequence.

Figure 5.1. A schematic illustration of the DNA sequences utilized in this investigation and structures of guanine and inosine. The photooxidant $[\text{Rh}(\text{phi})_2\text{bpy}']^{3+}$ was covalently tethered to one end of the DNA and its complementary sequence containing the guanine doublet sites was ^{32}P labeled at the 5' end, which is noted by *. The bridge energy was raised by including inosine, which has an oxidation potential of ~ 1.5 V vs. NHE [30], whereas guanine is ~ 1.3 V vs. NHE [24].



Guanine



Inosine

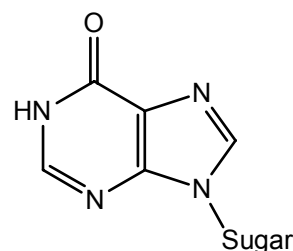


Figure 5.2. The long-range oxidation of 5'-³²P-end labeled DNA using Δ -[Rh(phi)₂bpy']³⁺ after 20% denaturing PAGE and phosphorimagery. For each sequence, the first two lanes are Maxam-Gilbert sequencing lanes. The 313 nm lane is the result of direct photocleavage after 10 minutes of irradiation at 313 nm. The 365 nm lane delineates oxidation after one hour of irradiation at 365 nm and followed by 10 % aqueous piperidine treatment. Dark lanes are samples that were prepared analogously to the irradiated 365 nm samples but were not irradiated and treated with piperidine. The samples contained the following: 1 μ M Rh-modified duplex, 20 mM Tris-Cl (pH 8), and 10 mM NaCl. The arrow delineates the proximal site, whereas, the boxes show the distal 5'-GG-3' site being marched out in 2 base pair increments.

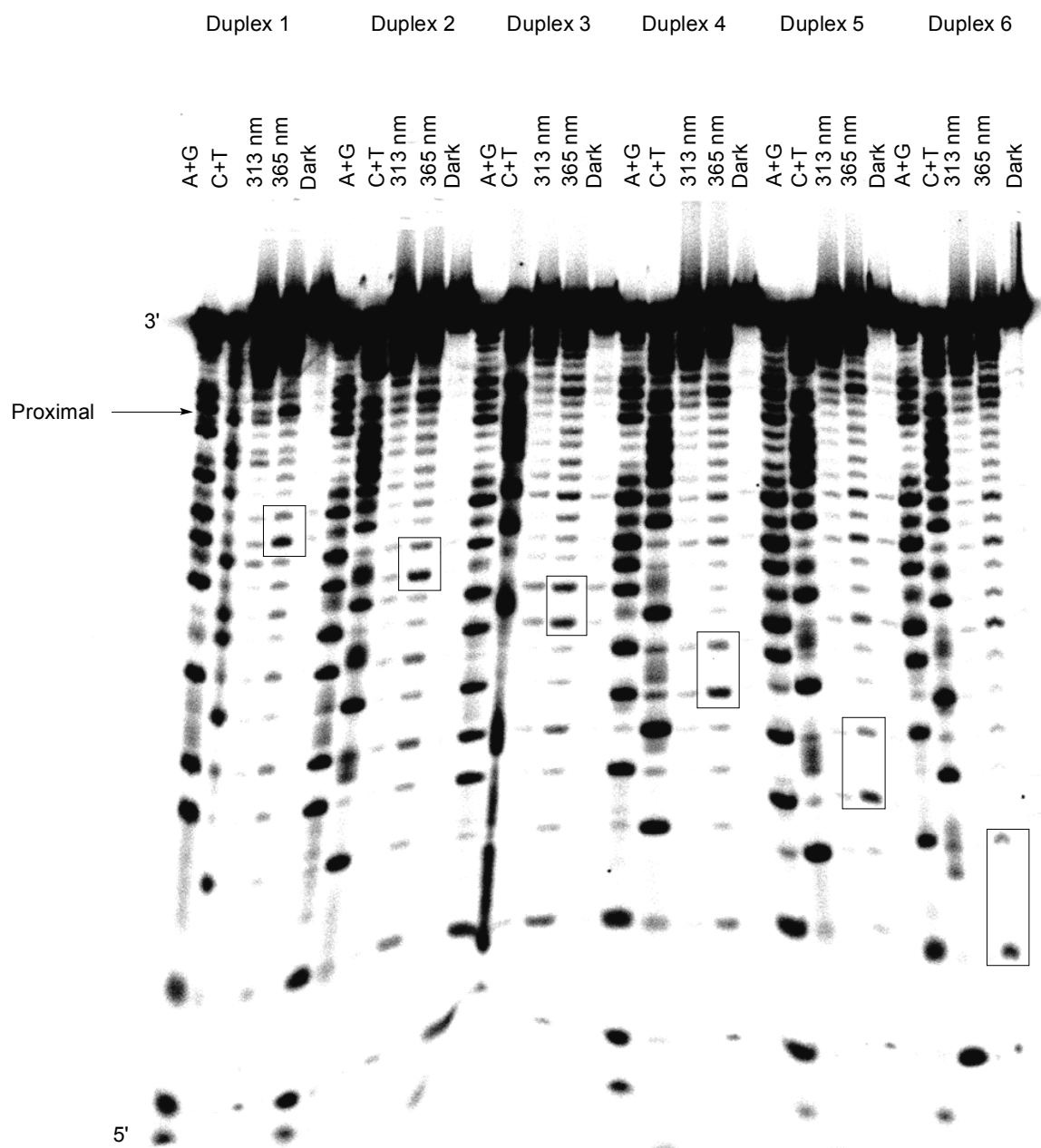
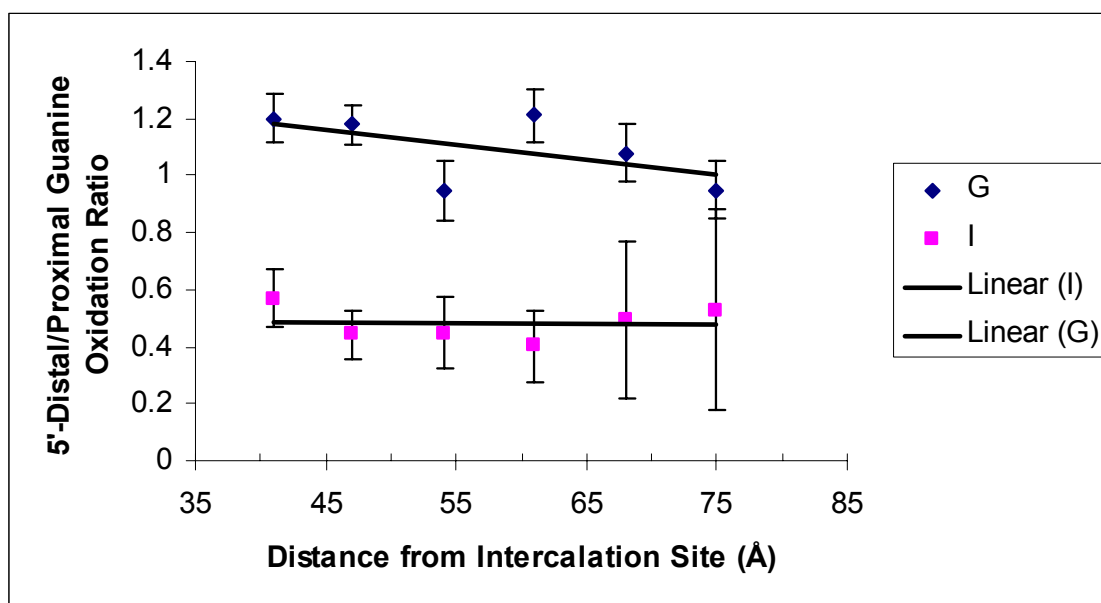


Figure 5.3. Plot of the 5'-G distal/proximal ratio versus distance from the intercalation site of Δ -[Rh(phi)₂bpy']³⁺. The G data, in which guanine bases are intervening between two 5'-CGGC-3' sites, are adapted from [5]. The I data, which has intervening inosine bases (Figure 5.1), reflect the result of three trials. Note the extremely modest decrease with increasing distance from 41 to 75 Å.



Thus we decided to investigate the attenuation in oxidative damage yield upon increasing the ionization potential of six 28 base-pair DNA bridges by the introduction of inosine, a guanine base analog that possesses a higher oxidation potential (~ 1.5 V vs. NHE) [30] than that of guanine (~ 1.3 vs. NHE) [24]. Figures 5.2 and 5.3 illustrate the effect on guanine oxidation of the addition of intervening inosines between two oxidatively sensitive 5'-GG-3' sites upon irradiation at 365 nm, treatment with piperidine, and phosphorimagery. To account for differential gel loading, the yield of oxidative damage at the distal site was normalized to that of the proximal site.

The concomitant addition of inosine steps and increase in distance between the proximal and distal guanine sites from 41 Å to 75 Å did not result in a marked decrease in the oxidative damage yield for the rhodium conjugates (Figure 5.3). In fact, the shallow distance dependence was analogous to that previously observed [5 and Figure 5.3]. Although the plot shows a slight decrease in the distal/proximal ratio from that previously obtained [5] and rather large experimental variance at 68 Å and 75 Å, all could be a result of the increasing inosine steps adding more duplex instability due to the loss of a hydrogen bond. However, a shallow distance dependence is observed. The high oxidation potential of rhodium may allow for direct charge injection into higher energy states of the intervening bridge medium and thus the inosine barrier may

be insufficient in buffering DNA CT utilizing this photooxidant. Indeed, as described in Chapter 4, the properties of the oxidant do play a pivotal role in modulating charge transport yields.

Parallel investigations have also been performed that explored the addition of *low* energy sites intervening between two 5'-GG-3' sites, utilizing covalently tethered $[\text{Rh}(\text{phi})_2\text{bpy}']^{3+}$ [32]. The investigation found that the addition of an intervening 5'-GGG-3', a single 5'-G-3', an 8-oxoguanine, or a deazaguanine did little to diminish oxidative damage yields at the 5'-GG-3' sites. In fact, the studies found that having an intervening deazaguanine, which has an estimated oxidation potential of ~ 1.0 V vs. NHE [33], resulted in a *higher* distal/proximal ratio. The importance of intervening bridge energetics and the photooxidant characteristics was further reiterated in the study of Nakatani *et al.* in which a cyanobenzophenone-substituted uridine ($^{\text{CNBP}}\text{U}$) was utilized as the oxidant with an intervening deazaguanine (^zG), deazaadenine (^zA), adenine (A) or guanine (G) contained in a TTBTT bridge, where *B* is one of the aforementioned bases, that was situated between two 5'-GGG-3' sites [34]. The 5'-G distal/proximal ratio increased in the order $\text{A} < ^z\text{A} < \text{G}$. Interestingly, the incorporation of a ^zG resulted in *complete* trapping of the charge at the ^zG site.

Although the $^{\text{CNBP}}\text{U}$ is able to perform long-range charge transport, its photochemical characteristics are not as well defined as those delineated for the

phi complexes of rhodium or the dppz complexes of ruthenium. Furthermore, it is not entirely clear that the $^{\text{CNBP}}\text{U}$ is as well coupled into the π -stack as other intercalating oxidants (e.g., anthraquinones, $[\text{Rh}(\text{phi})_2\text{bpy}']^{3+}$, $[\text{Ru}(\text{phen})(\text{dppz})(\text{bpy}')^{2+}$, etc.). Therefore the oxidative damage yield of $^{\text{CNBP}}\text{U}$ may be more compromised than that of the rhodium or ruthenium metallointercalators or other intercalators generally used in DNA CT studies. For instance, the poor stacking of the $^{\text{CNBP}}\text{U}$ may make it more vulnerable to variations in bridge energetics, as was evident in a report that investigated charge transport through a series of A/T steps (Chapter 2 and reference [11]).

The temperature dependence of long-range oxidation in the presence of bridging inosines and utilizing the $[\text{Rh}(\text{phi})_2\text{bpy}']^{3+}$ photooxidant

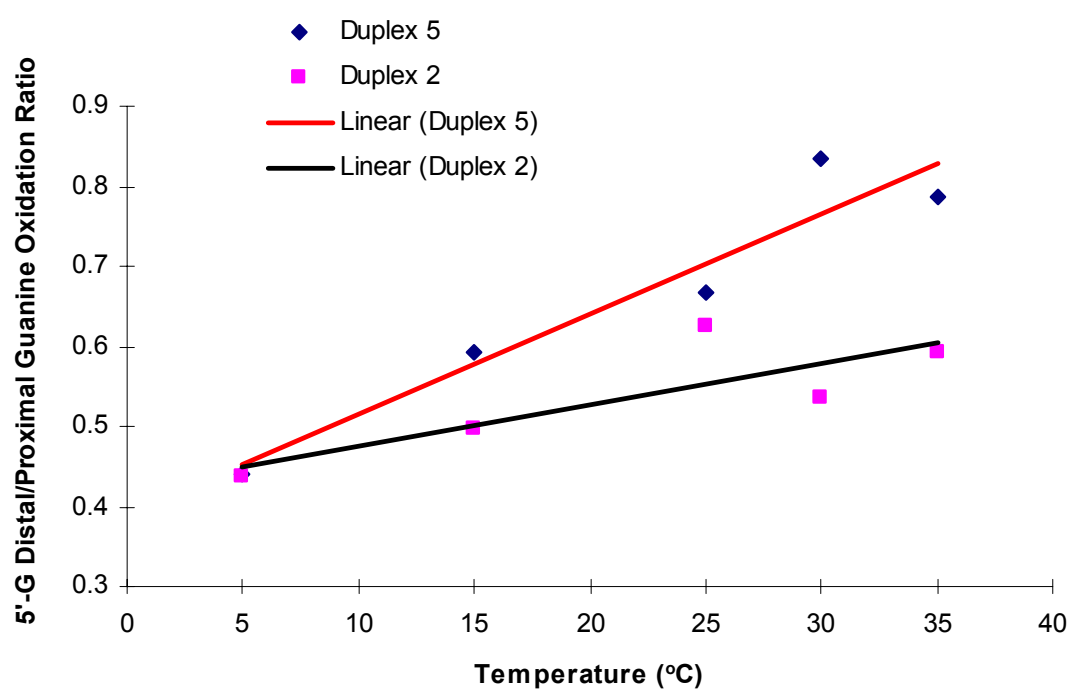
DNA is a dynamic molecule whose motions are proving to play an important role in modulating long-range CT [35]. As previously discussed in Chapter 1, a spectroscopic investigation of ethidium/deazaguanine assemblies delineated both 5 and 70 picosecond (ps) components, which was attributed to direct charge transport for those assemblies properly aligned and the timescale of ethidium motion within its intercalation site, hence leading to repositioning of the oxidant for CT, respectively [36]. Additionally, temperature studies, utilizing femtosecond spectroscopy to examine base-base CT between Ap^* and G, found

that base dynamics play an important role in modulating DNA CT yields and hence can also serve as gates of charge transport [37].

We also wanted to examine the temperature dependence and thus explore the effect of dynamics on DNA CT initiated by our higher energy rhodium conjugates. Assemblies 2 and 5 were chosen for study (Figure 5.1). In general, increases in distal/proximal ratios were observed in both assemblies with increasing temperature (Figure 5.4). At the lower temperatures, less efficient charge transport, as delineated by oxidative damage yield, occurs because of decreased DNA dynamics; this leads to a decrease in the probability of the DNA to be positioned in a conformation(s) that leads to efficacious CT (Chapter 2). However, at higher temperatures, the increased dynamics aid DNA CT for they allow those duplexes not properly configured upon charge injection to adopt other conformations that lead to more amenable electronic communication via the π -stack and thus permit the propagation of charge [35].

The temperature studies here and other investigations underscore the need for theoretical models that include the inherent contribution of DNA dynamics to CT. There are hints that if Nature does indeed take advantage of DNA CT that it probably *exploits* these DNA dynamics; for example, if the importance of CT within the cell is realized, perhaps Nature could take

Figure 5.4. A temperature dependence plot of 5'-G distal/proximal ratio for Assembly 2 and 5 (Figure 5.1). Utilizing both duplexes, an increase in distal guanine damage occurs with a concomitant decrease in proximal damage.



advantage of the flexibility of 5'-TA-3' sequences [38], the curvature of A-tracts [39], or the sequence-dependent localization or delocalization of introduced charge [40], hence utilizing all as means to protect critical genes from oxidative damage. Thus it is necessary to continue biochemical and spectroscopic investigations of sequence-dependent CT dynamics and energetics and to incorporate these elements into theoretical models to accurately provide a holistic description of the mechanism of DNA CT.

CONCLUSION

While we have emphasized the importance of back electron transfer and the photochemical characteristics of the photooxidant employed in DNA CT investigations (Chapter 4), one must also incorporate the overall bridge energetics of the DNA medium in attenuating the CT process. This was certainly underscored in studies utilizing the ^{CNBP}U oxidant, which appears to be extremely sensitive to the energetic identity of intervening bridge elements, whereas the ability of the [Rh(phi)₂bpy']³⁺ complex to oxidize all bases allows it to have energetic access to higher lying orbitals of the DNA bridge. Hence, studies are currently underway to examine whether rhodium *does* actually occupy all bases during the CT process.

REFERENCES

1. Watson, J.D.; Crick F. H. C. *Nature* **1953**, *171*, 737-738.
2. Dekker, C.; Ratner, M. A. *Physics World* **2001**, 29-33.
3. Murphy, C. J.; Arkins, M. R.; Jenkins, Y.; Ghatlia, N. D.; Bossman, S.; Turro, N. J.; Barton, J. K. *Science* **1993**, *262*, 1025-1029.
4. Arkin, M. R.; Stemp, E. D. A.; Holmlin, R. E.; Barton, J. K.; Hörmann, A.; Olson, E. J. C.; Barbara, P. F. *Science* **1996**, *273*, 475-480.
5. Núñez, M. E.; Hall, D. B.; Barton, J. K. *Chem. Biol.* **1998**, *6*, 85-97.
6. Henderson, P. T.; Jones, D.; Hampikian, G.; Kan, Y.; Schuster, G. B. *Proc. Natl. Acad. Sci. USA* **1999**, *96*, 8353-8358.
7. Núñez, M. E.; Barton, J. K. *Curr. Opin. Chem. Biol.* **2000**, *4*, 199-206.
8. Lewis, F. D.; Letsinger, R. L.; Wasielewski, M. R. *Acc. Chem. Res.* **2001**, *34*, 159-170.
9. Giese, B. *Acc. Chem. Res.* **2000**, *33*, 631-636.
10. Schuster, G. B. *Acc. Chem. Res.* **2000**, *33*, 253-260.
11. Nakatani, K.; Dohno, C.; Saito, I. *J. Am. Chem. Soc.* **1999**, *121*, 10854-10855.
12. a) Beratan, D. N.; Priyadarshy, S.; Risser, S. M. *Chem. Biol.* **1997**, *4*, 3-8. b) Priyadarshy, S.; Risser, S. M.; Beratan, D. N. *J. Biol. Inorg. Chem.* **1998**, *3*, 196-200.
13. Bolton, J. R.; Archer, M. D. *Advances in Chemistry Series* **1991**, *228*, 7-23.

14. Marcus, R. A.; Sutin, N. *Biochem. Biophys. Acta* **1985**, *811*, 265-322.
15. McConnell, H. M. *J. Chem. Phys.* **1961**, *3*, 508-515.
16. Gray, H. B.; Winkler, J. R. *Annu. Rev. Biochem.* **1996**, *65*, 537-561.
17. Murphy, C. J.; Arkin, M. R.; Jenkins, Y.; Ghatlia, N. D.; Bossmann, S. H.; Turro, N. J.; Barton, J. K. *Science* **1993**, *262*, 1025-1029.
18. Kelley, S. O.; Holmlin, R. E.; Stemp, E. D. A.; Barton, J. K. *J. Am. Chem. Soc.* **1997**, *119*, 9861-9870.
19. Fukui, K.; Tanaka, K. *Angew. Chem. Int. Ed.* **1998**, *37*, 158-161.
20. Kelley, S. O.; Barton, J. K. *Science* **1999**, *283*, 375-381.
21. Pascaly, M.; Yoo, J.; Barton, J. K. *J. Am. Chem. Soc.* **2002**, *124*, 9083-9092.
22. Felts, A. K.; Pollard, W. T.; Friesner, R. A. *J. Phys. Chem.* **1995**, *99*, 2929-2940.
23. Meggers, E.; Michel-Beyerle, M. E.; Giese, B. *J. Am. Chem. Soc.* **1998**, *120*, 12950-12955.
24. Steenken, S.; Jovanovic, S. V. *J. Am. Chem. Soc.* **1997**, *119*, 617-618.
25. Sugiyama, H.; Saito, I. *J. Am. Chem. Soc.* **1996**, *118*, 7063-7068.
26. Prat, F.; Houk, K. N.; Foote, C. S. *J. Am. Chem. Soc.* **1998**, *120*, 845-846.
27. Henderson, P. T.; Jones, D.; Hampikian, G.; Kan, Y.; Schuster, G. B. *Proc. Natl. Acad. Sci. USA* **1999**, *96*, 8353-8358.

28. Amouyal, E.; Homsy, A.; Chambron, J.-C.; Sauvage, J.-P. *J. Chem. Soc. Dalton Transactions* **1990**, 6, 1841-1845.
29. Holmlin, R. E.; Dandliker, P. J.; Barton, J. K. *Bioconjugate Chem.* **1999**, 10, 1122-1130.
30. Hush, N. S.; Cheung, A. S. *Chem. Phys. Lett.* **1975**, 34, 11-13.
31. Turro, C.; Evanhazav, A.; Bossmann, S. H.; Barton, J. K.; Turro, N. J. *Inorg. Chim. Acta* **1996**, 243, 101-108.
32. Rajski, S. R. personal communication.
33. Kelley, S. O.; Barton, J. K. *Chem. Biol.* **1998**, 5, 413-425.
34. Nakatani, K.; Dohno, C.; Saito, I. *J. Am. Chem. Soc.* **2000**, 122, 5893-5894.
35. O'Neill, M. A.; Barton, J. K. submitted.
36. Wan, C.; Fiebig, T.; Kelley, S. O.; Treadway, C. R.; Barton, J. K.; Zewail, A. H. *Proc. Natl. Acad. Sci. USA* **1999**, 96, 6014-6019.
37. O'Neill, M. A.; Becker, H.-C.; Wan, C.; Barton, J. K.; Zewail, A. H. *Angew. Chem. Int. Ed.* **2003**, 42, 5896-5900.
38. Dickerson, R. E. *Nucleic Acids Res.* **1998**, 26, 1906-1926.
39. Koo, H. S.; Drak, J.; Rice, J. A.; Crothers, D. M. *Biochemistry* **1990**, 29, 4227-4234.
40. Yoo, J.; Delaney, S.; Stemp, E. D. A.; Barton, J. K. *J. Am. Chem. Soc.* **2003**, 125, 6640-6641.

CHAPTER 6

Summary and Perspectives

In the fifty years since the determination of the molecular structure of DNA by Watson and Crick, the ability of the π -stacked array of base pairs to support charge transport (CT) has been conclusively delineated by numerous investigations. Fast rates of charge transport and a shallow dependence on distance have been shown for those donor and acceptor pairs that are well coupled into the π -stacked medium. Subsequent studies revealed that DNA could also serve as a reactant in CT and that the transport could occur over remarkable distances. Additional spectroscopic, electrochemical, and biochemical investigations of DNA CT have found it to be exquisitely sensitive to perturbations in the π -stack. DNA-binding proteins that disrupt the π -stacking of the base pairs, mismatches, and base bulges have all been found to attenuate charge transport. This wealth of experimental evidence provoked an investigatory shift in the DNA CT field from whether charge transport occurs to ruminations about the mechanism of the process.

The work described in this dissertation commenced in this highly charged intellectual environment. During this time, a single nucleotide hopping model that described DNA CT as that of hopping amongst easily oxidizable guanine steps and tunneling through higher energy adenine/thymine steps was being heavily touted as a dominant CT mechanism. However, this mechanistic oversimplification did not appear to elucidate the extraordinarily fast rates of

charge transport observed over a range of distances or the shallow dependence on distance of CT. An investigation utilizing 5'-functionalized rhodium assemblies and varying lengths of A/T sequences described here does not show marked decreases in oxidative damage yield, as would be expected for increasing the number of tunneling steps, but hints at a mechanism that is far more complicated than the proposed model of single nucleotide hopping. Hopping amongst inherent DNA domains, in which charge is injected into extended, transiently formed π -orbitals, the size of which is dictated by the DNA sequence, has been proposed as an alternative DNA CT mechanism and is more encompassing in describing experimental data.

Octahedral complexes comprised of phenanthrenequinone diimine (ϕ) complexes of rhodium and the dipyridophenazine (dppz) complexes of ruthenium have been extremely useful in studies of DNA CT. These complexes have chemically tunable ancillary ligands and intercalating ligands that permit them to have direct electronic communication with the π -stack. Additionally, these complexes are highly charged; the rhodium complexes possess a +3 charge and the ruthenium complexes a +2 charge. This led us to consider whether perhaps these highly charged complexes could influence the local potential at proximal guanine doublet (5'-GG-3') sites, leading to guanine oxidation ratios that would be greater than the expected one. Hence, ionic distribution studies

have been performed by simply changing the end label(s) of the strand containing the oxidatively sensitive 5'-GG-3' sites. This results in dramatic differences in oxidative damage yield at proximal and distal guanine sites, suggesting that the polarizability of the DNA π -stack should also be considered as an important factor when modeling DNA CT.

Although a variety of oxidants, e.g., metallointercalators, organic intercalators, and modified bases, have been shown to perform long-range oxidative damage to DNA, they yield varying oxidative results. Therefore, a systematic investigation of the yield of oxidative damage, using assemblies modified with either rhodium, ruthenium, anthraquinone, ethidium, or thionine were found to have remarkably different oxidative damage patterns, with ruthenium and anthraquinone garnering higher oxidative yields than all of the other oxidants, hence reiterating the fact that the photochemical characteristics of the oxidant play a key role in modulating CT yields. Additional studies utilizing N^2 -cyclopropylguanine (^{CP}G), a kinetically faster hole trap than the commonly employed 5'-GG-3' trap, also found differences amongst the oxidants, with the rhodium and ethidium assemblies possessing higher distal/proximal 5'- ^{CP}GG -3' ratios than that of anthraquinone or ruthenium. Furthermore, thionine, whose long-range oxidative ability was not established in biochemical studies, was found to effectively modify the ^{CP}G trap and delineated a complex distance

dependence using this trap, thus revealing the importance of competitive back electron transfer in attenuating CT yields for all oxidants employed in the investigation.

To probe the effect of bridge energetics on the CT process, rhodium-modified assemblies, containing varying numbers of inosine, which has a higher oxidation potential than guanine, were constructed. The intervening bridge medium did little to attenuate oxidative damage yields for rhodium, suggesting that perhaps CT using the rhodium oxidant, because of its ability to oxidize all DNA bases, involves injection into and transient occupation of all of the bridge elements.

With the burgeoning interest in the use of DNA in the field of microelectronics and the creation of effective biological sensors, it has become increasingly imperative to comprehend the mechanism(s) of DNA-mediated CT and those factors that attenuate the process. The work described in this thesis provides insight into some salient parameters that either impede or enhance the ability of DNA to support charge transport. This work has elucidated how the extent of electronic communication with and amongst the base pairs within the π -stack, dynamics, and stacking can efficiently modulate DNA CT.

One significant question that remains is whether Nature takes advantage of this remarkable ability of DNA biologically. If a charge is introduced via

endogenous or exogenous sources, is the charge funneled to particular regions to protect those that are vital to cellular function and maintenance? Does DNA sequence and hence packaging somehow protect other genetic regions? Only further study will elucidate the answers to these and other questions.

Meanwhile, it is essential to thoroughly investigate and understand the various photochemical systems that are utilized to examine and characterize DNA CT such that an accurate and general mechanism(s) of CT can be formulated.